

Modelling Calcium Signalling in In-Vitro Fertilisation

Layla Sadeghi Namaghi

Supervisors:

Katerina Kaouri

Thomas Woolley

A thesis submitted for the degree of
Master of Philosophy



School of Mathematics
Cardiff University
August 2022

Abstract

Calcium (Ca^{2+}) signalling plays a crucial, diverse role in the body (Berridge et al., 2003). We focus on the role of Ca^{2+} signalling in the fertilisation of mammalian eggs (Sanders et al., 2018). Many models of Ca^{2+} signalling rely on inaccurate dynamics of the inositol 1,4,5-triphosphate receptor (IP_3R) on the Endoplasmic Reticulum (ER) (Theodoridou et al., 2013). It is also frequently assumed that Ca^{2+} oscillations are driven by the emptying of the ER Ca^{2+} store and not by the IP_3R dynamics. Here, we develop a new ‘gating’ model for Ca^{2+} signalling in fertilisation that more accurately captures the open probability of the IP_3R dynamics, as a function of Ca^{2+} and IP_3 , as determined by Mak et al. (1998).

To develop a detailed understanding of gating models, we first study the models of Atri et al. (1993) and Li and Rinzel (1994). Subsequently, we study Mak et al. (1998), which includes the most up-to-date experimental data on the IP_3R dynamics. We also review how these data have been incorporated into a model by Kowalewski et al. (2006), though the latter is not a model for Ca^{2+} signalling in fertilisation.

Our model combines features of the Atri et al. (1993) model with the IP_3R data by Mak et al. (1998). It contains one ODE for $[Ca^{2+}]$ in the cytosol and another ODE for the percentage of non inactivated IP_3R . We perform linear stability analysis and solve the model numerically, varying $[IP_3]$ as the bifurcation parameter. This model accurately reproduces key experimental features, including the low frequency and large amplitude of Ca^{2+} oscillations in fertilisation. The model also captures that frequency and amplitude of Ca^{2+} oscillations increase as $[IP_3]$ is increased (Sanders et al., 2018). With this model, we hope to guide future experiments that could eventually improve clinical practice in In-Vitro Fertilisation.

Acknowledgements

Firstly, I would like to express my gratitude towards my outstanding supervisors, Dr. Katerina Kaouri and Dr. Thomas Woolley. They have both worked extremely hard to guide me through this project and introduce me to the field of academic research. Even through a pandemic, they have both put every effort into supporting me. I would like to thank them for their patience, wisdom and encouragement. I am so grateful for the opportunity to have worked with them both and hope to do so again in the future.

I would like to thank Prof. Karl Swann, of the Cardiff University School of Biosciences. Without him, this project would not have been possible. I will cherish many fascinating conversations we had about his work and the use of mathematical modelling in the world of biology.

I would also like express my thanks to all of the staff and students in the School of Mathematics. I feel truly lucky to be continuing my studies here with them all. Namely, I'm extremely grateful for the friendships I have made in Lucy, Josh, Tim, and Abhishek.

Finally, I'd like to thank my parents for their support throughout my studies. Their work ethic has always been my inspiration.

Contents

1	Introduction	5
1.1	Ca^{2+} signalling in fertilisation	5
1.1.1	Agonists, receptors and second messengers	7
1.1.2	Internal compartments	9
1.1.3	Internal calcium channels	9
1.2	Mathematical models for Ca^{2+} signalling	11
1.3	Project aims	15
1.4	Thesis overview	16
2	Ca^{2+} signalling models for fertilisation	18
2.1	The Atri et al. model	19
2.1.1	Model assumptions	21
2.1.2	Non-dimensionalisation of the Atri et al. model	24
2.1.3	Linear stability analysis	25
2.1.4	Simulations	27
2.2	The Li-Rinzel model	29
2.2.1	Simulations	33
3	Experimental data on IP_3R dynamics (Mak et al.)	36
4	A model incorporating the experimental data by Mak et al.	45
5	A new model for Ca^{2+} signalling in fertilisation	51
5.1	Linear stability analysis	55
5.2	Simulations	59
6	Summary, Conclusions and Further work	63
	References	65

A	A look into models with dynamic IP_3	72
B	Parameter Tables	78
C	MATLAB Code	83

Chapter 1

Introduction

Calcium in the form of Ca^{2+} ions is a life and death signal, acting as an intracellular messenger in the body, carrying information in cells to regulate their activity (Berridge et al., 2003). Ca^{2+} signals are relevant to many cell functions, for example muscle contractions and cell adhesion (Berridge et al., 2003). In this project, we study mathematical modelling of Ca^{2+} signalling in fertilisation of the mammalian egg. Our focus will be on deterministic, spatially homogeneous models, paying close attention to the dynamics of the IP_3 receptors (IP_3R). After studying the existing models and experimental data available, we derive a new model that successfully captures many of the key features that regulate Ca^{2+} signalling in a fertilising egg.

1.1 Ca^{2+} signalling in fertilisation

The cytosolic Ca^{2+} concentration in almost every cell type is carefully controlled by sophisticated mechanisms (Berridge et al., 2000). As a result, the Ca^{2+} shows complex spatiotemporal behaviour (Atri et al., 1993; Swann & Lai, 2013; Wallingford et al., 2001). These behaviours range from stochastic spiking, to regular oscillations, periodic waves, and spiral waves. The ECF has a Ca^{2+} concentration of around $1mM$, while active pumps and exchangers maintain the concentration of cytoplasmic Ca^{2+} at around $0.1\mu M$. Some intracellular compartments, for example the endoplasmic reticulum (ER) and mitochondria, have a comparatively high concentration of $100 - 800\mu M$ (Carreras-Sureda et al., 2018). High levels of cytosolic Ca^{2+} for prolonged periods of time can be cytotoxic (Berridge et al., 2000), hence Ca^{2+} regulation is very important. In this project, we aim to model Ca^{2+} signalling in fertilising eggs. During fertilisation, Ca^{2+} oscillations are triggered by PLC_ζ and are the essential trigger of embryo development. PLC_ζ is a testes-specific isoform of phospholipase

C (*PLC*) and is located in the sperm cytoplasm. *PLC* is an enzyme that is restricted to the plasma membrane. The number of Ca^{2+} oscillations influences the rate of embryo development (Swann & Lai, 2016). These Ca^{2+} oscillations have a large amplitude ($1\mu M$) and low frequency (time period >10 mins). The initial Ca^{2+} increase lasts approximately five minutes. Each subsequent Ca^{2+} rise is very rapid (1 sec) and the Ca^{2+} increases last for about 1 minute. Ca^{2+} oscillations in a fertilising mouse egg can be seen in Figure 1.1.

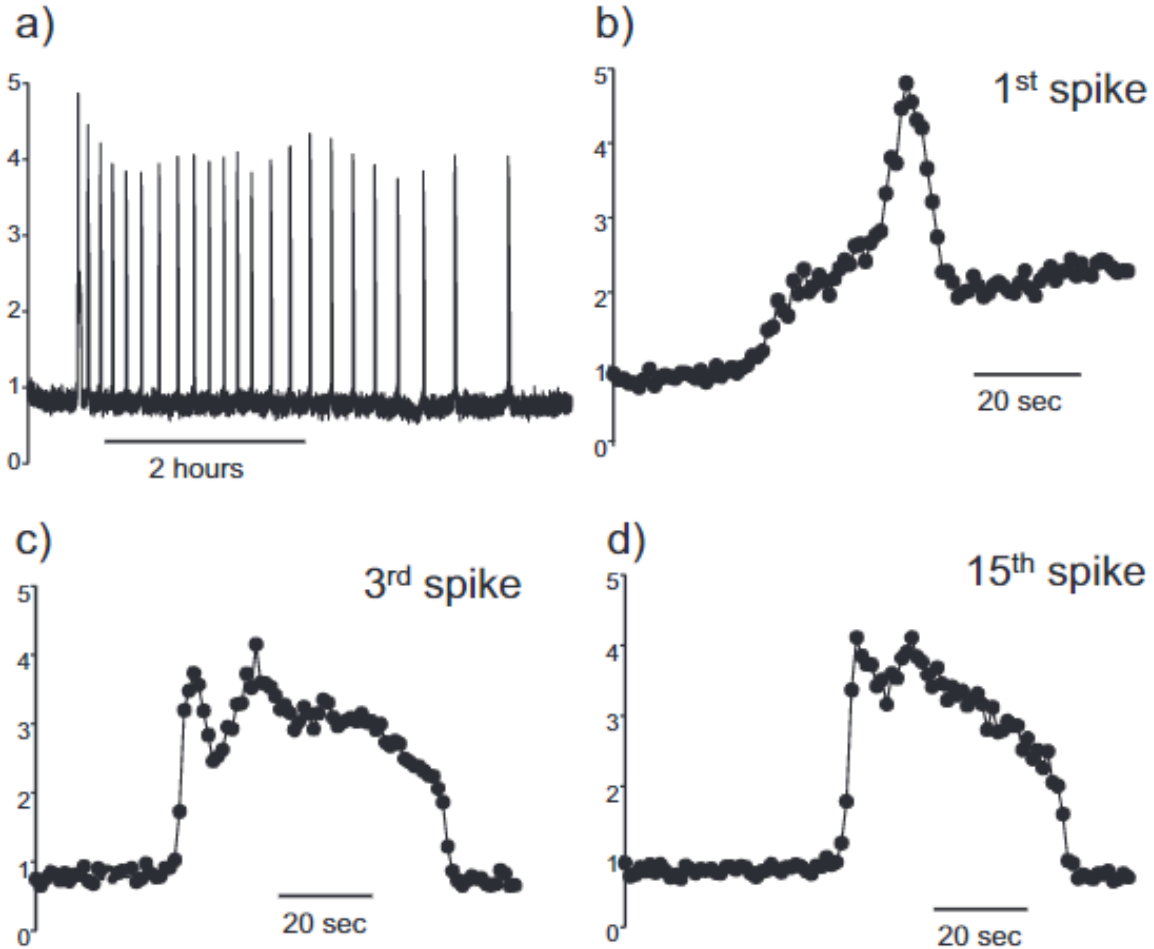


Figure 1.1: Intracellular Ca^{2+} oscillations in a fertilising mouse egg. This is measured by the fluorescence of the Ca^{2+} -sensitive dye Rhod dextran. The fluorescence is plotted as a ratio of the fluorescence versus time divided by the starting fluorescence. Once the sperm is added there are large increases in fluorescence ratio indicating Ca^{2+} increases in the cytoplasm. The amplitude of the Ca^{2+} oscillations is variable and likely to be in the range of $1 - 2\mu M$ (Swann & Lai, 2013). Source: Swann and Lai (2013).

1.1.1 Agonists, receptors and second messengers

The most important of the signalling pathways is the phosphatidylinositol signalling pathway (Berridge et al., 2000). Here, in a somatic cell, phospholipase C (*PLC*) is activated and splits another membrane molecule, phosphatidylinositol 4,5-bisphosphate (*PIP*₂), into inositol 1,4,5-triphosphate (*IP*₃) and diacylglycerol (DAG). The *IP*₃ that is released into the cytoplasm then binds to *IP*₃ receptors (*IP*₃*R*) which lie on the membrane of the endoplasmic/sarcoplasmic reticulum (ER/SR). The *IP*₃*R* are channels that release Ca^{2+} from the ER to the cytosol (Parys & Bezprozvanny, 1995).

In fertilisation, once sperm has fused with the egg membrane, the sperm *PLC*_ζ (an isoform of *PLC*) diffuses into the egg cytoplasm. Here, the *PLC*_ζ binds to *PIP*₂ which leads to the generation of *IP*₃. This *IP*₃ binds to the *IP*₃*R* on the ER, causing the ER to release Ca^{2+} . The increase in [Ca^{2+}] in the cytosol then stimulates the activity of *PLC*_ζ to generate more *IP*₃. Therefore, as *PLC*_ζ diffuses across the egg, this positive feedback loop occurs throughout the cytoplasm (Swann & Lai, 2016).

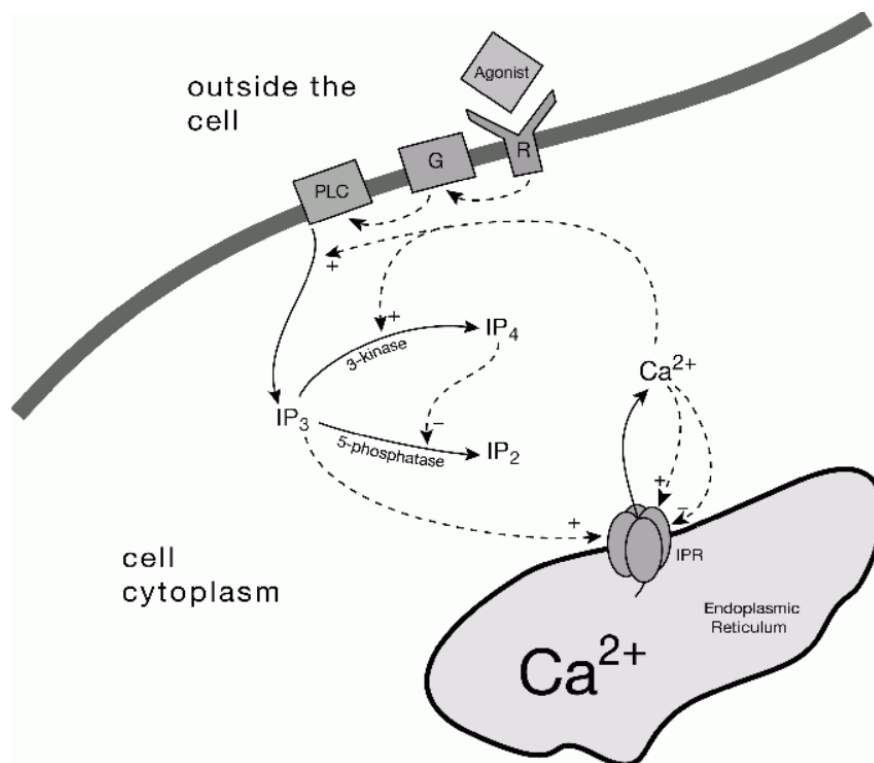


Figure 1.2: A schematic of the PLC pathway for Ca^{2+} signalling. R - Receptor, G - GPCR. Source: Sneyd (2007).

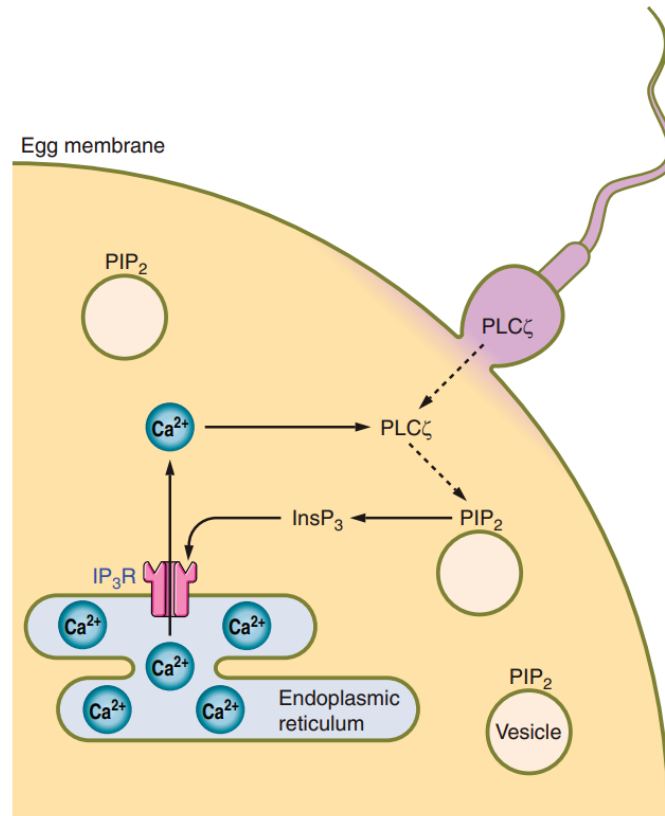


Figure 1.3: A schematic diagram showing the proposed mechanism of action of $PLC\zeta$ during fertilisation. Once sperm has fused with the egg membrane, the sperm $PLC\zeta$ diffuses into the cytoplasm. It then binds to PIP_2 and this leads to the generation of IP_3 . IP_3 binds to the IP_3R on the ER and this causes Ca^{2+} release from the ER. Source: Swann and Lai (2016).

1.1.2 Internal compartments

The most significant of intracellular compartments when it comes to Ca^{2+} signalling is the ER (Berridge & Galione, 1988). Its main function concerns protein synthesis, and it makes up approximately 10% of the total cellular volume. The ER is able to store a substantial amount of Ca^{2+} , and release it into the cytosol very quickly. The large amount of Ca^{2+} enters the ER via the sarcoplasmic/endoplasmic reticulum Ca^{2+} ATPases (SERCA) pumps, and escapes through two major types of receptor Ca^{2+} channels (Marks, 1997). These are the IP_3R and the ryanidine receptor (RyR).

The mitochondria in the cell are responsible for producing adenosine triphosphate (ATP) and also act as a Ca^{2+} store. It is still not well understood how the mitochondria interact with cytosolic Ca^{2+} . It is highly suspected that the ER is the main driving force for the intracellular Ca^{2+} fluxes, while the mitochondria might play a more passive modulatory role (Jouaville et al., 1995).

1.1.3 Internal calcium channels

As described above, Ca^{2+} is released from the ER through two types of receptors. The RyR is the largest known ion channel (Van Petegem, 2012; Fill & Copello, 2002). It is mainly found in cells other than eggs, such as cardiac cells and skeletal muscle cells. For this reason we do not go into further depth regarding this channel.

The second major intracellular Ca^{2+} channel is the IP_3 receptor (IP_3R) (Joseph, 1996; Patel et al., 1999; Taylor & Laude, 2002; Foskett et al., 2007; Mak & Foskett, 2015). The probability of the IP_3R being open is referred to throughout this thesis as the ‘*open probability*’ (P_O). At low cytosolic Ca^{2+} levels, an increase in the Ca^{2+} concentration leads to an increase in P_O . This starts a positive feedback process of Ca^{2+} , known as Ca^{2+} -induced Ca^{2+} release (CICR). At higher levels of Ca^{2+} concentration, P_O begins to decrease. In other words, the steady-state value of P_O is a biphasic function of Ca^{2+} (Parys et al., 1992). Figure 1.4 shows a graph of this based on experimental data (Mak et al., 1998). The IP_3R is also affected by IP_3 . An increase in cytosolic IP_3 concentration also increases P_O . We will go into further detail about this later as the IP_3R mechanisms and dynamics are a main feature of this thesis.

We have touched on the basics of Ca^{2+} signalling, and the schematic in Figure 1.3 provides a visual description of those. However, other aspects are specific to the type of cell considered.

Many studies and experiments have been carried out on the fertilisation of an aquatic frog (*Xenopus Laevis*), for example Busa and Nuccitelli (1985); Nuccitelli et al. (1993);

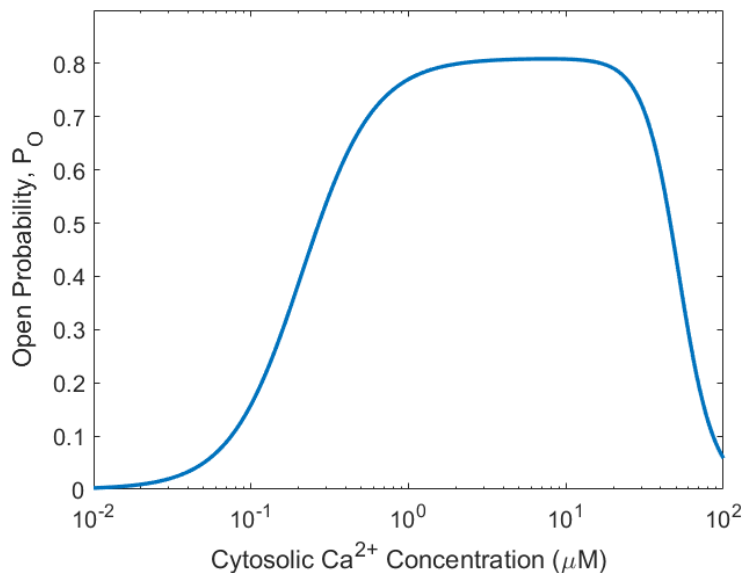


Figure 1.4: The open probability of the IP_3R , P_O , as a function of the cytosolic Ca^{2+} concentration (μM). This was plotted at an IP_3 concentration of $0.1\mu M$ using the equation for P_O and data from Mak et al. (1998). *Software*: MATLAB.

Fontanilla and Nuccitelli (1998). The diameter of their oocytes can be larger than $600\mu M$, around 50 – 100 times larger than an average cell ((Dupont et al., 2016), page 23). Their greater size means they are perfect for experimental investigations of Ca^{2+} signalling. Immature *Xenopus* oocytes show complex spatiotemporal organisation (Lechleiter et al., 1991), forming concentric circles and multiple spirals. A typical Ca^{2+} wave in a smaller cell cannot be observed in its entirety. Furthermore, there is not enough room for a spiral to form, and so Ca^{2+} waves take a form that is almost planar. In a larger cell like the *Xenopus* oocyte, it is possible to observe both the wave front and wave back, as well as spiral waves. Ca^{2+} blips and puffs are evoked by very low levels of IP_3 , while oscillations are observed in immature oocytes in response to sufficient amount of caged IP_3 (Marchant et al., 1999). These oscillations correspond to the repetitive Ca^{2+} waves that propagate throughout the cell during fertilisation (Berridge & Dupont, 1994; Thomas et al., 1996).

Upon fertilisation of an egg, sperm-egg fusion yields an alternative type of Ca^{2+} response in the way of a single slow Ca^{2+} wave inside the egg. It takes about four minutes for the wave to traverse the egg, with a high level of Ca^{2+} concentration maintained for the next 5 – 6 minutes after the propagation (Fontanilla & Nuccitelli, 1998). It is fortunate that there are detailed experimental data on *Xenopus* oocytes and on the elements of the Ca^{2+} toolbox that are relevant for eggs. The *Xenopus* egg is very similar to mammalian eggs, particularly in the type of IP_3R present which is a type 1 IP_3R . We also have accurate data of the IP_3R

dynamics (Mak et al., 1998). These data provide us with the opportunity to develop a new model that captures key features of the Ca^{2+} dynamics in the fertilisation of a mammalian egg. Such a model, to the best of our knowledge, does not exist in the literature.

1.2 Mathematical models for Ca^{2+} signalling

Models of Ca^{2+} signalling can be divided into four major subgroups. Firstly, they can be divided into deterministic and stochastic models, and secondly they can be divided into spatially homogeneous (ordinary differential equations, or ODEs) and spatially distributed models (partial differential equations, or PDEs). Ca^{2+} signalling is intrinsically stochastic and spatially distributed (Sun et al., 1998; Callamaras & Parker, 2000; Falcke, 2003). This makes the mathematical analysis of Ca^{2+} signals quite difficult. However, deterministic models can be useful for making predictions while they are easier to solve numerically than analogous stochastic models and so they remain a highly useful tool. In many cases, these predictions can (and have been) supported by experimental evidence and have been used extensively (Atri et al., 1993; De Young & Keizer, 1992; Dupont, 1998). For example, in Shuai and Jung (2002) the deterministic Li and Rinzel (1994) model is compared to two stochastic models and found to agree well when the number of IP_3R is large enough.

There is a spatial aspect to the Ca^{2+} oscillations at fertilisation, but the purely IP_3 induced Ca^{2+} oscillations, in oocytes, that we will model are uniform across the egg with no obvious wave. This was shown in imaging experiments (Carroll et al., 1994). We will therefore focus on deterministic, spatially homogeneous models, as a first approach to our challenge of creating a new model for Ca^{2+} signalling in fertilising eggs.

Figure 1.5 shows the Ca^{2+} fluxes in a cell. These fluxes are the following: into the cytosol through IP_3R from the ER ($J_{channel}$), out of the cytosol into the ER (J_{pump}), into cytosol through leak from the ER (J_{leak}), into the cell (J_{in}), and out of the cell (J_{pm}). We can define an ODE which represents the change in Ca^{2+} concentration in the cytosol over time, as follows:

$$\frac{dc}{dt} = J_{channel} - J_{pump} + J_{leak} + (J_{in} - J_{pm}), \quad (1.1)$$

where c represents the cytosolic Ca^{2+} concentration (μM). In the ODE above, each J flux represents the impact on the concentration within the cell due to the flux into or out of the cell, rather than the true flux that we see in Figure 1.5. The units of flux in the ODE are μMs^{-1} . We later show how true fluxes are translated into changes in concentration due to those fluxes using equation (2.3). Note that throughout this project, when referring to Ca^{2+}

concentration, we are referring to the concentration in the cytosol unless stated otherwise. Each type of flux can actually be modelled in different ways (Sneyd, 2007), depending on which elements are relevant.

In this thesis, we pay close attention to the so-called gating models. These are models which include one ODE for $[Ca^{2+}]$, as given in equation (1.1), and an ODE that models the proportion of non inactivated (or ‘openable’) IP_3R , n . This means that some IP_3R are fully inactivated (and cannot be opened), and the other IP_3R are closed but not inactivated, so can be opened. We wish to avoid the cytosolic Ca^{2+} oscillations depending on the ER Ca^{2+} store depleting as experimental evidence suggests that this does not drive oscillations during fertilisation (Sanders et al., 2018; Wakai et al., 2013). The equation for the proportion of non inactivated IP_3R , n , is given as follows:

$$\tau_n \frac{dn}{dt} = n_\infty(c) - n, \quad (1.2)$$

where n_∞ represents the steady state of n as a function of c , and τ_n is a time scale.

Alternatively, equation (1.1) is commonly coupled with a second ODE to account for the change in Ca^{2+} in the ER over time but this is not appropriate for modelling Ca^{2+} signalling in fertilisation since oscillations should not be driven by the Ca^{2+} store in the ER emptying (Sanders et al., 2018; Wakai et al., 2013). This equation is presented as follows:

$$\frac{dc_e}{dt} = \gamma(-J_{channel} + J_{pump} - J_{leak}), \quad (1.3)$$

where c_e represents Ca^{2+} concentration in the ER. Ca^{2+} in the ER oscillates passively in the case of fertilisation, so parameter values can be tuned such that (1.3) is approximately in steady state. The parameter γ represents the ratio of the volume of cytoplasm over the volume of the ER. This parameter is necessary since the volume of the ER is far less than that of the cytoplasm, making up just 10% of the total volume of the cell. This means that the flow of Ca^{2+} into the ER will cause a larger change in concentration in the ER than the flow of Ca^{2+} into the cytoplasm.

Generally, the ODEs (1.1), (1.2) and/or (1.3) can be coupled with other equations that could represent the state of the IP_3R , the states of the ATPase pumps, the Ca^{2+} buffers, or the IP_3 concentration, amongst others (Atri et al., 1993; De Young & Keizer, 1992; Dupont et al., 1991; Höfer, 1999).

We now briefly discuss the collection of models that have been constructed for Ca^{2+} signalling. One type of model for Ca^{2+} signalling is based on the assumption that the Ca^{2+} concentration in the ER remains constant as the store is quickly refilled from the cytoplasm

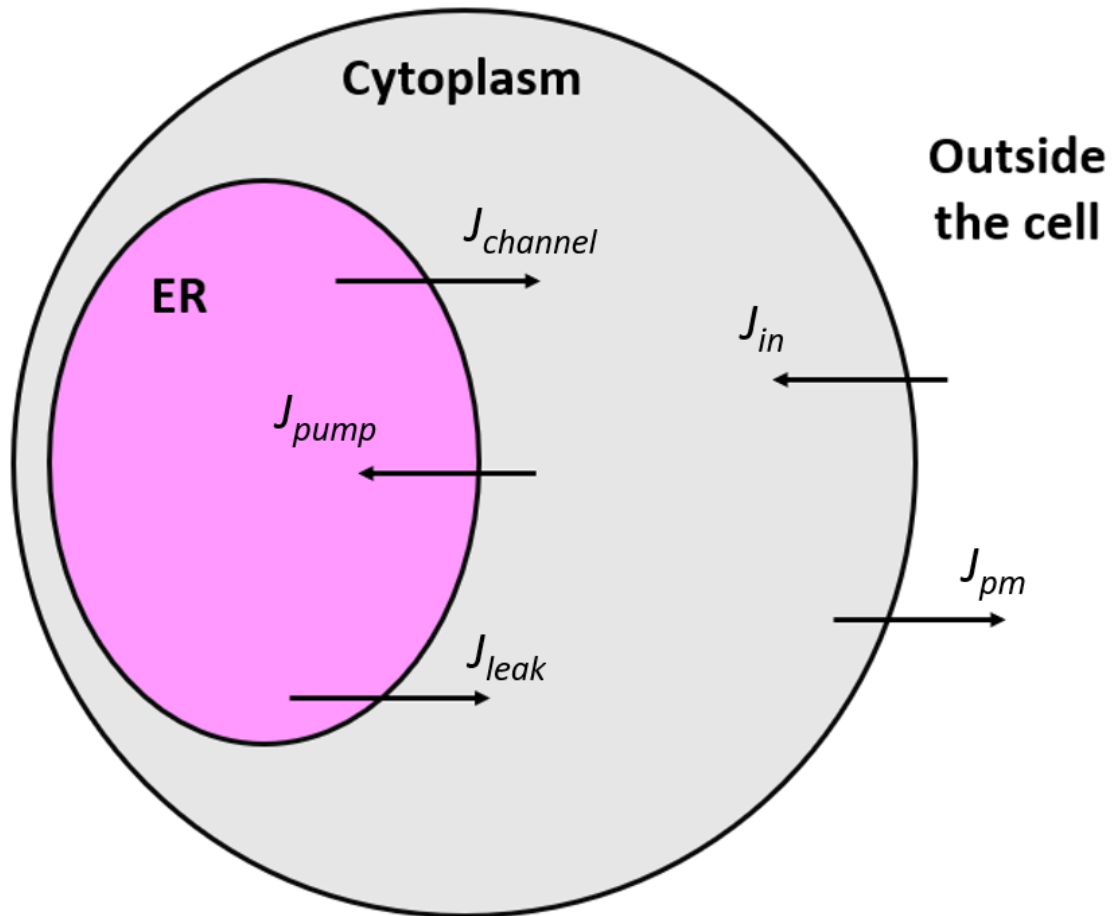


Figure 1.5: A diagram illustrating the fluxes in and out of the cell's cytoplasm typically modelled in a gating model, as in ODEs (1.1) and (1.2). Flux into the cytosol through IP_3R from the ER is represented by $J_{channel}$. Flux out of the cytosol back into the ER through SERCA pumps is represented by J_{pump} . There is also a leak of Ca^{2+} from the ER into the cytosol represented by J_{leak} . Flux into and out of the cytoplasm over the cell plasma membrane is represented by J_{in} and J_{pm} , respectively.

(Dupont et al. (2016), page 104). A model based on the ER refilling was derived by Dupont and Goldbeter (1993). Positive feedback of Ca^{2+} release is assumed, and this drives the Ca^{2+} oscillations. This type of model was developed before the dynamics of the IP_3R were discovered and therefore does not account for any Ca^{2+} -dependent inactivation of the IP_3R . The model relies on depletion of the ER Ca^{2+} store and the time period for oscillations is based on the time taken to refill the ER. One major problem that commonly occurs still in modern models is that the oscillations are assumed to emerge due to the ER store depleting and refilling. Experimental data from Sanders et al. (2018); Wakai et al. (2013) suggests that this is not the case for eggs.

One of the early models for the *Xenopus* oocyte was a gating model by Atri et al. (1993). We will refer to this as the ‘Atri model’ throughout this thesis. It is a simple, non-linear two-variable ODE model that gives rise to Ca^{2+} oscillations. The model is highly cited and still regarded to be very relevant today. The model is studied in detail in Chapter 2.

De Young and Keizer (1992) derived a model which we refer to as the ‘De Young-Keizer model’. Their kinetic model was based on experimental data on the IP_3R . It reproduces several in-vivo and in-vitro experimental results (Berridge, 1989; Mouillac et al., 1990; Smrcka et al., 1991). It has nine variables and assumes a positive-feedback mechanism of Ca^{2+} on IP_3 production.

Li and Rinzel developed a gating model by reducing the De Young-Keizer model, using the multiple scales method, to just two ODEs (Li & Rinzel, 1994). We refer to this as the ‘Li-Rinzel model’. Like in the Atri model, the variables are the cytosolic Ca^{2+} concentration and the proportion of non-inactivated IP_3R . This is another well-known gating model. The derived model retains the key features of the original De Young-Keizer model. We will take a thorough look at the Li-Rinzel model also in Chapter 2.

In the *Xenopus* oocyte, the intracellular waves exhibit complex spatiotemporal organisation (Lechleiter et al., 1991). In order to take the first step towards modelling Ca^{2+} waves in fertilising eggs, here we develop a deterministic gating (ODE) model for Ca^{2+} oscillations which accurately reproduces key experimental features in fertilising eggs. Previously, all models have incorporated IP_3R dynamics that depend on $[Ca^{2+}]$ and $[IP_3]$ in an inaccurate manner, and some rely on the ER store depleting and refilling to drive oscillations. Evidence (Sanders et al., 2018; Wakai et al., 2013) suggests that this refilling is not the main driving force for oscillations in fertilisation and that they are mainly driven by the IP_3R dynamics as published by Mak et al. (1998). We will derive a new model that incorporates the dynamics based on this more accurate data for how the IP_3R dynamics depend on $[Ca^{2+}]$ and IP_3 .

1.3 Project aims

In this thesis we study a series of the well-known deterministic, spatially homogeneous Ca^{2+} signalling models. We investigate how they work, paying close attention to the IP_3R dynamics that are known to be the driving force for oscillations. There is currently, to our knowledge, no Ca^{2+} model for fertilisation that contains the accurate type 1 IP_3R dynamics depending on $[Ca^{2+}]$ and $[IP_3]$ according to the data from Mak et al. (1998). Instead, many models for fertilisation rely on incorrect IP_3R dynamics and the ER Ca^{2+} store emptying to drive oscillations.

Our ultimate aim for this project is to develop a realistic model for Ca^{2+} oscillations that occur during fertilisation in mammalian eggs. The model should use the most current understanding of the mechanism of action of the type 1 IP_3R and of PLC_ζ . It should also reproduce the low frequency, large amplitude oscillations characteristic of fertilising mammalian eggs (shown in Figure 1.1). The type 1 IP_3R dynamics from Mak et al. (1998), that accurately show how the open probability depends on $[Ca^{2+}]$ and $[IP_3]$, must be incorporated. The model should not rely on the emptying of Ca^{2+} stores to drive the cytosolic Ca^{2+} oscillations. (Sanders et al., 2018). We aim to obtain such a model where the amplitude and frequency of Ca^{2+} oscillations increase as $[IP_3]$ increases, as per the experimental data from Sanders et al. (2018) and Sneyd et al. (2006).

This will be achieved by first studying several existing Ca^{2+} signalling models, out of the hundreds in the literature (Dupont et al., 2016). A subset of these are related to fertilisation (Atri et al., 1993; Sanders et al., 2018; Theodoridou et al., 2013). Many of these models appear to work well, but assume inaccurate IP_3R dynamics (Politi et al., 2006; Theodoridou et al., 2013; Sanders et al., 2018), and rely solely on the concept of ER store refilling as the driving force of the Ca^{2+} oscillations. We will take a step back from these recent models, many of which have three, or more, dynamic variables, and more parameters capturing other complex processes happening in the cell. We aim to develop a simple, two-variable model that incorporates experimental data for the open probability of the IP_3R by Mak et al. (1998). The Atri model was the first model developed for the *Xenopus* oocyte, but it is still a good model to start from as it captures the Ca^{2+} induced Ca^{2+} release mechanism operated by the ER, though depends on inaccurate data for how the IP_3R depends on Ca^{2+} and IP_3 . It is also a gating model with Ca^{2+} oscillations not driven by the ER store depleting, but by the presence of an ODE for the proportion of non-inactivated IP_3R , as required.

The IP_3R are channels that open and close to allow Ca^{2+} to pass from the ER into the cytosol. The flux of Ca^{2+} through the IP_3R is controlled by the probability of a single channel being open. The mechanism for the open probability of the IP_3R was identified by

Mak et al. (1998). These data have not been however, acknowledged sufficiently in recent Ca^{2+} modelling. They display some interesting features in regards to the dependence of the open probability on Ca^{2+} and IP_3 . We will deepen our understanding of these dynamics and explore how they can be incorporated into a Ca^{2+} model. We have been collaborating with Professor Karl Swann (Cardiff University), and his involvement has been crucial in this project. With insights from the Swann lab, we aim to present a new model, that accurately captures the Ca^{2+} oscillations, while using the correct dynamics from Mak et al. (1998). This will emulate the data from Sanders et al. (2018) and Sneyd et al. (2006) that tell us how the frequency and amplitude of Ca^{2+} oscillations behaves when $[IP_3]$ is increased. In this way, we aim to capture some of the complex features of Ca^{2+} signalling in eggs and in particular Ca^{2+} oscillations.

The experimental data from the Swann lab (see Sanders et al. (2018)) show that having IP_3 concentration as a dynamic variable is essential in a future model. In this work we set out to complete the initial important step towards this by deriving a two-variable model for Ca^{2+} signalling in fertilising eggs with the inclusion of the IP_3R dynamics from Mak et al. (1998) where IP_3 is a bifurcation parameter. This is the first step to reaching a three-variable model (with IP_3) that could inform future experiments and ultimately IVF clinical practice.

1.4 Thesis overview

We follow an incremental approach in this thesis. Firstly, we review current Ca^{2+} models and identify strengths and areas of improvement. We then analyse the true IP_3R dynamics in accordance with the data from Mak et al. (1998), and the equation that describes them. With this, we will then derive a system, based on an existing model, ensuring the addition of the accurate IP_3R dynamics.

In Chapter 2 we review and analyse several existing Ca^{2+} models, paying particular attention to those of Atri et al. (1993) and Li and Rinzel (1994). In this literature review we take note of the key features of each model, including investigating the IP_3R dynamics and its open probability. We also recognise the role of IP_3 as a bifurcation parameter. This is an essential feature that has to be included in any future Ca^{2+} model. In Chapter 3 we take a close look at the correct dynamics of the IP_3R as determined by Mak et al. (1998). We examine the data and the fairly complex ‘biphasic Hill function’ used in Mak et al. (1998) to describe these data. We acknowledge previous inaccuracies in the modelling of the IP_3R and improve them. In Chapter 4 we take a brief look at one model that has incorporated these dynamics already (Kowalewski et al., 2006) and discuss the relevance to our project.

In Chapter 5 we derive a new model - based on the Atri model but with the correct open probability equation derived from the data in Mak et al. (1998). Deriving this new model requires careful and thorough analysis of both the Atri model and the equation for the open probability. We solve the two-variable model numerically and we also perform linear stability analysis. This model matches key features of data from Sanders et al. (2018) and Sneyd et al. (2006) which show that the frequency and amplitude of Ca^{2+} oscillations increase as $[IP_3]$ is increases. In Chapter 6 we summarize our results propose future research directions.

Chapter 2

Ca^{2+} signalling models for fertilisation

There are many models of Ca^{2+} signalling available, including those derived by Theodoridou et al. (2013) and Politi et al. (2006). Sanders et al. (2018) is also based on these models. In the model by Theodoridou et al. (2013) there are three equations for cytosolic Ca^{2+} concentration, represented by c , Ca^{2+} concentration in the ER, represented by c_e , and cytosolic IP_3 concentration, represented by p . Since c_e plays more of a passive role (Sanders et al., 2018; Wakai et al., 2013), one should be able to replace it with a constant, with the system continuing to oscillate. In many models the IP_3R dynamics have been considered in the modelling of the flux of Ca^{2+} from the ER into the cytosol. However, these can be eliminated, or disregarded, in many instances with the systems still producing oscillations. For the model by Sanders et al. (2018) upon numerical experimentation, we found that oscillations are lost when c_e is taken out. This can be seen in Figure 2.1. This implies a dependence on ER store refilling, rather than IP_3R dynamics. By considering a gating model instead, for example the model by Atri et al. (1993), we have a two-variable model that does not consider Ca^{2+} in the ER as a dynamic variable. Regardless of this, it is still necessary that the model incorporates the correct IP_3R dynamics. The most recent data for IP_3R dynamics are discussed in Chapter 3, where we review the paper by Mak et al. (1998).

Taking the recent models mentioned as our starting point we resolve issues and correct the dependence on the IP_3R dynamics. We should avoid oscillations that depend on the ER store depletion. We are motivated to go back to basics and identify how to incorporate the open probability equation by Mak et al. (1998). We have briefly mentioned some well-established models for Ca^{2+} signalling in our introduction. Here we revisit these models in a detailed manner and decide which model would be suitable to incorporate the correct IP_3R dynamics into.

Below we study two key deterministic models for Ca^{2+} oscillations. We explore how they work, especially what drives the Ca^{2+} oscillations, and their biological representation. We

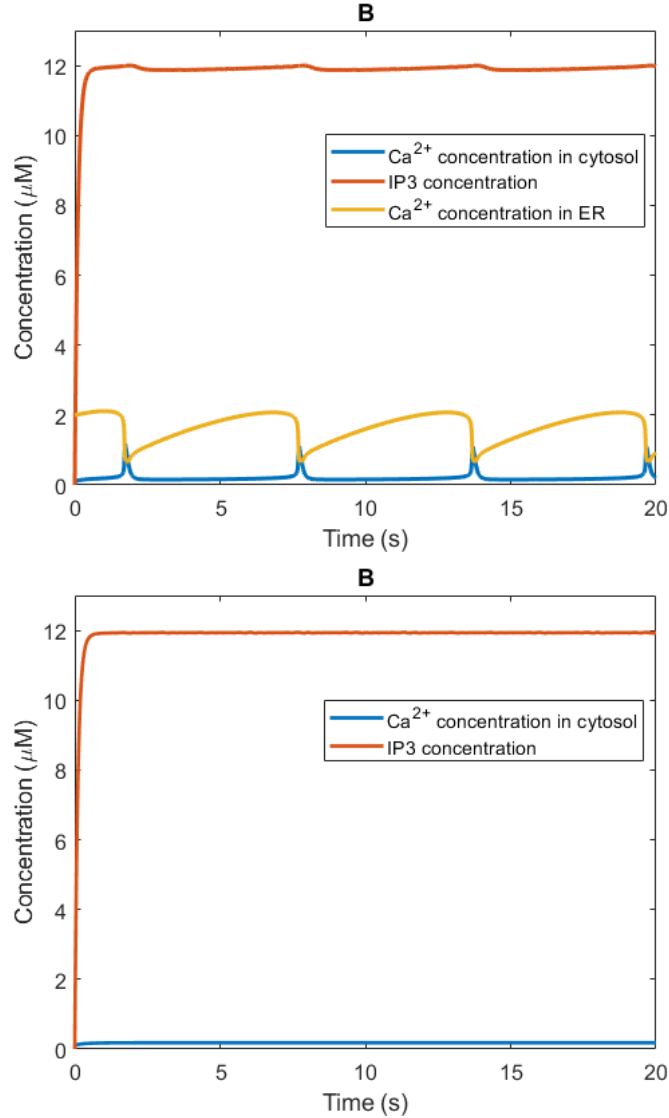


Figure 2.1: Ca^{2+} oscillations arising as solutions to the (Sanders et al., 2018) model. **(A)** Cytosolic Ca^{2+} , IP_3 , and Ca^{2+} in the ER oscillating. **(B)** A non oscillatory system of cytosolic Ca^{2+} and IP_3 , with the equation for Ca^{2+} in the ER having been taken out. This implies that oscillations depend on the ER store refilling. *Software:* MATLAB.

begin by looking at model by Atri et al. (1993) and the model by Li and Rinzel (1994).

2.1 The Atri et al. model

The first model we review was developed by Atri et al. (1993). It is the first deterministic Ca^{2+} model for the *Xenopus* oocyte. This model displays a fairly realistic representation of Ca^{2+} signals that occur during fertilisation. The model is based on experimental evidence

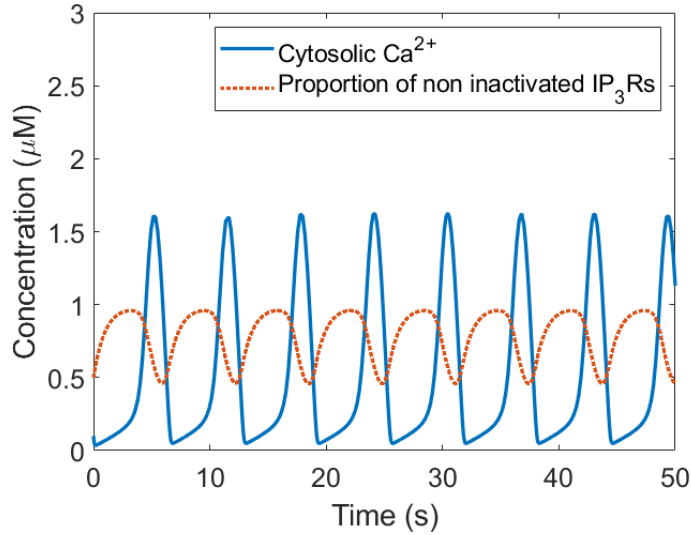


Figure 2.2: Ca^{2+} oscillations as solutions to the Atri Model, (2.5), (2.6), with $\mu(p) = 0.3$ (within oscillatory range). Parameter values are shown in Table B.1. Initial values of $0.1\mu M$ and 0.5 were taken for c and n respectively. Oscillations over time of 50 seconds. *Software:* MATLAB.

that the IP_3R is regulated by the cytosolic Ca^{2+} level in a biphasic manner (Finch et al., 1991). It is apparent in the experiments that Ca^{2+} release is inhibited by both low and high levels of cytosolic Ca^{2+} , and encouraged by intermediate levels of cytosolic Ca^{2+} . The inactivation of the IP_3R is a slower process than the activation (Finch et al., 1991). The model produces Ca^{2+} oscillations and travelling waves in the *Xenopus Laevis* oocyte with IP_3 concentration at a constant level.

The model consists of two ODEs, (2.1) and (2.2), where c represents cytosolic Ca^{2+} concentration (in μM) and n represents the proportion of non inactivated IP_3 receptors. The ODEs are:

$$\frac{dc}{dt} = J_{channel} - J_{pump} + J_{leakage}, \quad (2.1)$$

$$\tau_n \frac{dn}{dt} = \frac{K_{inh}^2}{K_{inh}^2 + c^2} - n. \quad (2.2)$$

The fluxes above are given by

$$\begin{aligned}
 J_{channel} &= k_{flux}n \left(\frac{p + \mu_0 K_{IP_3}}{K_{IP_3} + p} \right) \left(\frac{K_{act}b + c}{K_{act} + c} \right), \\
 J_{pump} &= \frac{V_e c}{K_e + c}, \\
 J_{leakage} &= \delta.
 \end{aligned}$$

The Ca^{2+} flux from the ER through the IP_3R into the cell cytosol is represented by $J_{channel}$. The Ca^{2+} flux by SERCA pumps from the cytosol to the cell's ER is represented by J_{pump} . The small flux of Ca^{2+} leaking out of the ER is represented by $J_{leakage}$. Parameter values and biological descriptions are given in Table B.1.

2.1.1 Model assumptions

The single channel model

A few assumptions are made about the IP_3R in the Appendix of Atri et al. (1993). These are:

- The IP_3R consists of three independent binding sites.
- A single molecule of IP_3 binds to the IP_3 activation site (site 1). A single molecule of Ca^{2+} binds to the Ca^{2+} activation site (site 2), and two molecules of Ca^{2+} bind to the Ca^{2+} inhibitory site (site 3).
- Activation of sites 1 and 2, and inactivation of site 3 together permits Ca^{2+} to pass through the IP_3R . Hence Ca^{2+} is involved in both positive and negative feedback.
- When Ca^{2+} and IP_3 levels are zero, basal flux through the IP_3R is still assumed as there is still a nonzero probability of activation of sites 1 and 2.
- The number of open channels is responsible for the total flux of Ca^{2+} from the ER to the cytosol.

In $J_{channel}$ there are three terms multiplying each other, p_1 , p_2 , and p_3 , which give the probability that a single channel is open. p_1 and p_2 represent the probabilities that sites 1 and 2 are activated, respectively. The probability that Ca^{2+} is not bound to site 3 (inactivation site) is represented by p_3 . We can, therefore, say that the total steady-state Ca^{2+} flux through IP_3R is given by the following:

$$I_T = Nip_1p_2p_3,$$

where i is the Ca^{2+} current through a single open IP_3R and N is the total number of IP_3R .

In this paper it is assumed that the volume of a channel, V , is constant. By this assumption, we can convert the Ca^{2+} current to an impact of the flux on the concentration in the cytosol, given by $J_{channel}$:

$$J_{channel} = \frac{Ni p_1 p_2 p_3}{2FV}, \quad (2.3)$$

where F represents Faraday's constant. $J_{channel}$ is the Ca^{2+} flux through the ER into the cytosol and has units μMs^{-1} . It is directly proportional to the number of IP_3R on the ER, N . The units of F are CM^{-1} and the units of i are μCs^{-1} . N is dimensionless and V has units of volume. p_1 , p_2 , and p_3 are true fluxes, in number of molecules per channel per second. To get to the final form of $J_{channel}$, let $k_{flux} = Ni/2FV$. Each of p_1 , p_2 , and p_3 are modelled as functions of Ca^{2+} and IP_3 , as labelled below. Note that we refer to p_1 as a function $\mu(p)$.

At steady state,

$$J_{channel} = k_{flux} \underbrace{\left(\frac{p + \mu_0 K_{IP_3}}{K_{IP_3} + p} \right)}_{p_1 = \mu(p)} \underbrace{\left(\frac{K_{act} b + c}{K_{act} + c} \right)}_{=p_2} \underbrace{\left(\frac{K_{inh}^2}{K_{inh}^2 + c^2} \right)}_{=p_3}. \quad (2.4)$$

It is an assumption of the Atri model that the expression for $J_{channel}$ valid at steady state also holds for the temporarily evolving system and this allows us to write ODEs (2.1) and (2.2). It is not our intention in this work to question this assumption.

In this thesis, we aim to derive a more accurate model for Ca^{2+} signalling at fertilisation. An area to focus and improve is the incorporation of IP_3R dynamics. The Atri model uses data (Parys et al., 1992) that inaccurately capture how the IP_3R dynamics depend on $[Ca^{2+}]$ and $[IP_3]$ during fertilisation. We now have more accurate data for this from Mak et al. (1998). It is therefore necessary to look closely at the components p_1 , p_2 , and p_3 , as they synthesize the open probability of the IP_3R .

We can begin by studying p_1 further. As labelled above, we have called this $\mu(p)$. μ_p is the probability that a single molecule of IP_3 binds to site 1. From experimental data, this probability is given to be $\mu_0 = 0.567$ when $IP_3 = 0$. The model then assumes that for non-zero $[IP_3]$ the probability increases according to a Hill function and saturates at the value 1. This Hill function is not fitted experimentally. The half-maximal activation constant for IP_3 is given by K_{IP_3} . Note that $\mu_0 + \mu_1 = 1$, where μ_1 is the proportion of IP_3R that are not activated at $IP_3 = 0 \mu M$.

Next, p_2 is the probability that Ca^{2+} binds to activation site 2. The half-activation constant (the proportion of IP_3R that are activated by the binding of Ca^{2+}) here is given

by K_{act} . The parameter b is the proportion of IP_3R that have site 2 activated in the absence of bound Ca^{2+} and represents a basal current through the IP_3R .

Finally, the last component accountable for the opening of the IP_3R is p_3 , which represents the probability that Ca^{2+} is not bound to inhibitory site 3. The half-maximal inactivation constant is K_{inh} . In p_3 , the Hill coefficient of 2 shows that this is a more cooperative process than the binding in sites 1 and 2 (in p_1 and p_2), according to the data collected. According to the experiments, when Ca^{2+} increases quickly, the IP_3R is activated quickly and is deactivated very slowly. This is why site 3 takes a while to reach its steady state, hence the constant time scale, $\tau_n = 2s$ in equation (2.2). This is despite the fact that sites 1 and 2 obtain a fast equilibrium with IP_3 and Ca^{2+} .

The parameters b , K_{act} , and K_{inh} for this model were all chosen by fitting to the experimental data in Parys et al. (1992). We will revisit the functions of p_1 , p_2 , and p_3 and the way the open probability is modelled in Chapter 4, where we derive a new model.

Dynamic behaviour of the IP_3R

Equation (2.4) represents the steady flux through the IP_3R for fixed Ca^{2+} , but we must note that the channel reacts in a certain manner to a varying cytosolic Ca^{2+} level. It is evident from the data in Finch et al. (1991) that when the cytosolic Ca^{2+} concentration rapidly increases, the IP_3R activates quickly and deactivates at a slower pace. This motivates the assumption that the binding of sites 1 and 2 quickly reach an equilibrium with IP_3 and cytosolic Ca^{2+} , while site 3 reaches its steady state proportional to the time constant τ_n . We obtain equation (2.1) when we write p_3 as n for notational convenience in equation (2.4). Note that the way in which the IP_3R has been modelled shares similarities with the modelling of the IP_3R subunits in the Hodgkin and Huxley (1952) model of electrical impulse propagation in the nerve axon, hence the Atri model is considered a gating model. In both models, constants were chosen in order to reproduce a specific steady-state curve for the open probability of the specific channels. In the Hodgkin-Huxley equations, these are the sodium and potassium channels as a function of voltage, and in the Atri model, this is the IP_3R as a function of Ca^{2+} and IP_3 . The variable n , for the proportion of non inactivated IP_3R , is directly analogous to the inactivation variable h in the Hodgkin-Huxley equations. Time constants in the equations for n and h account for the delay in activation and inactivation after changes in $[Ca^{2+}]$ and voltage, respectively.

The modelling of the IP_3R in the Atri model is very similar to other models, particularly the model by De Young and Keizer (1992). Both of the models show similar results. Both feature a separation of time scales of Ca^{2+} -dependent activation and inactivation of the

IP_3R , where activation takes places faster than inactivation (Finch et al., 1991).

We have discussed which parts of this model represent Ca^{2+} flux through to the cytosol (in $J_{channel}$), and that J_{pump} represents the SERCA pumps back into the ER. The latter is given by the Michaelis-Menten function. It is acknowledged in the paper by Atri et al. (1993) that incorporation of more detail in this term would be beneficial to the model when more experimental evidence is available. The model is not driven by ER Ca^{2+} depletion as the ER concentration is assumed to remain constant (and high). This emphasizes the importance of the role that the IP_3R dynamics and the IP_3 concentration play in facilitating the cytosolic Ca^{2+} oscillations. That being said, as we see later, the IP_3R dynamics that are used in the Atri model are based on outdated experimental data. A replacement in the dynamics is therefore due. We will do this in Chapter 3 with updated data from Mak et al. (1998).

2.1.2 Non-dimensionalisation of the Atri et al. model

We non-dimensionalise equations (2.1) and (2.2) by substituting in $c = K_{act}\bar{c}$, $t = \tau_n\bar{t}$, and $n = \bar{n}$, as in Kaouri et al. (2019). The process of non-dimensionalisation is discussed in Murray (1989). Dropping the bars for notational purposes, we get the following:

$$\frac{dc}{dt} = \mu(p)K_1n \left(\frac{b+c}{1+c} \right) - \frac{Vc}{K+c}, \quad (2.5)$$

$$\frac{dn}{dt} = \frac{K_2^2}{K_2^2 + c^2} - n, \quad (2.6)$$

where $K_1 = K_f\tau_n/K_{act}$, $V = V_e\tau_n/K_{act}$, $K = K_e/K_{act}$ and $K_2 = K_{inh}/K_{act}$. Note that the $J_{leakage}$ term has been ignored now since $\tau_n\delta/K_{act}$ is of a much lower order of magnitude in comparison to the other terms. Parameter values are given in Table B.1.

As discussed above, oscillations emerge when IP_3 is at an appropriate level - not too low or too high. This means that $\mu(p) = p_1$ is a bifurcation parameter. In Figure 2.5, we see a solution of the equations (2.5) and (2.6) with $\mu(p) = 0.3$, which is within oscillatory range. Figure 2.6 shows what happens when $\mu(p)$ has a value of 0.2886 and 0.6 respectively. When $\mu(p) = 0.2886$, the variables c and n almost immediately reach their steady state values. As the parameter is increased to $\mu(p) = 0.6$ the simulation begins with oscillations that slowly decay over time until c and n reach their steady states.

From the non-dimensionalisation, we have reduced the system down to seven parameters. We will go on to find the equilibria of equations (2.5) and (2.6) as well linearise the equations, and find the stability of the equilibria.

2.1.3 Linear stability analysis

To begin our linear stability analysis, we look for the steady states (equilibria) of the equations, which are nodes, given at the points where $dc/dt = 0$ and $dh/dt = 0$. This leads to a fourth-order polynomial. On solving for our bifurcation parameter, $\mu(p)$, we get

$$\mu(p) = \frac{Vc(c^3 + c^2 + c + 1)}{K_1c^2 + K_1(b + K)c + K_1bK},$$

as in Kaouri et al. (2019). We can find a range of values for c and $\mu(p)$ that result in oscillations by evaluating the expression above. We can find this range by solving $d\mu(p)/dc = 0$. We get the following two fold bifurcation points:

$$c = 0.22281 \Rightarrow \mu(p) = 0.28925,$$

$$c = 0.33374 \Rightarrow \mu(p) = 0.28814.$$

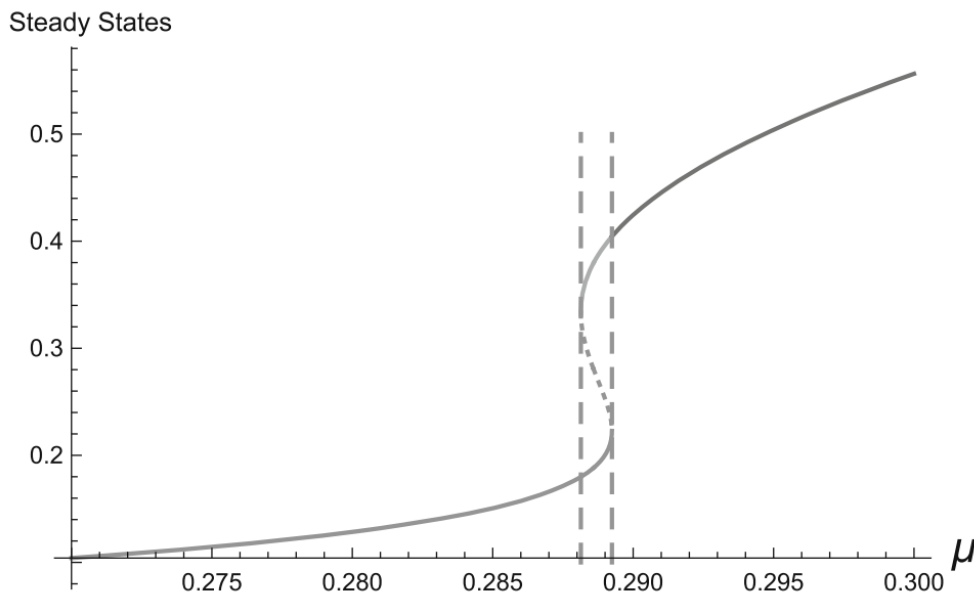


Figure 2.3: A graph that shows the steady states of the non-dimensionalised form of the model, (2.5), (2.6). The steady states are shown as a function of the bifurcation parameter $\mu(p)$. We can see that as $\mu(p)$ increases, there is one steady state. There is a double (degenerate) steady state at $\mu(p) = 0.28814$. There are then three steady states, followed by another double (degenerate) steady state at $\mu(p) = 0.28925$. Finally, there is just one steady state for all $\mu(p) > 0.28925$. Source: Kaouri et al. (2019).

To identify the bifurcations of the Atri model, we start by linearising the system near its

steady states. Then, for each steady state we compute the Jacobian matrix. Let

$$\begin{aligned}\frac{dc}{dt} &= F(c, n), \\ \frac{dn}{dt} &= G(c, n).\end{aligned}$$

The Jacobian matrix is given by

$$J = \begin{pmatrix} J_{1,1} & J_{1,2} \\ J_{2,1} & J_{2,2} \end{pmatrix},$$

where

$$J_{1,1} = \frac{\partial F}{\partial c}, J_{1,2} = \frac{\partial F}{\partial n}, J_{2,1} = \frac{\partial G}{\partial c}, J_{2,2} = \frac{\partial G}{\partial n},$$

are evaluated at steady-state. The characteristic polynomial of the system is given by

$$\lambda^2 - T(J)\lambda + D(J) = 0,$$

where the trace, determinant and discriminant are defined respectively as follows:

$$\begin{aligned}T(J) &= J_{1,1} + J_{2,2}, \\ D(J) &= J_{1,1}J_{2,2} - J_{1,2}J_{2,1}, \\ Disc(J) &= (T(J))^2 - 4D(J).\end{aligned}$$

The trace, determinant and discriminant are important in the understanding of the qualitative behaviour of the system. Our trace and determinant are given by

$$\begin{aligned}T(J) &= \frac{\mu(p)K_1n}{c+1} - \frac{\mu(p)K_1n(b+c)}{(c+1)^2} - \frac{V}{K+c} + \frac{Vc}{(K+c)^2} - 1, \\ D(J) &= -\frac{\mu(p)K_1n}{c+1} + \frac{\mu(p)K_1n(b+c)}{(c+1)^2} + \frac{V}{K+c} - \frac{Vc}{(K+c)^2} + \frac{2\mu(p)K_1(b+c)c}{(c+1)(c^2+1)^2},\end{aligned}$$

where λ represents the eigenvalues. We can therefore solve the characteristic polynomial to find these eigenvalues. Eigenvalues, λ , are given by the following:

$$\lambda = \frac{T(J) \pm \sqrt{T(J)^2 - 4D(J)}}{2}.$$

In Kaouri et al. (2019) is a complete list of bifurcations of the system. These are found by

determining the nature of the roots of the polynomial over a range of values for $\mu(p)$. The list of bifurcations from Kaouri et al. (2019) is as follows.

- $0 < \mu < 0.27828$: one stable node.
- $\mu = 0.27828$: the stable node becomes a stable spiral (bifurcation $Disc = 0$)
- $\mu = 0.28814$: Stable spiral present. Also, a saddle and an unstable node emerge (bifurcation $Det = 0$, fold point)
- $\mu = 0.28900$: the stable spiral becomes an unstable spiral. The other two steady states are still a saddle and an unstable node. ($Tr = 0$, Hopf bifurcation)
- $\mu = 0.28924$ the unstable spiral becomes an unstable node, and we have two unstable nodes and a saddle ($Disc = 0$)
- $\mu = 0.28925$: one unstable node ($Det = 0$, fold point)
- $\mu = 0.28950$: the unstable node becomes an unstable spiral ($Disc = 0$)
- $\mu = 0.49500$: the unstable spiral becomes a stable spiral. ($Tr = 0$, Hopf bifurcation)

2.1.4 Simulations

We now look at the simulations of the Atri model in different bifurcation regimes. We use the `ode45` function in MATLAB (MathWorks, 2020) to solve the reduced equations, (2.5) and (2.6), with various values of $\mu(p)$. Figure 2.5 shows Ca^{2+} oscillations as solutions to the Atri Model, (2.5), (2.6), with $\mu(p) = 0.3$ (within oscillatory range). Figure 2.6 also shows Ca^{2+} oscillations as solutions to the Atri model (2.5), (2.6). In **A**, there is a simulation with $\mu(p) = 0.2886$ (too low to be in the oscillatory range). Here, both c and n quickly go to their respective steady state values. In **B**, there is a simulation with $\mu(p) = 0.6$ (too high to be in the oscillatory range). Oscillations start with a large amplitude and dampen over time.

Bifurcation diagram

Non-dimensionalisation has reduced the number of parameters in the system. Equations (2.5) and (2.6) can be used to generate a bifurcation diagram for $\mu(p)$ against c . Figure 2.4 (Kaouri et al., 2019) shows the changes in the qualitative behaviour of the system as $\mu(p)$ increases, generated with the XPPAUT continuation software (Ermentrout, 2002). They show the amplitude and frequency of limit cycles, respectively, as the bifurcation parameter

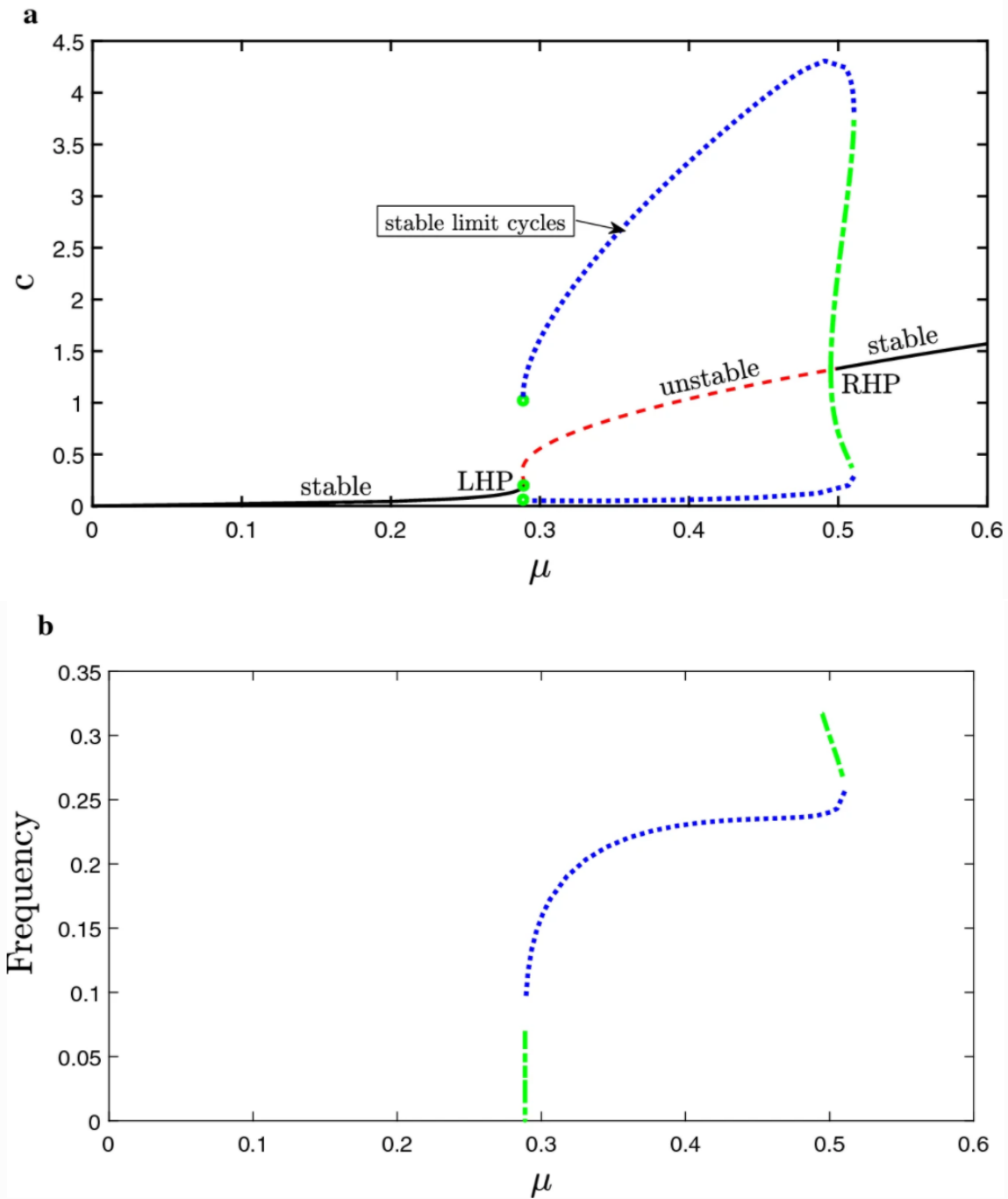


Figure 2.4: Bifurcation diagrams for the non-dimensionalised Atri model (2.5), (2.6) as $\mu(p)$ increases. **(a)** Amplitude of calcium oscillations (limit cycles). The blue dots show the stable limit cycles while the green dashes show the unstable limit cycles. Note the presence of the left Hopf point (LHP) and the right Hopf point (RHP). **(b)** Frequency of the limit cycles. Source: Kaouri et al. (2019).

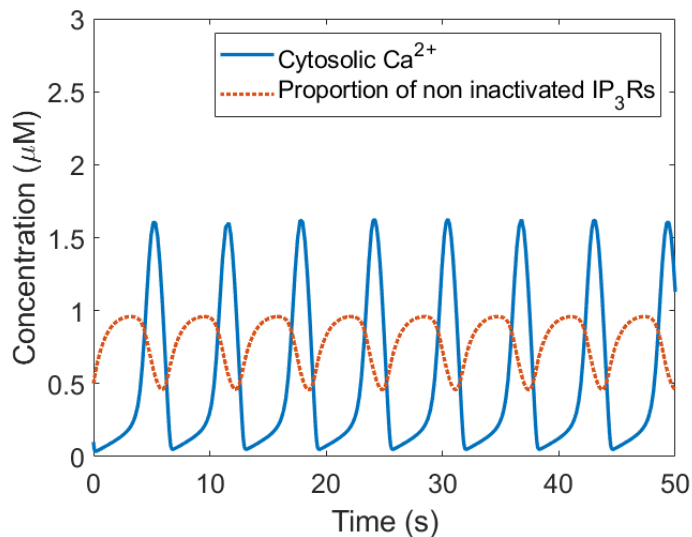


Figure 2.5: Ca^{2+} oscillations as solutions to the Atri Model, (2.5), (2.6), with $\mu(p) = 0.3$ (within oscillatory range). Parameter values are shown in Table B.1. Initial values of $0.1\mu M$ and 0.5 were taken for c and n respectively. Oscillations over time of 50 seconds. *Software:* MATLAB.

$\mu(p)$ increases. In Figure 2.4a we see for what values of $\mu(p)$ we have stable and unstable limit cycles, and the two Hopf points. The figures show that as $\mu(p)$ is increased, oscillations increase more in amplitude than they do in frequency. The range of $\mu(p)$ that gives oscillations is $0.289 < \mu < 0.495$.

We have now presented in detail the Atri et al. (1993) model and its derivation, linear stability analysis and bifurcation analysis. This model captures key Ca^{2+} signalling features but uses outdated data to model the IP_3R dynamics. More recent experiments and data have shown that the probabilities p_1 , p_2 , and p_3 are more accurately modelled by Mak et al. (1998). We will incorporate the latter IP_3R dynamics in a model later in the thesis.

Next, we present in detail the Li-Rinzel model and we compare it to the Atri model.

2.2 The Li-Rinzel model

The Li and Rinzel (1994) model shares many key features with the Atri model. It is also a two-variable gating model obtained by reducing the 9-variable De Young and Keizer (1992) model for Ca^{2+} oscillations mediated by IP_3R . It is based on the assumption of there being three binding sites for the IP_3R - those are the sites responsible for IP_3 regulation, Ca^{2+} activation and Ca^{2+} inactivation. The Li-Rinzel model has a bifurcation diagram almost identical to that of the De Young-Keizer model, and is analogous in its form to the

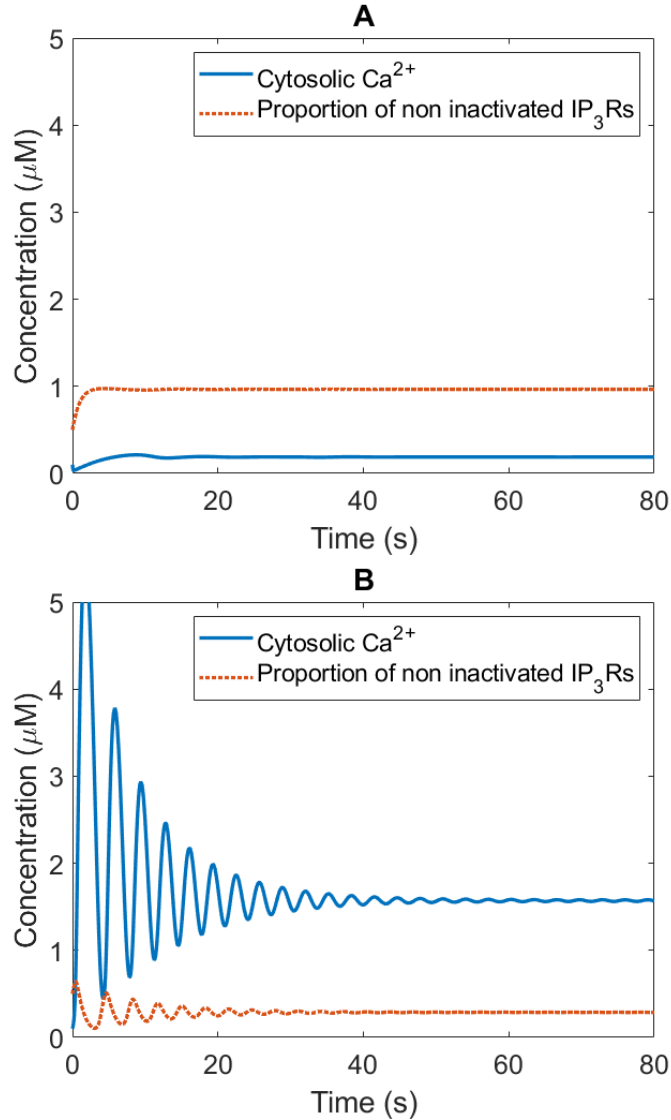


Figure 2.6: Ca^{2+} oscillations as solutions to the Atri model (2.5), (2.6). Parameter values are shown in Table B.1. Initial values of 0.1 and 0.5 were taken for c and n , respectively. **(A)** Simulation with $\mu(p) = 0.2886$ (too low to be within oscillatory range). Here, both c and n quickly go to their respective steady state values. **(B)** Simulation with $\mu(p) = 0.6$ (too high to be within oscillatory range). Oscillations start with a large amplitude and dampen over time. *Software:* MATLAB.

Hodgkin-Huxley equations (Hodgkin & Huxley, 1952), a gating model for plasma membrane electrical excitability. The bifurcation diagram for the Li-Rinzel model also compares closely to the bifurcation diagram of the Atri model. The Li-Rinzel model retains the most important dynamic features of the De Young-Keizer model and is able to reproduce experimental observations (Bezprozvanny et al., 1991; Watras et al., 1991). The two-variable Li-Rinzel model is as follows:

$$\frac{dc}{dt} = \left(v_1 \left(\frac{p}{p + K_{IP_3}} \right)^3 \left(\frac{c}{c + K_{act}} \right)^3 n^3 + \epsilon \right) (c_0 - (1 + c_1)c) - \frac{V_e c^2}{K_e^2 + c^2}, \quad (2.7)$$

$$\frac{dn}{dt} = A(c + K_{inh}) \left(\frac{K_{inh}}{c + K_{inh}} - n \right), \quad (2.8)$$

where c is the cytosolic Ca^{2+} concentration and n is the proportion of non inactivated IP_3R . The maximal rate of Ca^{2+} release is given by v_1 . The half-activation constant for IP_3 binding to activation site 1 is given by K_{IP_3} . In all cells, there are SERCA pumps on the ER which allow Ca^{2+} to be pumped back into the ER. Here, this flux is assumed to be governed by a Hill function which saturates for a sufficiently high value of Ca^{2+} . The maximal SERCA pump rate is given by V_e , and the half-activation constant for the SERCA pumps is K_e . A parameter to characterize the slow time scale of Ca^{2+} inactivation is given by A . The half-maximal inactivation constant for Ca^{2+} binding to the inhibitory site 3 is K_{inh} . Finally, ϵ represents the Ca^{2+} leak out of the ER.

Model assumptions

The Ca^{2+} permeability of the IP_3R is its maximum permeability times the channels open probability. The Li-Rinzel model (2.7), (2.8), is built on assuming the existence of three binding sites on each subunit of the channel. Similarly to the model assumptions for the Atri model, we have the sites for:

- A single molecule of IP_3 binds to the IP_3 activation site (site 1).
- A single molecule of Ca^{2+} binds to the Ca^{2+} activation site (site 2).
- Two molecules of Ca^{2+} bind to the Ca^{2+} inhibitory site (site 3).

These three binding processes are not necessarily assumed to be independent. Firstly, IP_3 binding depends on whether the Ca^{2+} inhibitory site is occupied, while Ca^{2+} binding to its inhibitory site also depends on whether the receptor already has an IP_3 molecule bound. However, these two processes are independent of Ca^{2+} binding to its activation site. This

independence gives rise to some symmetries in the binding rate constants. For generality, we assume that three binding processes depend on each other, with no symmetry assumed.

The channel's open probability at equilibrium is expressed as

$$\left(\frac{p}{p + K_{IP_3}}\right)^3 \left(\frac{c}{c + K_{act}}\right)^3 \left(\frac{K_{inh}}{K_{inh} + c}\right)^3. \quad (2.9)$$

This fits to experimental data of the bell-shaped Ca^{2+} dependence and the sigmoidal IP_3 dependence of the IP_3R open probability at equilibrium (Bezprozvanny et al., 1991; De Young & Keizer, 1992).

Dynamic behaviour of the IP_3R

The De Young-Keizer model was reduced to the two-variable Li-Rinzel model. As a consequence of time scale separation, it turns out that the effect of specific gating processes are independent of the kinetics of a slower gating process but dependent on all faster gating processes. This means that the channel opening by IP_3 seems to be independent of Ca^{2+} binding to either the activation or inhibitory site since it is faster than those processes.

The Li-Rinzel model can be compared to the Atri model. They hold many similarities and are still widely used by modellers today. The equation for n is almost identical in the Atri model and the Li-Rinzel model. The equations for c hold very similar structures in both of these models. Equation (2.7) represents cytosolic Ca^{2+} concentration (μM) and can be compared to equation (2.1) from the Atri model. Equation (2.8) represents the proportion of non inactivated IP_3R and can be compared to equation (2.2). Like equation (2.1), equation (2.7) has a positive term for Ca^{2+} flux into the cytosol, with Hill functions of order 1. We can compare p_1 , p_2 , p_3 from the Atri model to the equivalent terms here. The probability of IP_3 binding to its activation site is represented again by a Hill equation, $p/(p + K_{IP_3})$. This implies that no IP_3R are activated when there is no IP_3 present, or in other words the open probability of the IP_3R is 0. The term here corresponds to p_1 in the Atri model. The probability of Ca^{2+} binding to its activation site is represented by $c/(c + K_{act})$. This term corresponds to p_2 in the Atri model. Finally, the probability that Ca^{2+} is not bound to its inhibitory site is represented by $K_{inh}/(K_{inh} + c)$. This is a Hill function of order 1, in comparison to p_3 in the Atri model being a Hill function of order 2. The three terms for probabilities p_1 , p_2 and p_3 are raised to the third power in the Li-Rinzel model. As discussed, these probabilities are all modelled by Hill functions. The simplified equation is analogous, mathematically, to the Hodgkin and Huxley (1952) model of plasma membrane electrical excitability. In the Li-Rinzel model, c (analogous to the membrane voltage) is the

major regulator of the IP_3R and the concentration gradient $c - c_0$ (analogous to the voltage deviation from the Nernst reversal potential) is the driving force for oscillations. In both models, channel activation and inactivation appear as separate factors with first-order gating kinetics. There is also a negative term in equation (2.7) representing Ca^{2+} being pumped back into the ER. This term for the SERCA pumps is a Hill function of order 2. This is similar to what we have in the Atri model in equation (2.1).

2.2.1 Simulations

In Figure 2.7 we present the bifurcation diagram from the Li-Rinzel model (2.7)-(2.8). This bifurcation diagram shows good agreement between the Li-Rinzel model and the De Young-Keizer model. The reduction from nine to two variables is therefore appropriate. The reduction in the number of variables is useful because the model can then be very quickly studied and intuition about the system dynamics can be extracted easily.

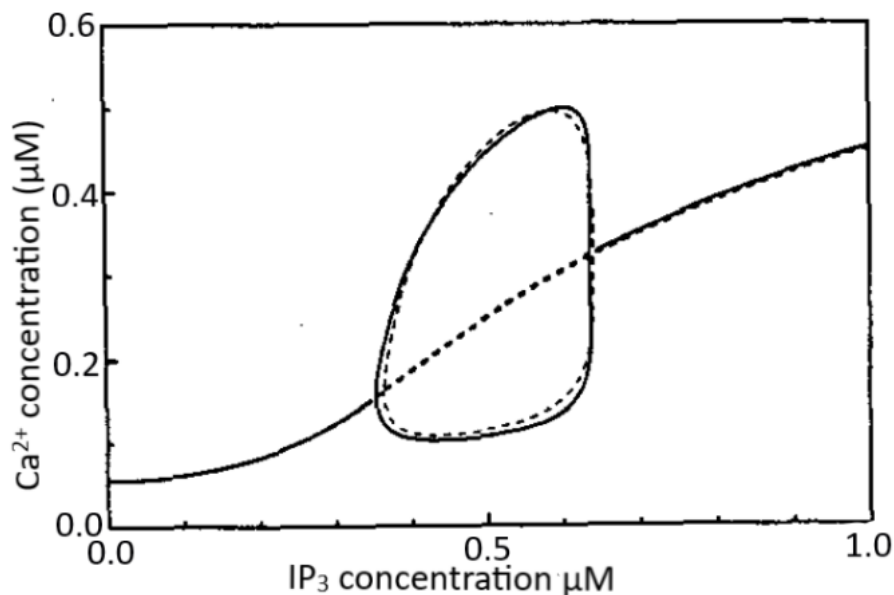


Figure 2.7: Bifurcation diagram with bifurcation parameter p for the Li-Rinzel model, (2.7)-(2.8). Source: Li and Rinzel (1994).

Presented in Figure 2.8 are the Ca^{2+} oscillations arising as solutions to the Li-Rinzel model (2.7)-(2.8). These oscillations occur with IP_3 concentration at $0.6\mu M$. Parameter values are given in Table B.2. There is a range of concentration for IP_3 for which we obtain oscillations. Shown in Figure 2.9 are graphs where the IP_3 concentration is too low ($0.2\mu M$) to obtain oscillations, and too high to obtain oscillations ($1\mu M$), respectively. When $[IP_3] < 0.47325\mu M$, the solution reaches steady state. Where the IP_3 concentration

is too high, the solution decays to the steady state in an oscillatory manner.

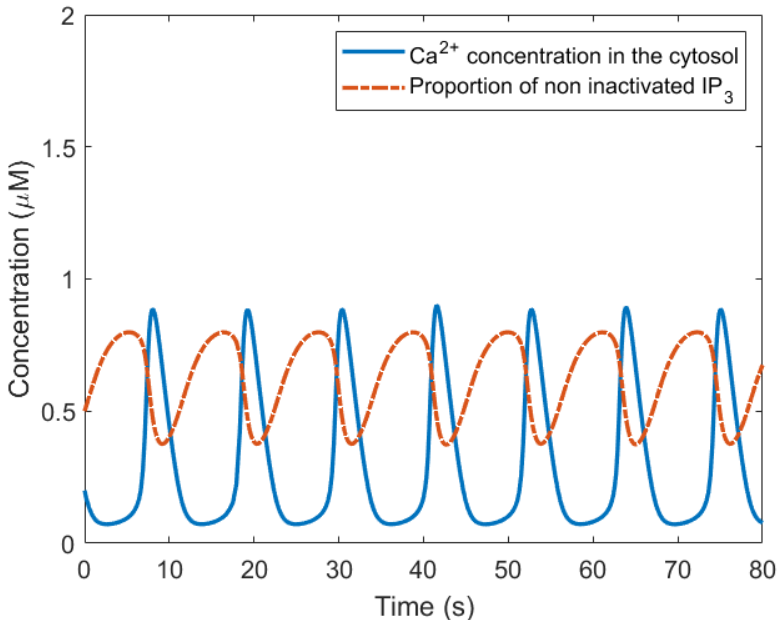


Figure 2.8: Cytosolic Ca^{2+} oscillations arising as solutions to the Li-Rinzel model, (2.7), (2.8). Parameter values used are in Table 2.8. To be within oscillatory range, the IP_3 level, p , was chosen to be $0.6\mu M$. Initial conditions applied were $0.2\mu M$ and $0.5\mu M$ for cytosolic Ca^{2+} and for the proportion of non inactivated IP_3R , respectively. *Software*: MATLAB.

We have now studied two famous gating models - the Atri model and the Li-Rinzel model. As discussed in the Introduction, many modellers have built on these two-variable models to derive more complex Ca^{2+} signalling models. Having studied the IP_3R dynamics in these models, in the next chapter we go on to review more up-to-date data of these dynamics from experiments carried out by Mak et al. (1998), and how these data were fitted to an equation for the open probability of the IP_3R . Our aim is to eventually find a way to incorporate these more detailed and exact IP_3R dynamics into a model for Ca^{2+} signalling in fertilising eggs.

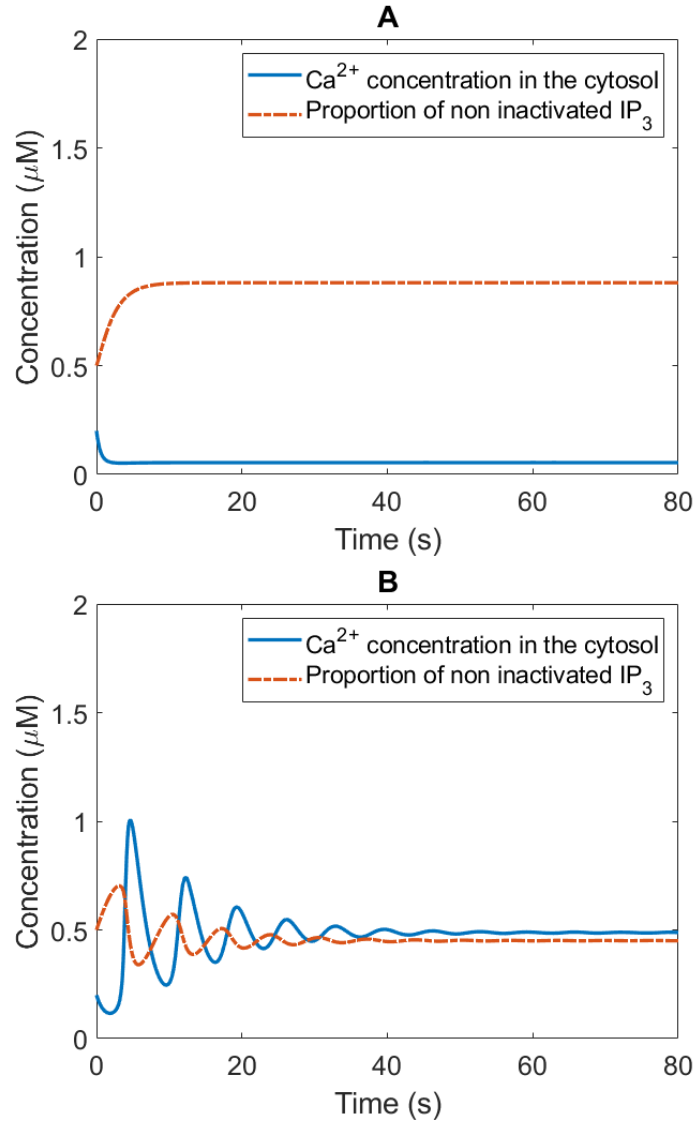


Figure 2.9: Decaying Ca^{2+} oscillations arising as solutions to the two-variable minimal model by Li and Rinzel (1994), (2.7)-(2.8). Parameter values used are shown in Table 2.8. Initial conditions applied were $0.2\mu\text{M}$ and 0.5 for cytosolic Ca^{2+} and the proportion of non inactivated IP_3R respectively. **(A)** $IP_3 = 0.2\mu\text{M}$, too low to be within oscillatory range. **(B)** $IP_3 = 1\mu\text{M}$, too high to be within oscillatory range. *Software:* MATLAB.

Chapter 3

Experimental data on IP_3R dynamics

(Mak et al.)

There is an abundance of models for Ca^{2+} signalling, as discussed. In this work we aim to develop an accurate model for Ca^{2+} signalling occurring in the mammalian egg at fertilisation. We are therefore concerned with modelling the IP_3R on the ER accurately. For an oocyte, the only Ca^{2+} -releasing channels are the IP_3R as the RyR are not expressed in the ER membrane (Dupont et al., 2016). The open probability of the IP_3R is controlled by several ligands, the most significant of which are IP_3 and Ca^{2+} . Henceforth, we will refer to the open probability of the IP_3R as P_O . P_O is given as follows:

$$P_O = p_1 p_2 p_3, \quad (3.1)$$

where p_1 and p_2 , respectively, represent the probabilities that sites 1 and 2 (for IP_3 and Ca^{2+}) are activated, and p_3 is the probability that Ca^{2+} is not bound to site 3, as in Atri et al. (1993). This relatively simple equation presented in Atri et al. (1993) is shown in equation (2.4). Constants were chosen in order to reproduce the steady-state curve for P_O , based on data by Parys et al. (1992). The time constant in equation (1.2) for n accounts for the delay between activation and inactivation. A typical timescale for activation of site 3 used in gating models like those of Atri et al. (1993) and Li and Rinzel (1994) is 1-2 seconds. These can be seen in equations (2.1) and (2.7). This estimate is based on older data from Finch et al. (1991), Combettes et al. (1994), Dufour et al. (1997), and Marchant and Taylor (1998). However, we now have at our disposal experimental data from Mak et al. (1998) that accurately capture how the IP_3R dynamics depend on $[Ca^{2+}]$ and $[IP_3]$ during fertilisation. The newer data confirm the accuracy of this estimate of 1-2 seconds for the measurement of the time dependence but give more details on how the open probability

depends on both Ca^{2+} and IP_3 . To fully understand how the open probability of the IP_3R behaves, it is important to study the steady-state open probability as a function of IP_3 and Ca^{2+} . For fixed IP_3 concentration, the shape of P_O is a bell-shaped function of cytosolic Ca^{2+} concentration. P_O increases at low Ca^{2+} , reaches a peak, and then decreases at high Ca^{2+} . This can be seen in Figure 3.3. The precise shape of this curve is dependent upon the IP_3R type and the cell type in some cases. Old data from Kaftan et al. (1997) and Hagar et al. (1998) suggest a maximum P_O of less than 0.1. This statistic contradicts more recent studies that estimate to be P_O from 0.3 to 0.8 (Mak et al., 1998). The data in Mak et al. (1998) are single channel data from native membranes as opposed to some artificial system where we cannot say if the exact conditions mimic the cell. This means that we have data which show a very close replicate of how a real egg behaves.

The experimental data provided by Mak et al. (1998) provide detailed information about the IP_3R gating mechanisms as Ca^{2+} and IP_3 bind to the IP_3R , activating Ca^{2+} release from the ER. These dynamics drive complicated cytoplasmic Ca^{2+} signals, including temporal oscillations and propagating waves. It is evident that both positive and negative feedback of cytosolic Ca^{2+} controls the IP_3 -mediated Ca^{2+} release. The experiment was carried out under rigorously defined conditions using patch clamp of the IP_3R in the ER membrane of isolated *Xenopus Laevis* oocyte nuclei. The results provided detailed information about how the IP_3R works and the dependence on cytosolic Ca^{2+} and IP_3 . In Figure 3.1 typical traces of single-channel current for different levels of Ca^{2+} are shown. When cytosolic Ca^{2+} concentration is at steady-state ($0.01 - 0.1\mu M$), P_O was low, and some short open intervals of $\tau_O < 3ms$ are observed. These open intervals were interlaced with much longer closed intervals of approximately $\tau_C = 100ms$, as seen in Figure 3.2. As the Ca^{2+} level rose from $0.1\mu M$ to $1\mu M$, P_O drastically increases up to 0.8, with τ_O increasing to around $10ms$ and τ_C decreasing to around $2ms$. Figure 3.2 from Mak et al. (1998) shows the mean time of closed-channel (τ_C) and open-channel (τ_O), as a function of the cytosolic Ca^{2+} level.

Ca²⁺ dependence of the gating of the IP₃R

In the experiment, Mak et al. (1998) expected to observe a narrow bell-shaped curve for P_O when the cytosolic Ca^{2+} is approximately $300nM - 1\mu M$ (Bezprozvanny & Ehrlich, 1995; Bezprozvanny et al., 1991; Stehno-Bittel et al., 1995; Masamitsu, 1990). However, the results clearly showed that the open probability of the gate remained elevated at approximately 0.8 with saturating levels of IP_3 ($10\mu M$) applied to the cytosol to fully stimulate at various levels of Ca^{2+} concentrations. This can be seen in Figure 3.3. It was only upon increasing the Ca^{2+} levels above $20\mu M$ that the open probability, P_O , drastically started to decrease. This

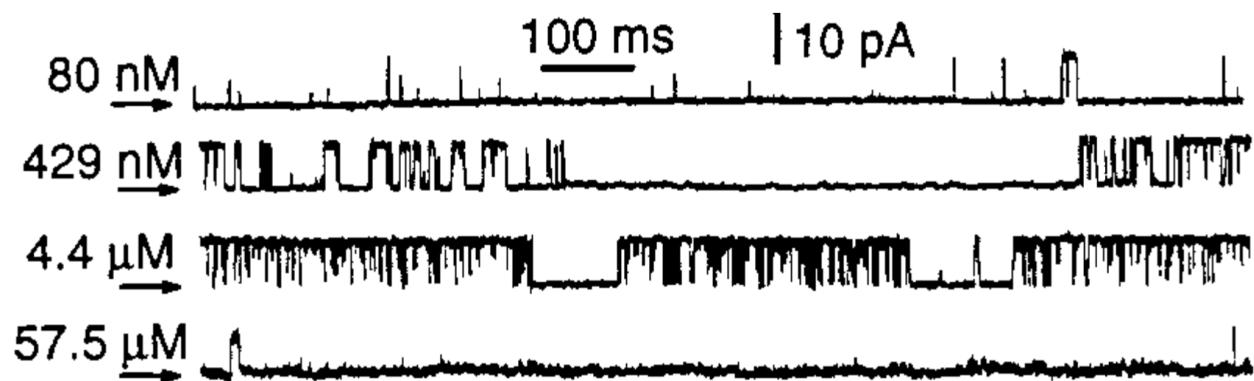


Figure 3.1: Closed-channel current levels in each trace recorded at various levels of Ca^{2+} : 80 nM , 429 nM , $4.4\text{ }\mu\text{M}$ and $57.5\text{ }\mu\text{M}$, in the presence of $10\text{ }\mu\text{M}$ of IP_3 . Source: Mak et al. (1998).

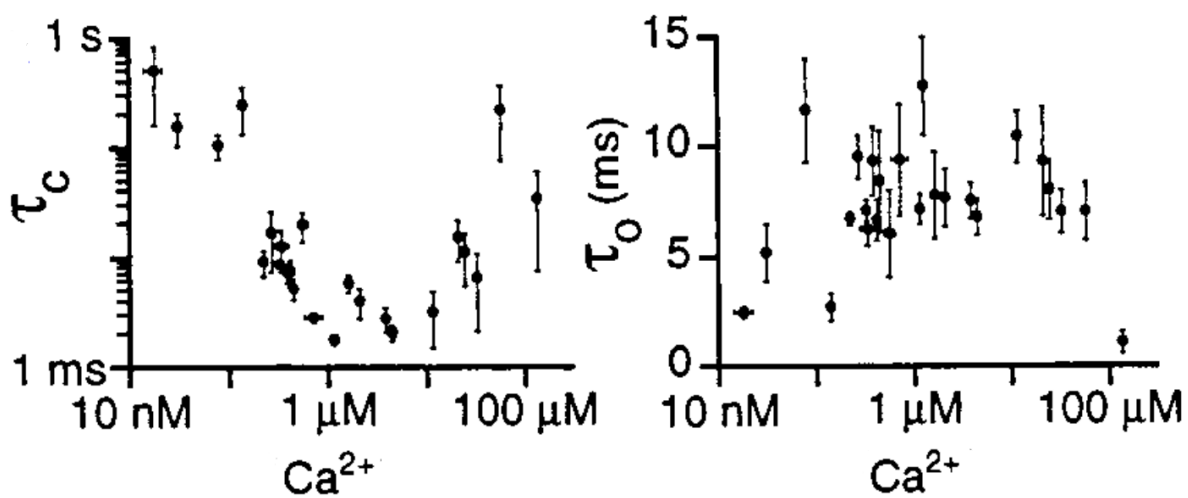


Figure 3.2: Mean time of closed-channel (τ_C) and open-channel (τ_O), in the presence of $10\text{ }\mu\text{M}$ of IP_3 , as a function of the cytosolic Ca^{2+} level. Source: Mak et al. (1998).

is due to the two distinct types of functional Ca^{2+} binding sites, activating and inhibitory ones.

Mak et al. (1998) derived an equation to accurately model their experimental data for the open probability of the IP_3R . This equation for P_O is considered a breakthrough in the modelling of the IP_3R dynamics. It is formatted slightly differently to the open probability in other models, as follows.

$$P_O = P_{max} \left(\frac{1}{1 + \left(\frac{K_{act}}{c}\right)^{H_{act}}} \right) \left(\frac{1}{1 + \left(\frac{c}{K_{inh}}\right)^{H_{inh}}} \right), \quad (3.2)$$

where

$$K_{inh} = K_{\infty} \left(\frac{1}{1 + \left(\frac{K_{IP_3}}{p}\right)^{H_{IP_3}}} \right). \quad (3.3)$$

This equation is phenomenological, based on experimental data obtained for the single channel IP_3R . The first parenthesis in equation (3.2) models Ca^{2+} binding to the activation site. The second parenthesis models Ca^{2+} binding to the inhibitory site. K_{inh} depends on IP_3 binding to its activation site. Recall that previous models, (2.1)-(2.2) and (2.7)-(2.8), had these terms for the three sites as three separate parentheses.

Equation (3.2) is a ‘biphasic Hill equation’, as referred to in Mak et al. (1998). The shape of this as a graph has P_O increasing, reaching a peak, and then decreasing. This can be seen fitting to the data in Figure 3.3. Parameter values are given in Table B.4. The maximum probability of the IP_3R channel being open, P_{max} , is given as 0.81. This was chosen based on the experimental data where 0.81 was shown to be the maximum value, as seen in Figure 3.3. This equation models the two distinct types of binding sites for Ca^{2+} - the activation and inhibitory sites. The activation and inhibition of the IP_3R by Ca^{2+} are very cooperative processes and this is represented by the Hill coefficients chosen, $H_{act} = 1.9 \pm 0.3$ and $H_{inh} = 3.9 \pm 0.7$. These also suggest that it is necessary for Ca^{2+} to bind to two of four monomers to open the IP_3R channel in the presence of IP_3 , and for Ca^{2+} to bind to all four monomers to prevent opening of the channel (Mak et al., 1998).

Lowering the IP_3 concentration did not affect Ca^{2+} activation parameters or the Hill coefficient for the term representing Ca^{2+} binding to the inhibitory site, H_{inh} . This did however decrease the half-maximal inhibitory Ca^{2+} , K_{inh} . Also observed was a functional half-maximal activating IP_3 concentration, K_{IP_3} , at $50nM$ and a corresponding Hill coefficient, H_{IP_3} , at 4 for IP_3 . From these results it is apparent that Ca^{2+} is a receptor agonist, as it stimulates the opening of the channel with sufficient IP_3 present (Berridge et al., 2000).

The evidence suggests that the sole function of IP_3 is to relieve Ca^{2+} inhibition. The results of the experiments are shown in Figure 3.3.

Dependence of P_O on IP_3

The results of the experimental data in Mak et al. (1998) suggest that the open probability of the IP_3R is relatively insensitive to Ca^{2+} until it reaches a quite high concentration. This insensitivity is in contrast to previous models which have assumed a higher affinity of Ca^{2+} binding to the inhibitory site. This was, therefore, further investigated by Mak et al. (1998) but there was evidently no change in Ca^{2+} dependence with ranging concentration of IP_3 . This is proof that the IP_3R has a low-affinity IP_3 binding site with binding coefficients greater than $0.1\mu M$. There are many biochemical data that match this (Mauger et al., 1994; Taylor & Traynor, 1995; Taylor & Richardson, 1991; Joseph, 1996). As IP_3 was lowered to less than $0.1\mu M$, the channel became more sensitive to Ca^{2+} inhibition, as seen in Figure 3.3. For example, at $0.033\mu M$ of IP_3 , K_{inh} was brought all the way down to $9.5\mu M$, though constants for Ca^{2+} binding to the activation site were unaffected. In comparison, at an IP_3 concentration of $10\mu M$, K_{inh} lies at $54\mu M$. When much lower levels of IP_3 were applied, there was a significant reduction in both the maximum open probability, P_{max} and the range of Ca^{2+} for which the channel was active. With K_{inh} as the only IP_3 -sensitive parameter, equation (3.3), accurately fits with experimental data carried out for a wide range of IP_3 concentrations. Mak et al. (1998) concluded that the effect of IP_3 binding is not to enable Ca^{2+} binding to the activation site, but to ameliorate Ca^{2+} binding to the inhibitory site. Previously, it was thought that the effect of the binding was to enable activation of the IP_3R by Ca^{2+} (Mauger et al., 1994; Taylor & Richardson, 1991; Taylor & Traynor, 1995; Joseph, 1996), but the data from Mak et al. (1998) suggest otherwise. The dependence of K_{inh} on the IP_3 concentration is described with the Hill equation (3.1). Figure 3.4 shows P_O against Ca^{2+} concentration with various chosen levels of IP_3 (and the respective values for K_{inh} according to equation (3.2)). Figure 3.3 shows how the derived equation for P_O fits the data well.

As discussed, the only IP_3 -concentration-sensitive parameter here is K_{inh} . This parameter was shown to decrease with decreasing IP_3 . The equation for K_{inh} indicates that the IP_3R has a single class of functional IP_3 binding sites. Figure 3.5 demonstrates how K_{inh} varies with increasing IP_3 . Table 3.1 presents a range of numerical values computed for K_{inh} at fixed IP_3 . Also shown in Figure 3.5 are examples of the bell shape attained with normalised P_O vs. Ca^{2+} . These were computed from equation (3.2) with three different values for IP_3 chosen.

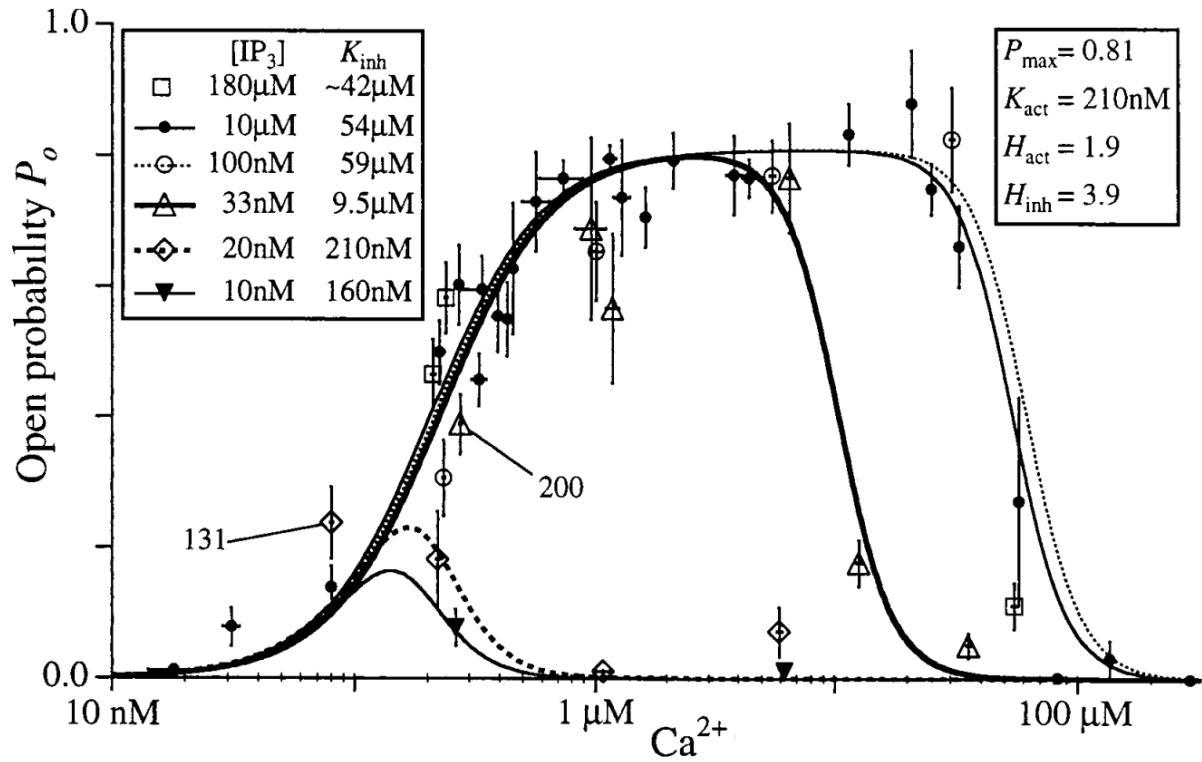


Figure 3.3: P_o as Ca^{2+} varies, at different levels of IP_3 . We can see how the equation (3.2) fits the data well. Source: Mak et al. (1998).

IP_3 (μM)	K_{inh} (μM)
180	~ 42
10	54
0.1	59
0.033	9.5
0.02	0.21
0.01	0.16

Table 3.1: K_{inh} (μM) for given IP_3 concentrations (μM) from equation (3.3). See also Figure 3.5.

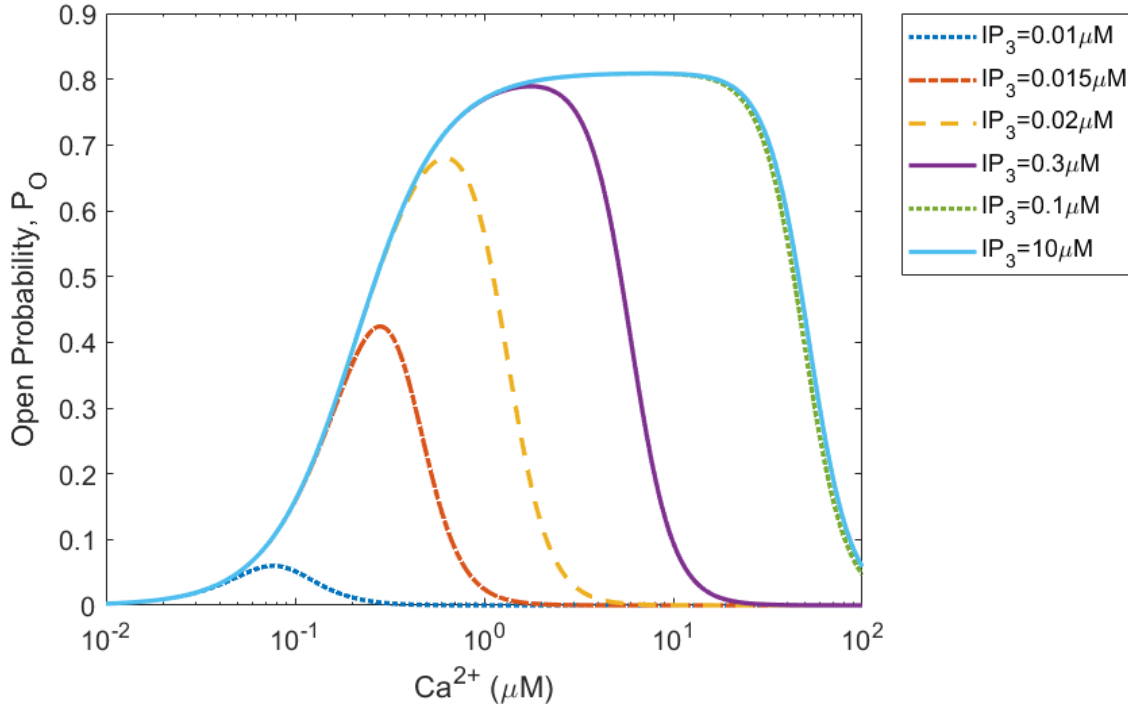


Figure 3.4: The open probability (3.2) of IP_3 , P_O , as a function of the cytosolic Ca^{2+} for a series of IP_3 values. Parameters used are shown in Table B.4. *Software*: MATLAB.

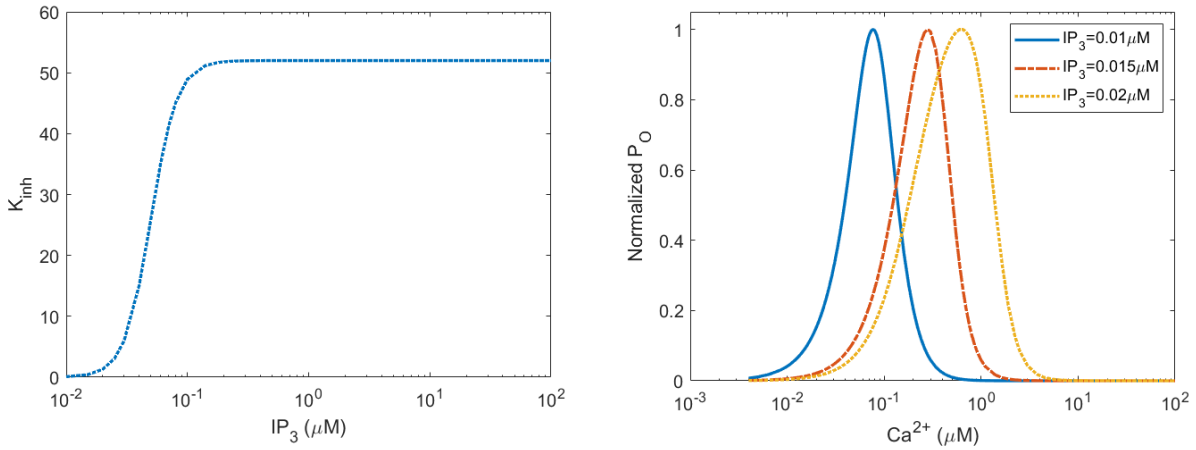


Figure 3.5: (Left) K_{inh} for increasing IP_3 concentration (μM). (Right) Bell-shaped normalised P_O vs. cytosolic Ca^{2+} concentration, from equation (3.2). The blue solid line is for $IP_3 = 0.01\mu M$, with a maximum point of 0.09. The red dashed line is for $IP_3 = 0.015\mu M$, with a maximum point of 0.49. Finally, the yellow dotted line is for $IP_3 = 0.02$, with a maximum at 0.71 (Mak et al., 1998). *Software*: MATLAB.

The maximum inhibitory Ca^{2+} binding coefficient is given by K_∞ . This parameter was assigned a value of $52 \pm 4\mu M$ at a saturating IP_3 concentration. The value of K_{IP_3} derived

is a close match to the dissociation constant in IP_3 binding assays as well as the necessary IP_3 concentration needed to stimulate Ca^{2+} release (Mauger et al., 1994; Taylor & Traynor, 1995; Joseph, 1996; Meyer et al., 1988). The large Hill coefficient of 4 ± 0.5 for H_{IP_3} in equation (3.3) is due to IP_3 activation of the IP_3R being a very cooperative process (Meyer et al., 1988; Finch et al., 1991; Carter & Ogden, 1997; Dufour et al., 1997). This means that we require IP_3 binding to all four monomers to open the gate of the channel through relieving Ca^{2+} inhibition. Figure 3.6 portrays the theoretical P_O equation, (3.2), for different levels of Ca^{2+} as IP_3 is increased.

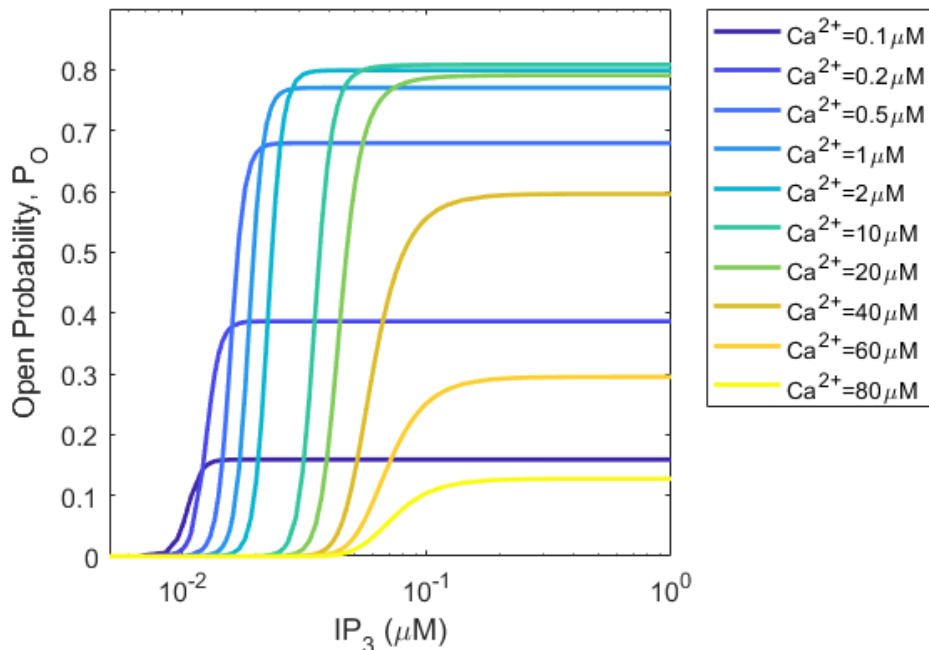


Figure 3.6: Replication of Figure 3c in Mak et al. (1998). It displays P_O from equation (3.2) vs. cytosolic IP_3 concentrations, at various levels of cytosolic Ca^{2+} concentrations. *Software:* MATLAB.

As seen in Figure 3.4, the data from Mak et al. (1998) clearly show a bell-shaped relationship between P_O and Ca^{2+} with a sharp peak for $Ca^{2+} < 1\mu M$ at low ($< 0.02\mu M$) IP_3 . The experiments imply that although cytosolic Ca^{2+} (at low concentrations) and IP_3 both activate the IP_3R channel, they do so in different ways. Like a conventional agonist, Ca^{2+} binding at low levels directly activates the channel. When the IP_3 concentration is low, Ca^{2+} is more likely to bind to the inhibitory site because of its higher affinity ($K_{inh} < K_{act}$). When the IP_3 concentration is higher, this is reversed. A visual representation of this is shown in Figure 3.7 (Mak et al., 1998).

The experimental data and corresponding equation fitted to them in Mak et al. (1998),

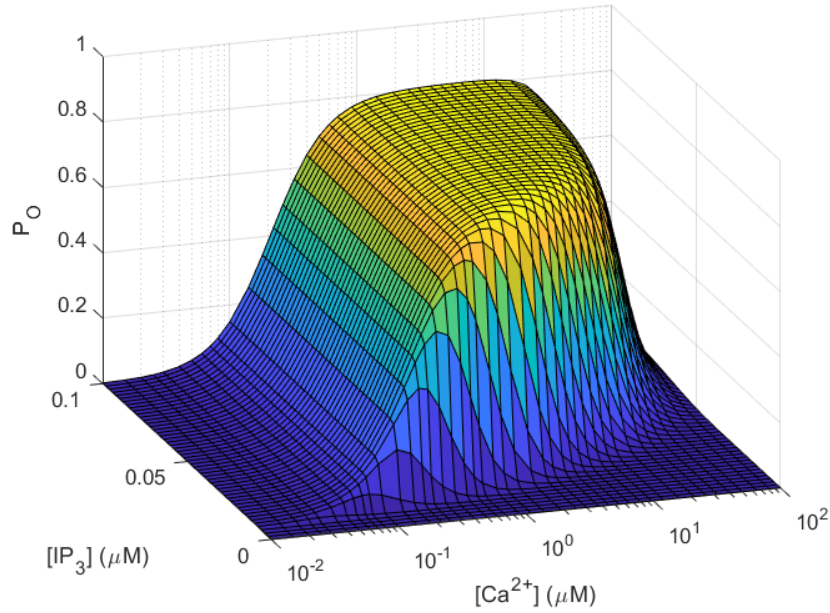


Figure 3.7: P_O vs. IP_3 vs. Ca^{2+} . P_O works at low, ‘activating’, levels of Ca^{2+} . P_O varies with changing IP_3 concentration. We can also see the effects on P_O at high, ‘inhibitory’, levels of Ca^{2+} . Parameter values used are shown in Table B.4 (Mak et al., 1998). *Software:* MATLAB.

(3.2), is the most up to date equation for the open probability of the IP_3R , capturing that IP_3 mediates its effects by modulating the affinity of Ca^{2+} inhibitory sites (Mak et al., 1998). It is thus, a vital component of a Ca^{2+} signalling model at fertilisation. We will therefore endeavor to develop a model with this P_O , using the structure of the Atri model. To achieve this we must study carefully the Atri model and see how we can replace appropriately the components modelling Ca^{2+} binding to its activation site, Ca^{2+} binding to its inhibitory site, and IP_3 binding to its activation site.

Before doing so, we study the model by Kowalewski et al. (2006) where they have incorporated the open probability curve by Mak et al. (1998) into a Ca^{2+} signalling model. We present a summary of this model in the following chapter.

Chapter 4

A model incorporating the experimental data by Mak et al.

A Ca^{2+} signalling model derived by Kowalewski et al. (2006) is currently the only model that includes the open probability, P_O , as modelled in (3.2) by Mak et al. (1998). As discussed previously, the open probability is the probability of the IP_3R being open at any time. Kowalewski et al. (2006) derived two models that differed in the way that the opening and closing of the IP_3R worked. These models are based on the model in De Young and Keizer (1992), and the data for the open probability in Mak et al. (1998). Each model by Kowalewski et al. (2006) produces Ca^{2+} oscillations with different frequencies and amplitudes.

The motivation for their work was to derive a model, based on previous experimental studies, of Ca^{2+} signalling in renal proximal tubular cells following exposure to ouabain (Aizman et al., 2001; Miyakawa-Naito et al., 2003) and after bacterial infection that may cause a fairly common and severe kidney disease in infants (Uhlén et al., 2000). The paper aims at modelling the impact of store-operated Ca^{2+} on the intracellular Ca^{2+} oscillations, assuming a large concentration gradient between Ca^{2+} in the ER and the cytosol. A large concentration gradient is generally assumed in models of Ca^{2+} signalling (Berridge et al., 2003), though for oocytes the depletion of the ER is not an essential driving force for oscillations (Sanders et al., 2018; Wakai et al., 2013). As discussed in the previous chapter, the Ca^{2+} signals in oocytes are driven by the open probability of the IP_3R and hence the IP_3R dynamics (Mak et al., 1998). In Kowalewski et al. (2006) it is acknowledged that the IP_3R are a key mediator of the Ca^{2+} signals (Patterson et al., 2004), but it is assumed the oscillations are mainly driven by depletion of the Ca^{2+} stored in the ER. The model, therefore, depends upon the activation of store-operated channels on the plasma membrane, rather than receptor-operated channels on the ER, which allow entry of external Ca^{2+} ions

into the cytoplasm (Putney et al., 2001; Parekh & Penner, 1997; Parekh & Putney Jr, 2005; Katrik et al., 2002; Berridge, 1995). As a result, they arrive at a reasonably complex model, with a large number of variables. We study this model below and analyse the way in which the experimental data for P_O , see equation (3.2), has been used.

The model consists of eight ODEs, with the following eight variables : cytosolic Ca^{2+} , c , Ca^{2+} in the ER, c_e , Ca^{2+} in the extracellular volume, c_{EC} , cytosolic IP_3 , p , cytosolic G proteins, G , store-operated channels in the plasma membrane, (SOC), cytosolic Ca^{2+} influx factor, (CIF_{cyt}), and in the ER, (CIF_{ER}). The extracellular volume is assumed to be infinite. The model is as follows:

$$\frac{dc}{dt} = \frac{S_{ER}}{V_{ER}}\beta(J_{channel} - XJ_{pump}) - \frac{S_{PM}}{V_{cyt}}\beta(YJ_{in} - J_{pm}), \quad (4.1)$$

$$\frac{dc_e}{dt} = \frac{S_{ER}}{V_{ER}}\beta(-J_{channel} + XJ_{pump}), \quad (4.2)$$

$$\frac{dc_{EC}}{dt} = 0 \text{ (The extracellular volume is 'infinite')}, \quad (4.3)$$

$$\frac{dp}{dt} = \begin{cases} G_{signal}I_{deg}p_{max} - I_{deg}p, & \text{if } t > t_0. \\ -I_{deg}p, & \text{otherwise.} \end{cases} \quad (4.4)$$

$$\frac{dG}{dt} = k_Gc - I_GG, \quad (4.5)$$

$$\frac{d(SOC)}{dt} = \frac{S_{PM}}{V_{cyt}}k_{SOC}CIF_{cyt} - I_{SOC}SOC, \quad (4.6)$$

$$\frac{d(CIF_{cyt})}{dt} = \frac{S_{ER}}{V_{ER}}\theta_{c_e}v_{CIF}(CIF_{ER} - CIF_{cyt}) - \frac{S_{PM}}{V_{cyt}}k_{SOC}CIF_{cyt}, \quad (4.7)$$

$$\frac{d(CIF_{ER})}{dt} = -\frac{S_{ER}}{V_{ER}r_{ER}}\theta_{c_e}v_{CIF}. \quad (4.8)$$

The Ca^{2+} fluxes are given by

$$\begin{aligned}
J_{channel} &= (V_{IP_3R} + V_{leakER})(c_e - c), \\
J_{pump} &= \frac{V_e c}{K_e + c}, \\
J_{in} &= \frac{V_p c^2}{K_p^2 + c^2}, \\
J_{pm} &= (V_{SOC} + V_{leakPM})(c_{EC} - c), \\
G_{signal} &= 1 - \frac{G^n}{G^n + K_{1/2,G}^n}, \\
V_{SOC} &= v_{SOC} SOC, \\
\theta &= \begin{cases} 1, & \text{if } c_e < c_{e,min}. \\ 0, & \text{otherwise.} \end{cases}
\end{aligned} \tag{4.9}$$

The biological representations and values of each parameter is given in Table B.5. Flux through the IP_3R is represented by $J_{channel}$. Flux across the cell plasma membrane is represented by J_{in} , and is dependent on the CIF and the SOC channel activity. The two different functions for the V_{IP_3R} term (coloured in blue in equation (4.9)) are presented in equations (4.10) and (4.11). They are based on the IP_3R dynamics in the De Young-Keizer model and on the Mak et al. (1998) equation for P_O (equation (3.2)), respectively. For V_{IP_3R} they choose either

$$V_{IP_3R_1} = v_1 \left(\frac{cpd_2}{(cp + pd_2 + d_1d_2 + cd_3)(c + d_5)} \right), \tag{4.10}$$

or

$$V_{IP_3R_2} = v_{IP_3R} P_O. \tag{4.11}$$

We have equations for cytosolic Ca^{2+} and Ca^{2+} in the ER given by (4.1) and (4.2) respectively.

The first model in Kowalewski et al. (2006) uses equation (4.10), which was also used in Baker et al. (2002). This is not specific to any subtype of IP_3R . The second model uses equation (4.11) with P_O , as derived by Mak et al. (1998). We examine how this was implemented and if it fits with the biological representation intended. V_{IP_3R} vs. IP_3 and $[Ca^{2+}]$, for equations (4.10) and (4.11) respectively, are compared in Figures 4.1A and B. The graphs show how the fluxes $V_{IP_3R_1}$ and $V_{IP_3R_2} = v_{IP_3R} P_O$ depend on the IP_3 and Ca^{2+}

concentrations, respectively. The graphs are quite different. In Figure 4.1B we can see that the IP_3 concentration saturates at around $0.03\mu M$. When $[IP_3] > 0.3\mu M$, the behaviour of $V_{IP_3R_2}$ does not change significantly as $[Ca^{2+}]$ changes. This is in contrast to Figure 4.1A where there is a strong IP_3 dependence and the flux is inhibited by very high levels of Ca^{2+} . As $[IP_3]$ increases beyond $0.1\mu M$, the maximum point in the graph in Figure 4.1A would continue to grow in a linear manner. However, as we can see in Figure 4.1B, the bell-shaped curve has reached a plateau upon increasing levels of $[IP_3]$. Although the first model presented in Kowalewski et al. (2006) used the IP_3R dynamics from the De Young-Keizer model (4.10), these were implemented in a different way, as the De Young and Keizer (1992) model is not a gating model. Both models in Kowalewski et al. (2006) included the open probabilities (from equations (4.10) and (4.11)) in $J_{channel}$.

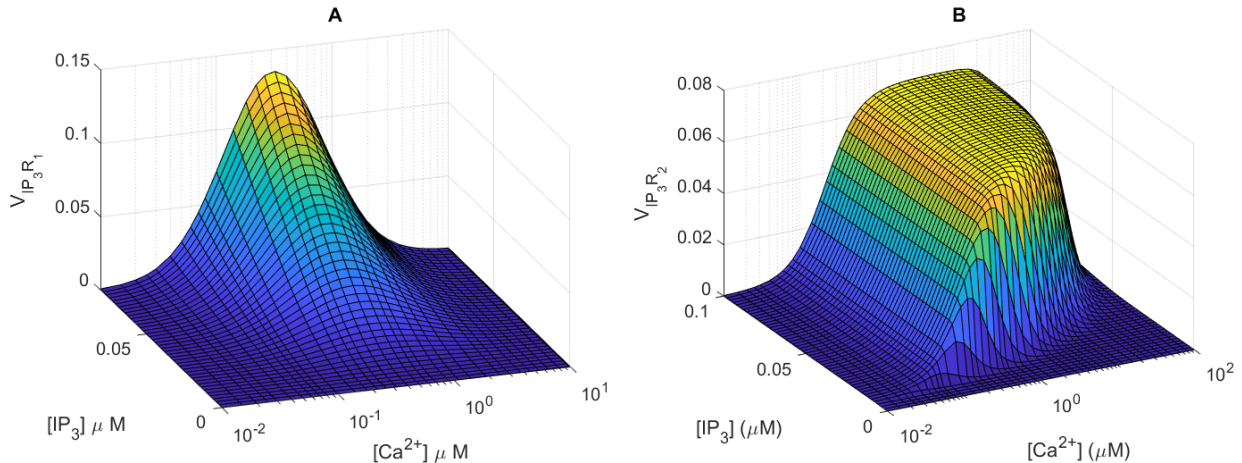


Figure 4.1: (A) $V_{IP_3R_1}$ vs. $[IP_3]$ and $[Ca^{2+}]$ (μM). (B) $V_{IP_3R_2}$ vs. $[IP_3]$ and $[Ca^{2+}]$ (μM). (Kowalewski et al., 2006; De Young & Keizer, 1992; Mak et al., 1998) *Software*: MATLAB.

The two models by Kowalewski et al. (2006) exhibit different oscillatory responses for Ca^{2+} , as seen in Figure 4.2. With equation (4.10), Ca^{2+} oscillations with a higher frequency and lower amplitude are generated. A fundamental difference is that the model with equation (4.11) has Ca^{2+} oscillating for all IP_3 concentrations higher than $0.012\mu M$, whereas with equation (4.10) these oscillations were triggered only between 0.030 and $0.043\mu M$ (Kowalewski et al., 2006).

Taking a closer look at the equation for IP_3 , (4.4), the IP_3 concentration starts off at an extremely low level. (See also Table 4.1). After a certain amount of time, $t_0 = 500s$, a reaction is assumed to begin. IP_3 has been modelled to degrade linearly with a time constant $1/I_{deg}$. Meanwhile, it is also produced by a reaction controlled by the signal G_{signal} . The G_{signal} lies between 0 and 1, and $[IP_3]$ lies between 0 and $IP_{3,max}$. In this model, $[IP_3]$ depends on G (a hypothetical species), that depends on $[Ca^{2+}]$. This is because production

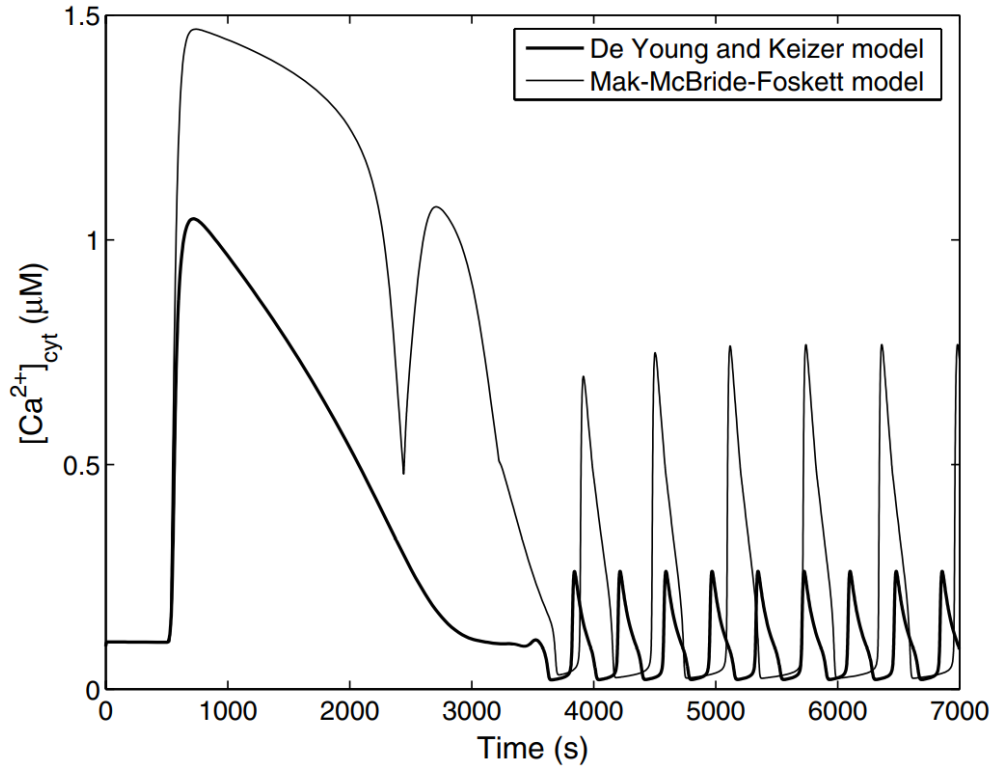


Figure 4.2: Ca^{2+} oscillations arising from the two different models by Kowalewski et al. (2006). The ‘*De Young and Keizer model*’ uses equation (4.10) (De Young & Keizer, 1992). The ‘*Mak-McBride-Foskett model*’ uses equation (4.11) (Mak et al., 1998). Source: Kowalewski et al. (2006). The large difference in their transients is due to the parameters v_1 and v_{IP_3R} chosen which represent the maximum Ca^{2+} permeability across the IP_3R .

of G is proportional to Ca^{2+} and degradation happens at the rate of $I_G[G]$. The parameter $K_{1/2,G}$ is the inactivation constant for the signalling mechanism (Kowalewski et al., 2006).

A phenomenological model for activating the SOC has been used as the exact mechanism has not yet been identified. The model by Kowalewski et al. (2006) has a diffusible messenger and a CIF, and is built upon the idea that CIF exits the ER and binds to a plasma membrane channel. CIF leaves the ER fast and the Ca^{2+} concentration in there decreases. When reaching the plasma membrane, CIF then binds to and activates SOC. The SOC are then deactivated after a while so long as more CIF has not been released into the cytosol. Within the ER CIF is regenerated at a slow pace but only let out when the ER Ca^{2+} level is lower than the threshold of $10\mu M$ (Kowalewski et al., 2006).

Variable	Initial value
Cytosolic IP_3	$1pM$
ER Ca^{2+}	$100\mu M$
ER CIF	$0.1\mu M$
Cytosolic G	0
Cytosolic Ca^{2+}	$95nM$
Extracellular Ca^{2+}	$950\mu M$
Cytosolic CIF	0
Active SOC in plasma membrane	0

Table 4.1: Initial values used for the models in Kowalewski et al (Kowalewski et al., 2006).

Both models in Kowalewski et al. (2006) generate Ca^{2+} oscillations (see Figure 4.2). However, it is difficult to compare these oscillations to Ca^{2+} oscillations at fertilisation as many other variables (that are not relevant to the cell type we are looking at) are included. The models rely on the existence of SOC, for example. One explanation for the activation of SOC is the assumed depletion of Ca^{2+} from the ER. As previously discussed, a model where Ca^{2+} released from the ER is a driving force for oscillations is not appropriate for Ca^{2+} signalling in fertilisation. Experimental data in Sanders et al. (2018); Wakai et al. (2013) suggest that cytosolic Ca^{2+} oscillations in an egg rely on the IP_3R dynamics to be the main driving force, and that ER store depletion plays a much less significant role. The model by Kowalewski et al. (2006) is therefore not appropriate for the mammalian egg. We must derive a new model that is appropriate incorporating the data from Mak et al. (1998).

We hence face the challenge of appropriately incorporating the open probability from equation (3.2) into a new model that does not strongly depend on depletion of Ca^{2+} from the ER. We will use the knowledge acquired from this chapter and our literature review to derive a new such model in Chapter 5.

Chapter 5

A new model for Ca^{2+} signalling in fertilisation

We have completed, in Chapter 2, a literature review of several Ca^{2+} signalling models, focusing on the models by Atri et al. (1993) and by Li and Rinzel (1994). These are two minimal gating models that are still widely used. We have also studied in Chapter 3 the work by Mak et al. (1998) which gives accurate data for the open probability of the IP_3R , P_O , as $[IP_3]$ and $[Ca^{2+}]$ vary. In this chapter we are going to present the derivation of a new model for Ca^{2+} signalling in fertilisation. This will also be a gating model but, in an appropriate manner, it will incorporate for the first time the most up-to-date IP_3R dynamics from Mak et al. (1998).

The Atri et al. (1993) model is a good starting point for creating a new gating model since it is a minimal model capturing many of the salient features of Ca^{2+} signalling while not including an equation for $[Ca^{2+}]$ in the ER. Deciding how to best incorporate the equation for P_O from Mak et al. (1998) is not straightforward so we have explored several options. In the model by Kowalewski et al. (2006), P_O was inserted into the equation for cytosolic Ca^{2+} as a multiplicative term for the flux entering the cytosol from the ER. This term is referred to as $J_{channel}$ in Chapter 4 (see equation (4.9)). We explored this idea but it does not quite fit in a gating model, as gating models include terms for the IP_3R dynamics in both ODEs, rather than just the equation for Ca^{2+} . We, therefore, chose an alternative approach of splitting up the equation for P_O given in Mak et al. (1998) in an appropriate manner, as detailed below.

Revisiting the biological representation behind each term in the Atri model, (2.1)-(2.2), the probability of IP_3 binding to its activation site on the IP_3R is represented by p_1 , the probability of Ca^{2+} binding to its activation site on the IP_3R is represented by p_2 , and the

probability of Ca^{2+} binding to the inhibitory site is represented by p_3 . As given in Chapter 2, these probabilities are, respectively, given as follows:

$$p_1 = \frac{p + \mu_0 K_{IP_3}}{K_{IP_3} + p}, \quad p_2 = \frac{K_{act} b + c}{K_{act} + c}, \quad p_3 = \frac{K_{inh}^2}{K_{inh}^2 + c^2}.$$

To construct a new Ca^{2+} signalling model, we split up the equation for P_O in Mak et al. (1998), as follows:

$$P_{O1} = \left(\frac{c^{H_{act}}}{c^{H_{act}} + K_{act}^{H_{act}}} \right),$$

$$P_{O2} = \left(\frac{K_{inh}^{H_{inh}}}{K_{inh}^{H_{inh}} + c^{H_{inh}}} \right),$$

where

$$K_{inh} = K_{\infty} \left(\frac{p^{H_{IP_3}}}{p^{H_{IP_3}} + K_{IP_3}^{H_{IP_3}}} \right).$$

Here, P_{O1} represents the probability of Ca^{2+} binding to the activation site on the IP_3R and depends on the half-maximal activation constant, K_{act} , and on the Hill coefficient, $H_{act} = 1.9 \pm 0.3$. P_{O1} increases with Ca^{2+} . P_{O2} represents the probability of Ca^{2+} binding to its inhibitory site. This depends on Ca^{2+} and K_{inh} , where K_{inh} depends on IP_3 . As $[Ca^{2+}]$ increases, P_{O2} decreases. As $[IP_3]$ increases, K_{inh} increases, and hence P_{O2} increases. Plots of P_{O1} as a function of Ca^{2+} and P_{O2} as a function of Ca^{2+} and IP_3 can be seen in Figures 5.1A and 5.1C.

To construct a new Ca^{2+} signalling model from the Atri model, we replace $p_1 p_2$ in $J_{channel}$ (in equation (2.1) for cytosolic Ca^{2+}) with P_{O1} . Moreover, we replace p_3 (in equation (2.2) for the proportion of non inactivated IP_3R) with P_{O2} . Plotting p_1 , p_2 , p_3 , P_{O1} , P_{O2} as functions of Ca^{2+} and IP_3 in Figure 5.1, we observe similarities and differences. In Figures 5.1A and 5.1B, we see that P_{O1} behaves similarly to $p_1 p_2$. Note that the scales are slightly different here as k_{flux} is a multiplicative factor in the $J_{channel}$ term in the Atri model. However, in Figures 5.1C and 5.1D, we see that P_{O2} and p_3 behave very differently. As the IP_3 concentration increases, p_3 does not change very much. In contrast, there is a far more significant change in P_{O2} as $[IP_3]$ increases, particularly for lower levels of IP_3 . This IP_3R behaviour emerging from the experiments in Mak et al. (1998) is a crucial feature included in our new model. Figure 5.1F shows $p_1 p_2 p_3$ vs. IP_3 for different levels of Ca^{2+} . For lower levels of Ca^{2+} , $p_1 p_2 p_3$ barely changes as $[IP_3]$ changes. The dependence on higher levels of Ca^{2+} is also very minimal. In comparison, there is clearly far more change in $P_{O1} P_{O2}$ as $[Ca^{2+}]$ and $[IP_3]$ vary,

as seen in Figure 5.1E. Similarly, in Figure 5.2A we plot $p_1p_2p_3$ vs. IP_3 for selected levels of Ca^{2+} and this can be compared to Figure 5.2B where we plot P_O vs. Ca^{2+} and IP_3 . We see once again that $p_1p_2p_3$ from the Atri model does not change significantly with increasing levels of IP_3 , whereas $P_{O1}P_{O2}$ from Mak et al. (1998) does.

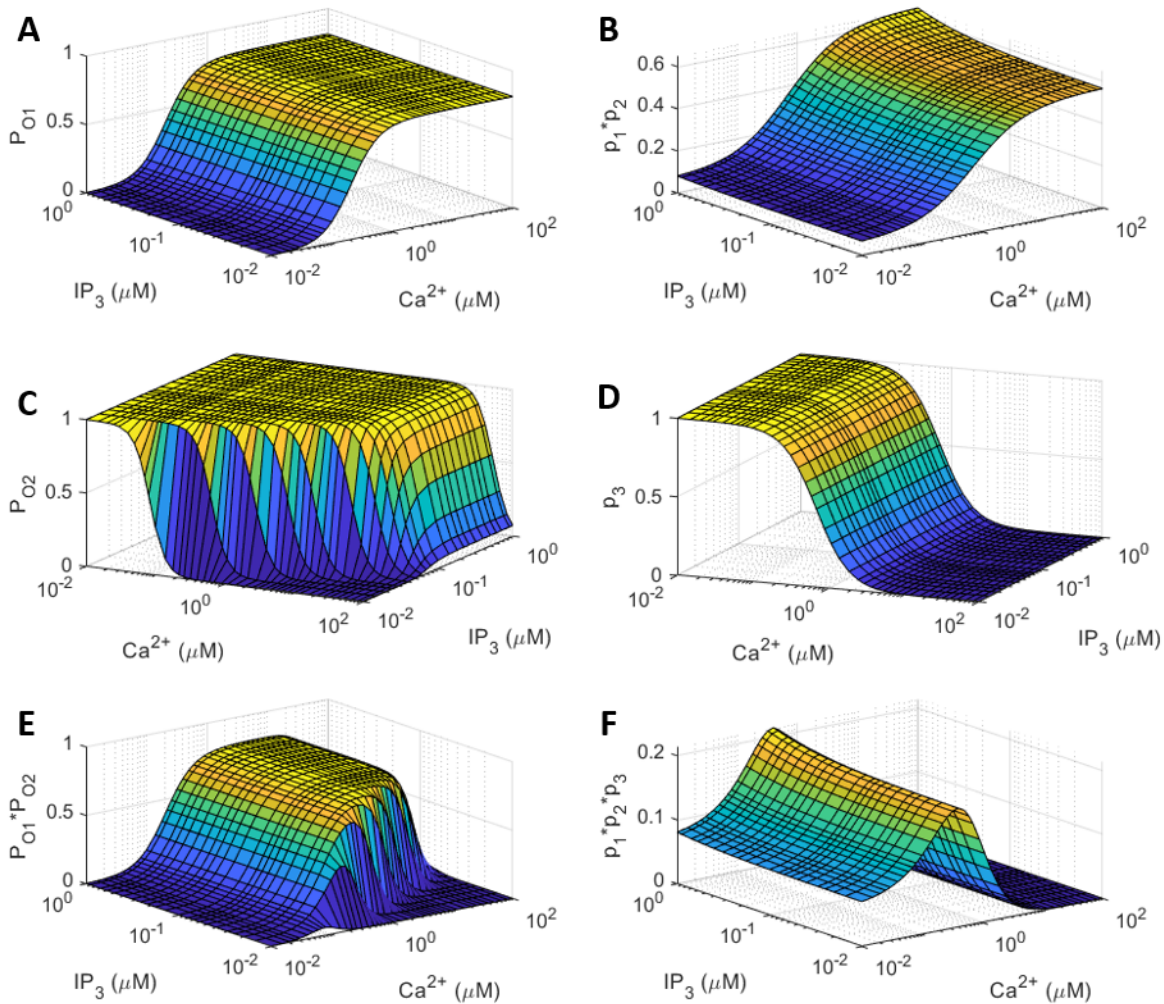


Figure 5.1: (A) P_{O1} vs. $[Ca^{2+}]$ and $[IP_3]$. (B) p_1p_2 vs. $[Ca^{2+}]$ and $[IP_3]$. (C) P_{O2} vs. $[Ca^{2+}]$ and $[IP_3]$. (D) p_3 vs. $[Ca^{2+}]$ and $[IP_3]$. (E) $P_O = P_{O1}P_{O2}$ vs. Ca^{2+} and IP_3 . (F) $p_1p_2p_3$ vs. Ca^{2+} and IP_3 . P_{O1} and P_{O2} are from Mak et al. (1998). p_1 , p_2 and p_3 are from Atri et al. (1993). *Software:* MATLAB.

Finally, Figures 5.3A and 5.3B are compared. In the former, $p_1p_2p_3$ is plotted as $[Ca^{2+}]$ increases for different levels of $[IP_3]$. We see that $p_1p_2p_3$ does not change as $[IP_3]$ goes from $0.01\mu M$ to $0.1\mu M$. It does change significantly when $[IP_3]$ reaches $10\mu M$ though. This once again illustrates that in the Atri model, the open probability of the IP_3R does not vary much

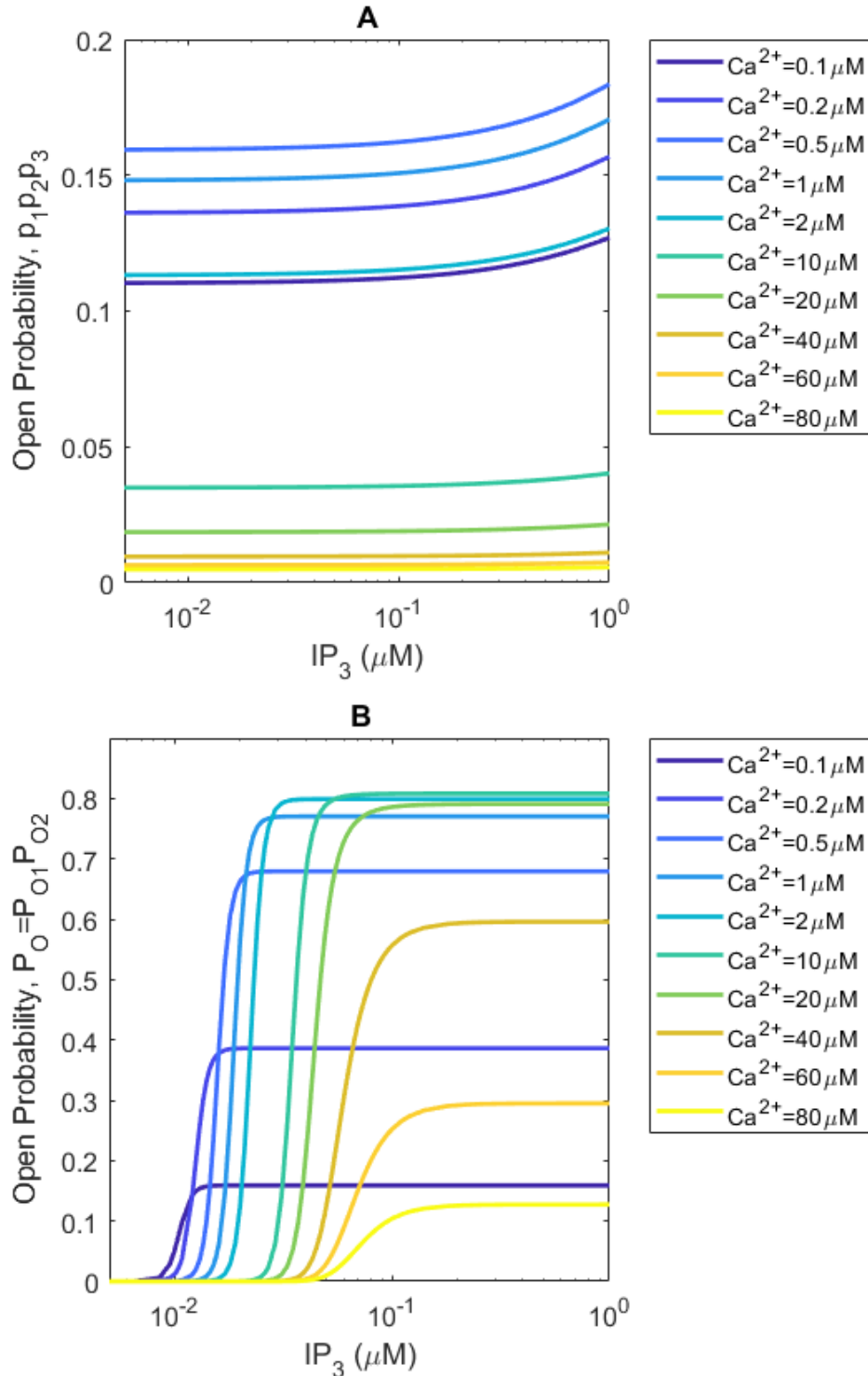


Figure 5.2: **(A)** $p_1 p_2 p_3$ (Atri model) vs. cytosolic IP_3 concentrations at various levels of cytosolic $[Ca^{2+}]$. Parameter values used are shown in Table B.1. **(B)** $P_{O1} P_{O2}$ (Mak et al., 1998) vs. cytosolic IP_3 concentrations at various levels of cytosolic $[Ca^{2+}]$. Parameter values used are shown in Table B.4. The Ca^{2+} values here were chosen to mirror the ones used in figure 3c in Mak et al. (1998). *Software*: MATLAB.

at low levels of $[IP_3]$. In contrast, the IP_3R dynamics derived in Mak et al. (1998) depend on $[IP_3]$ and $[Ca^{2+}]$ significantly, as seen in Figure 5.3B. These comparisons demonstrate the importance of implementing the IP_3R dynamics from Mak et al. (1998) in a new model.

One less researched Ca^{2+} flux is that of the SERCA pump, modelled by J_{pump} in equation (2.1). Atri et al. (1993) used a simple Hill function to model it and acknowledged it could be improved when more experimental data would be made available. For this reason we use more recent Ca^{2+} models to improve this term. In particular, we use the expression $V_e c^2 / (K_e^2 + c^2)$ from Politi et al. (2006) who derived a sophisticated gating model with cytosolic Ca^{2+} , the proportion of non inactivated IP_3R , Ca^{2+} in the ER and IP_3 as dynamic variables. They used a SERCA pump flux term with a Hill coefficient of 2, and the half-activation constant was given as $K_e = 0.1 \mu Ms^{-1}$. These parameter values are based on Lytton et al. (1992) and Camello et al. (1996).

Summarising, the inclusion of the IP_3R dynamics from Mak et al. (1998) and the SERCA pump flux term from Politi et al. (2006) leads us to a new model for Ca^{2+} signalling in fertilisation:

$$\frac{dc}{dt} = K_{flux} n P_{O1} - \frac{V_e c^2}{K_e^2 + c^2}, \quad (5.1)$$

$$\frac{dn}{dt} = g(P_{O2} - n). \quad (5.2)$$

This model has qualitative agreement to the data (Mak et al., 1998). Note that mouse eggs oscillate for some time in a Ca^{2+} -free medium (Sanders et al., 2018). One can ‘isolate’ mouse eggs so that no efflux or influx takes place and in this case, they can oscillate for many hours (Wakai et al., 2013). This implies that Ca^{2+} exchange with the extracellular medium is not necessary for Ca^{2+} oscillations (page 246 in Dupont et al. (2016)), (Yao & Parker, 1994). Hence, in the Atri model, the $J_{leakage}$ term is not essential for Ca^{2+} oscillations. We therefore disregard any leakage flux component in our model.

The next step is to perform a linear stability analysis of the model (5.1)-(5.2) and show that the model can generate oscillations for a range of IP_3 values that are compatible with experimental findings.

5.1 Linear stability analysis

We will now carry out the linear stability analysis of our new model (5.1)-(5.2) in order to determine if an oscillatory regime exists and for which IP_3 values. In Mak et al. (1998) a range for each parameter value is given. We use values in these ranges, and we also use the

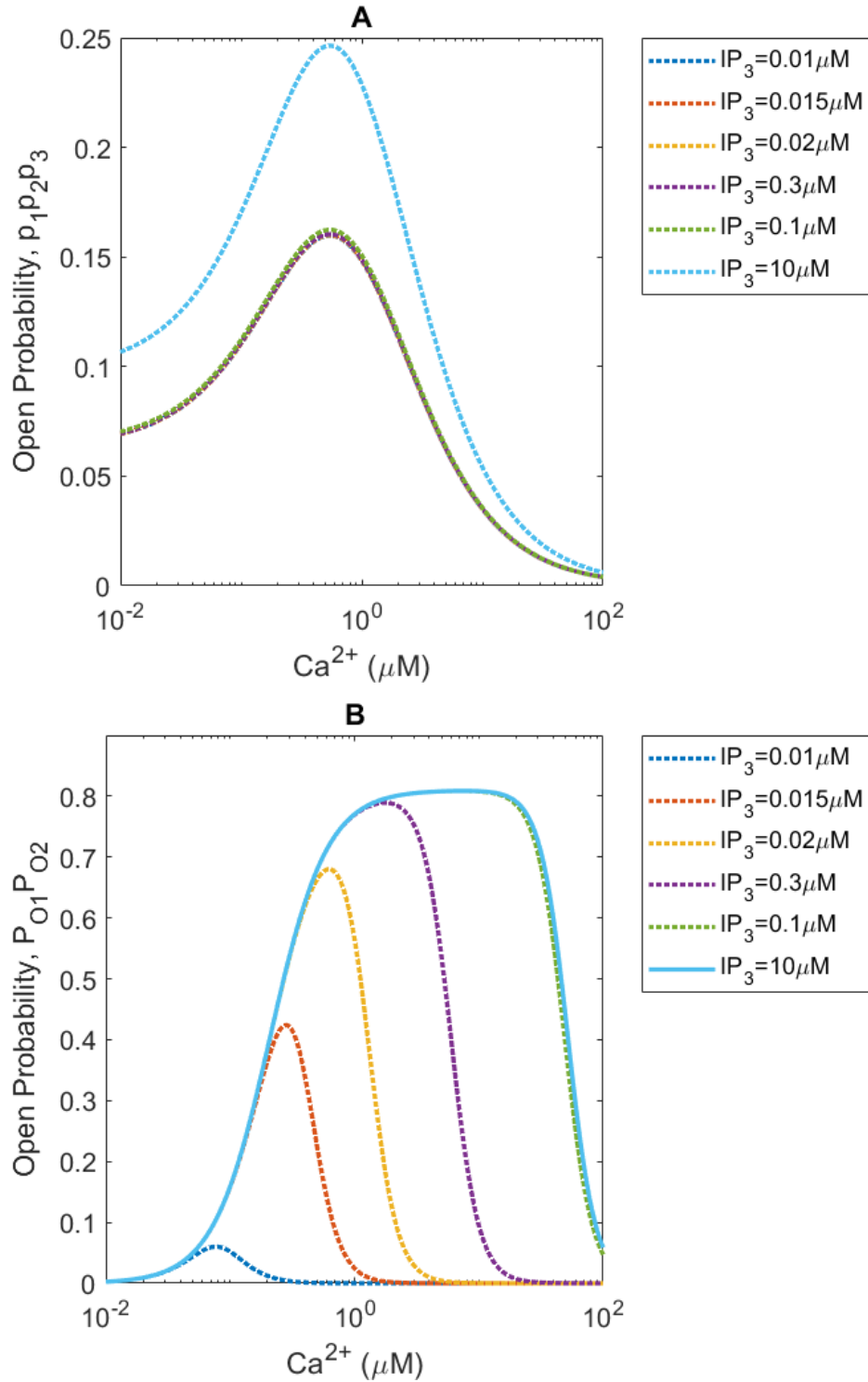


Figure 5.3: (A) $p_1 p_2 p_3$ (from the Atri model) as a function of cytosolic Ca^{2+} for various IP_3 levels of interest. Parameter values used are shown in Table B.1. (B) $P_{O_1} P_{O_2}$ (from Mak et al., 1998) as a function of cytosolic Ca^{2+} for various IP_3 levels of interest. Parameter values used are shown in Table B.4. *Software:* MATLAB.

half-activation constant in J_{pump} as in the Politi et al. (2006) model. We leave k_{flux} and V_e undetermined mutually. We know that k_{flux} measures the maximum flux from the ER to the cytosol, and V_e measures the maximum flux from the cytosol to ER. We assume that proteins are constant in a cell over the period of oscillations. We can also expect steady states of around $0.1\mu M$ for Ca^{2+} (Berridge et al., 2003; Kline & Kline, 1992), and n varies between 0 and 1 since it represents a proportion. Additionally, we must ensure a steady state value of approximately $0.01\mu M$ for IP_3 (Mak et al., 1998; Swann, 2021). This is a reasonable assumption since it is below the level that stimulates the opening of the IP_3R .

We set $dc/dt = dn/dt = 0$ to find the steady states. We have

$$\begin{aligned} F(c, n) &= k_{flux}n \left(\frac{c^{H_{act}}}{c^{H_{act}} + K_{act}^{H_{act}}} \right) - \frac{V_e c^2}{K_e^2 + c^2} \\ &= 0, \end{aligned} \tag{5.3}$$

$$\begin{aligned} G(c, n) &= g \left(\frac{K_{inh}^{H_{inh}}}{K_{inh}^{H_{inh}} + c^{H_{inh}}} - n \right) \\ &= 0, \end{aligned} \tag{5.4}$$

where

$$K_{inh} = K_\infty \frac{p_{IP_3}^h}{p^{h_{IP_3}} + k_{IP_3}^{h_{IP_3}}},$$

where we have four unknowns: c , n , k_{flux} , and V_e .

We then determine the Trace, Determinant, and Discriminant of the Jacobian matrix of the system (5.3) and (5.4). The partial derivatives are

$$\frac{\partial F}{\partial c} = \frac{k_{flux}n c^{H_{act}} H_{act}}{c(c^{H_{act}} + K_{act}^{H_{act}})} - \frac{k_{flux}n (c^{H_{act}})^2 H_{act}}{(c^{H_{act}} + K_{act}^{H_{act}})^2 c} - \frac{2V_e c}{K_e^2 + c^2} + \frac{2V_e c^3}{(K_e^2 + c^2)^2}, \tag{5.5}$$

$$\frac{\partial F}{\partial n} = \frac{k_{flux} c^{H_{act}}}{c^{H_{act}} + K_{act}^{H_{act}}}, \tag{5.6}$$

$$\frac{\partial G}{\partial c} = -g \frac{\left(\frac{K_\infty p^{h_{IP_3}}}{p^{h_{IP_3}} + k_{IP_3}^{h_{IP_3}}} \right)^{H_{inh}} c^{H_{inh}} H_{inh}}{\left(\left(\frac{K_\infty p^{h_{IP_3}}}{p^{h_{IP_3}} + k_{IP_3}^{h_{IP_3}}} \right)^{H_{inh}} + c^{H_{inh}} \right)^2 c}, \tag{5.7}$$

$$\frac{\partial G}{\partial n} = -g. \tag{5.8}$$

Hence, the Trace, Determinant and Discriminant are defined respectively as follows:

$$T(c, n) = \frac{\partial F}{\partial c} + \frac{\partial G}{\partial n},$$

$$D(c, n) = \frac{\partial F}{\partial c} \frac{\partial G}{\partial n} - \frac{\partial F}{\partial n} \frac{\partial G}{\partial c},$$

$$Disc(c, n) = (T(c, n))^2 - 4D(c, n).$$

Solving equations (5.3) and (5.4) and setting constraints so that $T(c, n) > 0$, $D(c, n) > 0$, $Disc(c, n) < 0$, we obtain appropriate steady state values and parameters values for k_{flux} and V_e . The steady states obtained are $c_s = 0.08\mu M$ and $n_s = 0.60$ (which are within a reasonable range (Berridge et al., 2003; Kline & Kline, 1992; Swann, 2021)) when $k_{flux} = 4.89$, $V_e = 1$.

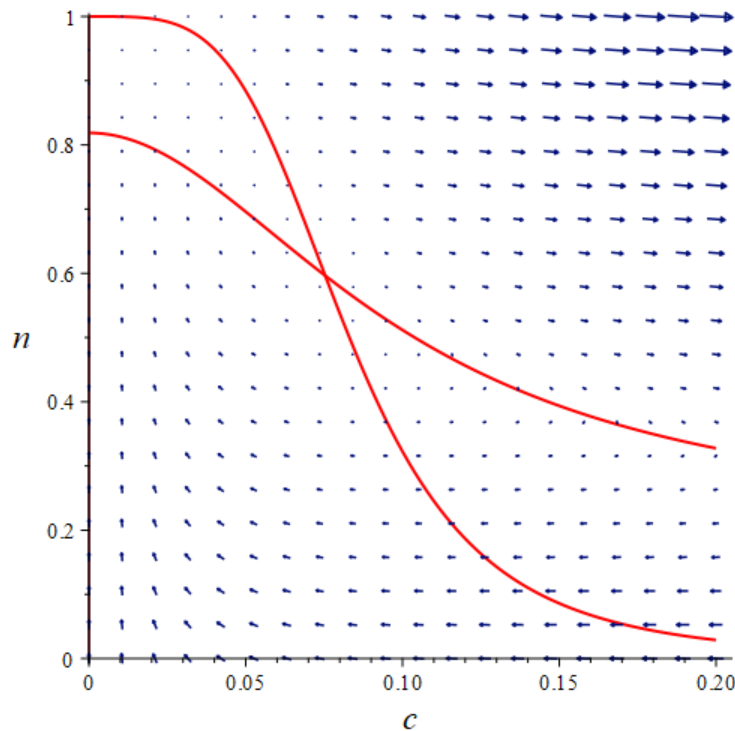


Figure 5.4: The nullclines of the system (5.3)-(5.4), with $k_{flux} = 4.89$, $V_e = 1$ and parameter values as given in Table 5.1. The steady state is where the lines intersect. Arrows indicate the vector field. *Software:* Maplesoft.

Evaluating the Trace, Determinant and Discriminant at the steady state value $c = 0.08$

gives:

$$\begin{aligned} T(c_s, n_s) &= 1.79, \\ D(c_s, n_s) &= 2.74, \\ \text{Disc}(c_s, n_s) &= -7.76. \end{aligned}$$

5.2 Simulations

We have completed the linear stability analysis, and decided on parameter values shown in Table 5.1.

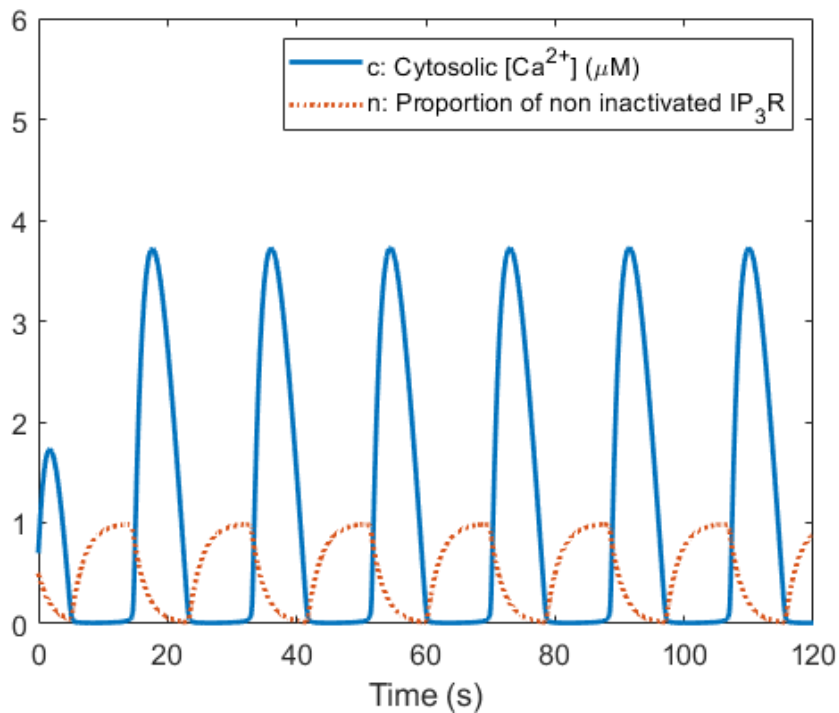


Figure 5.5: Ca^{2+} oscillations arising from the system (5.1)-(5.2), blue solid lines, with $p = 0.01\mu M$. The proportion of non inactivated IP_3R is also plotted, with a red dashed line. Parameter values are given in Table 5.1. *Software*: MATLAB.

Oscillations generated by the model (5.1)-(5.2) can be seen in Figure 5.5, where $p = 0.01\mu M$. Our model reproduces the low frequency, large amplitude oscillations characteristic of fertilising mammalian eggs (shown in Figure 1.1). We need to examine the exact range of values of p for which these oscillations exist, if the oscillations change in that range, and if the experimental findings in Sanders et al. (2018) are replicated.

We can determine the range of p for which the ODE system (5.1)-(5.2) yields oscillations by plotting the Trace, Determinant, and Discriminant at the steady states, and determining the range for which $T > 0$, $D > 0$, and $Disc < 0$ (unstable spiral). We find that this range is $0.0085 \leq p \leq 0.014$ which is extremely small. This can be seen in Figure 5.7.

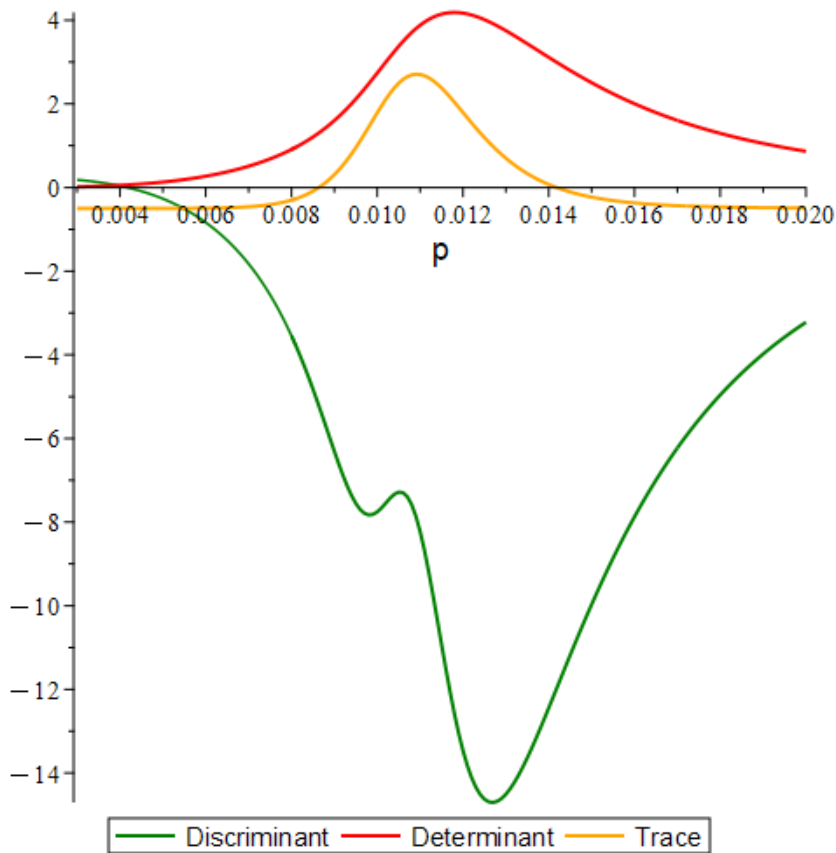


Figure 5.6: Trace, Determinant, and Discriminant for the system of equations (5.3)-(5.4) for varying bifurcation parameter p . Parameter values are as in Table 5.1. *Software:* MATLAB.

In order to enlarge the range of p to be $0.01\mu M \leq [IP_3] \leq 1\mu M$ for which the system is oscillatory, a non-linear scaling of equation (5.1) would be needed. Unfortunately, this is beyond the scope of this project. This scaling should render the left Hopf point at approximately $[IP_3] = 0.01\mu M$, and the right Hopf point at $[IP_3] \approx 1\mu M$ (Swann, 2021).

Regardless of the oscillatory range of p being an order of magnitude inaccurate, we can still analyse the behaviour of the oscillations. Figure 5.7 shows the oscillations for $p = 0.0085$ and $p = 0.014$, respectively, at each end of the oscillatory range. Both the amplitude and frequency of oscillations increase as the IP_3 concentration is increased, as seen in experiments (Sanders et al., 2018). However, the amplitude increase is more pronounced than the frequency increase.

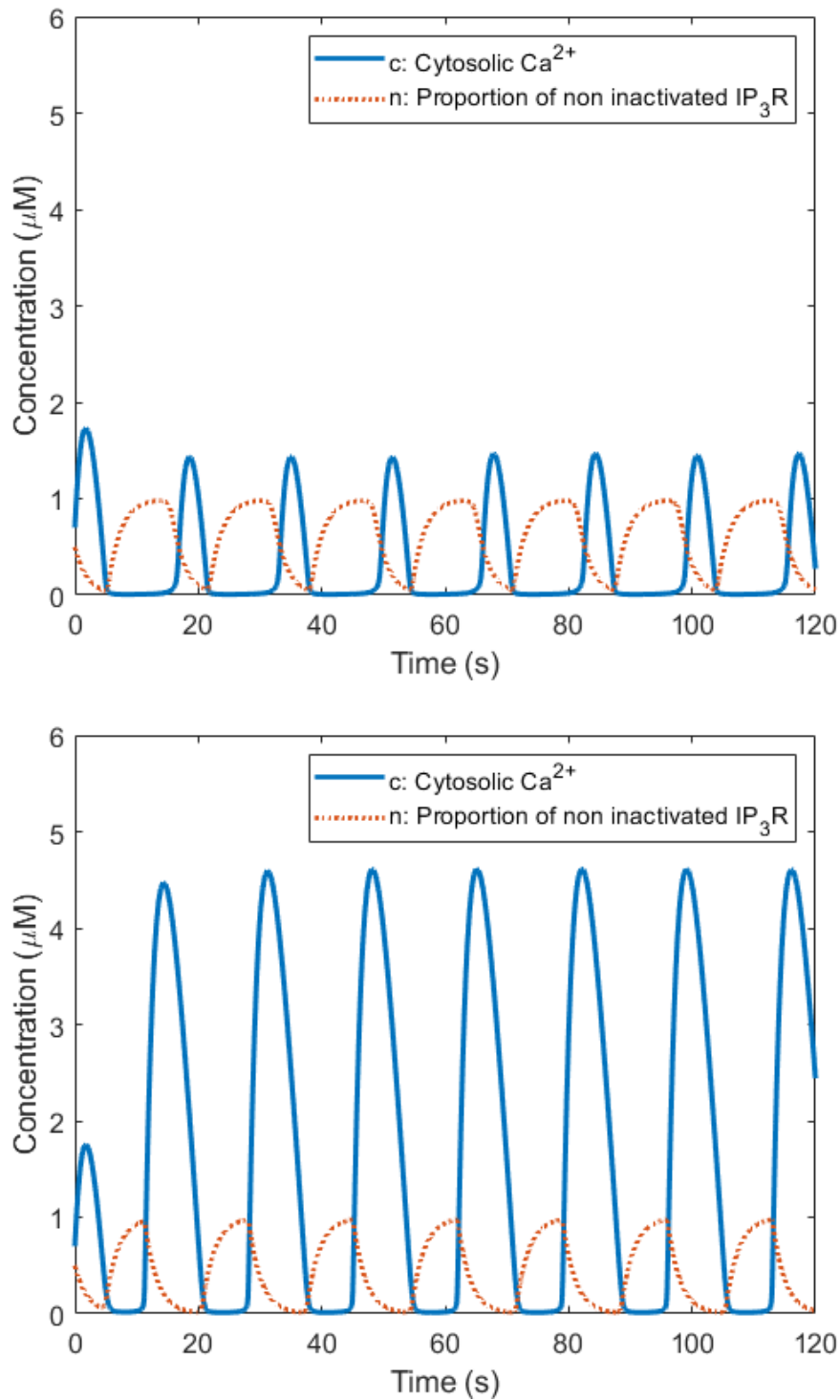


Figure 5.7: Ca^{2+} oscillations exhibited by new model (5.1)-(5.2), for (a) $p = 0.0085$ and (b) $p = 0.014$. We observe both ends of oscillatory region. *Software: MATLAB.*

Our new model (5.1)-(5.2) produces Ca^{2+} oscillations of higher frequency when there is

a higher concentration of IP_3 present in the cytosol. This result is in agreement with the experiments by Sanders et al. (2018). Previous models of Ca^{2+} signalling (Atri et al., 1993; Li & Rinzel, 1994; De Young & Keizer, 1992; Sanders et al., 2018; Theodoridou et al., 2013) have assumed outdated IP_3R dynamics, and instead relied on the ER store refilling to drive oscillations. We know that this is not the case for Ca^{2+} signalling in fertilisation (Sanders et al., 2018; Wakai et al., 2013). We have managed to reproduce key aspects of the experimental findings of Sanders et al. (2018) with our new two-variable model which incorporates the correct IP_3R dynamics from Mak et al. (1998). However, the data from Sanders et al. (2018) and Sneyd et al. (2006) show that IP_3 concentration is not constant and needs to be a dynamic variable in a Ca^{2+} model for fertilising eggs. Obtaining a new model closer to the data from Sanders et al. (2018) and Mak et al. (1998) was of foremost importance and is the first step to reaching a more complex three-variable model with dynamic IP_3 . We have derived a model that does not depend on the ER store emptying and refilling, as the data from Sanders et al. (2018) and Wakai et al. (2013) suggest. We have also managed to incorporate the IP_3R dynamics for fertilisation, that accurately depend on $[Ca^{2+}]$ and $[IP_3]$, as found by Mak et al. (1998). The next step of incorporating an ODE for IP_3 is beyond the scope of this project and is left for future work.

Note that the data from Sneyd et al. (2006) are in agreement with the data from Sanders et al. (2018), though experiments were carried out on pancreatic acinar cells and airway smooth muscle cells. Sneyd et al. (2006) also derived two models with an ODE for IP_3 , based on the Atri model and the Li-Rinzel model. We study these models in Appendix A.

Parameters used in new model	Value
K_{flux}	$8.6 \mu Ms^{-1}$
K_{act}	$0.2 \mu M$
H_{act}	2
V_e	$1 \mu Ms^{-1}$
K_e	$0.1 \mu M$
K_∞	$52 \mu M$
K_{IP_3}	$0.05 \mu M$
H_{IP_3}	4
g	0.5
h	0.5

Table 5.1: Parameters used in new model, (5.1)-(5.2).

Chapter 6

Summary, Conclusions and Further work

In this project we studied several Ca^{2+} signalling models, focusing on the IP_3R dynamics as determined in the experiments of Mak et al. (1998). In Chapter 1 we introduced the basic biological processes of Ca^{2+} signalling, focusing on those of a mammalian egg at fertilisation. We also briefly reviewed the Ca^{2+} models by Atri et al. (1993), Li and Rinzel (1994), Dupont and Goldbeter (1993) and De Young and Keizer (1992). Different models have been developed for different cell types. Many models and a substantial amount of experimental data are available for the *Xenopus* oocyte, which is similar to a mammalian egg. The most recent Ca^{2+} models for fertilisation (Theodoridou et al., 2013; Sanders et al., 2018; Politi et al., 2006) are not built with the correct IP_3R dynamics determined by Mak et al. (1998). Many models rely on the refilling of the ER store to drive Ca^{2+} oscillations, which is not the case for fertilisation (Sanders et al., 2018; Wakai et al., 2013). We have thus developed a new gating model where we do not have Ca^{2+} in the ER as a dynamic variable. This model reproduces key experimental features from Sanders et al. (2018) and Mak et al. (1998) as the frequency and amplitude of Ca^{2+} oscillations increase as $[IP_3]$ increases. The model also uses the data and fitted equation from Mak et al. (1998), and relies on the IP_3R dynamics to drive Ca^{2+} oscillations.

In Chapter 2, we analysed in detail two well-established gating models; the model by Atri et al. (1993) and the model by Li and Rinzel (1994). We paid close attention to key features, varying the IP_3 concentration as a bifurcation parameter and how the Ca^{2+} behaviour changes accordingly. We studied in detail the bifurcation diagrams of both models (Kaouri et al., 2019; Li & Rinzel, 1994). We also looked in depth at the individual terms in these models, particularly those that describe the open probability for the IP_3R .

In Chapter 3 we studied the open probability equation by Mak et al. (1998). This involved studying how the three binding sites on an IP_3R work (the activation of site 1 by IP_3 , the activation of site 2 by Ca^{2+} , and the deactivation of site 3 by Ca^{2+}) work. These three

binding processes occur with a certain probability, and these probabilities determine the overall probability of the IP_3R being open and allowing Ca^{2+} to pass through from the ER to the cytosol. The net flux of Ca^{2+} out of the ER is determined by the number of open IP_3R . We examined the experimental data (Mak et al., 1998) which were approximated by equation (3.2) derived for P_O .

In Chapter 4 we studied the model by Kowalewski et al. (2006). They used the equation for P_O by Mak et al. (1998), but the latter model relied upon store depletion of the ER to drive oscillations, rather than the opening and closing of the IP_3R . We require the opening and closing of the IP_3R to actually be the driving force for Ca^{2+} oscillations in our model, as previously discussed and thus, the model by Kowalewski et al. (2006) is therefore not appropriate for Ca^{2+} signalling in fertilisation.

In Chapter 5, we derived a new Ca^{2+} signalling model for fertilisation, (5.1)-(5.2). We used the Atri model (2.1)-(2.2), and the open probability equation for the IP_3R , P_O , by Mak et al. (1998), (3.2). We implemented P_O into the Atri model by splitting it into two terms P_{O1} and P_{O2} , given in equation (3.2), and substituted these into the Atri system in the place of the corresponding binding probabilities. P_{O1} represents the probability of Ca^{2+} binding to the activation site on the IP_3R , and P_{O2} represents the probability of Ca^{2+} binding to its inhibitory site. We also used the half-activation constant in J_{pump} as in the Politi et al. (2006) model. Our model reproduced the low frequency, large amplitude oscillations characteristic of fertilising mammalian eggs. We then performed simulations with increasing IP_3 concentration and parameter values as in Table 5.1. We showed that the oscillation amplitude and frequency increase as IP_3 concentration increases. The results are in agreement, qualitatively, with experiments carried out by Sneyd et al. (2006) and Sanders et al. (2018). The frequency of Ca^{2+} oscillations increases as $[IP_3]$ increases, as shown in Figure 5.7. Sneyd et al. (2006) and Sanders et al. (2018) show what happens when a large amount of IP_3 is suddenly released in the cell. These data were also in agreement with how our system behaves. Unfortunately, the range of IP_3 giving rise to Ca^{2+} oscillations in our model is between $p = 0.0085$ and $p = 0.014$. This should be adjusted to be between approximately $p = 0.01$ and $p > 1$ (μM) (Mak et al., 1998; Swann, 2021) using a non-linear scaling. A scaling is also needed for Ca^{2+} to oscillate between resting levels at $0.1\mu M$, and peaks at $1\mu M$, but this is outside the scope of this work.

In further work, one could incorporate a third ODE for IP_3 in a new model. We have introduced the correct IP_3R dynamics into our model and tested it with constant IP_3 . Evidence from Sanders et al. (2018) suggests that there is a positive feedback of Ca^{2+} on PLC_ζ , and this leads to oscillations of IP_3 . In Appendix A we briefly looked into modelling this and studied higher dimensional models by Sneyd et al. (2006). Once a third ODE for

IP_3 has been incorporated, our new model could be used to make novel predictions for future experiments.

Furthermore, stochastic modelling can be a direction for further work. As previously discussed, Ca^{2+} signalling is intrinsically a stochastic process, so it is logical to develop stochastic models. The IP_3R either open or close and these states change depending on random fluctuations induced by thermal noise. When many IP_3R open, a global spike of Ca^{2+} can occur (page 98 in Dupont et al. (2016)). Furthermore, one could look at modelling spatially extended systems (PDEs) rather than spatially homogeneous (ODEs). Cells are spatially distributed and Ca^{2+} concentration varies across the cell.

References

- Aizman, O., Uhlén, P., Lal, M., Brismar, H., & Aperia, A. (2001). Ouabain, a steroid hormone that signals with slow calcium oscillations. *Proceedings of the National Academy of Sciences*, *98*(23), 13420–13424.
- Atri, A., Amundson, J., Clapham, D., & Sneyd, J. (1993). A single-pool model for intracellular calcium oscillations and waves in the *Xenopus Laevis* oocyte. *Biophysical Journal*, *65*(4), 1727–1739.
- Baker, H. L., Errington, R. J., Davies, S. C., & Campbell, A. K. (2002). A mathematical model predicts that calreticulin interacts with the endoplasmic reticulum Ca^{2+} -ATPase. *Biophysical Journal*, *82*(2), 582–590.
- Berridge, M. J. (1989). *Cell to cell signalling: from experiments to theoretical models* (A. Goldbeter, Ed.). Academic Press, New York.
- Berridge, M. J. (1995). Capacitative calcium entry. *Biochemical Journal*, *312*(Pt 1), 1.
- Berridge, M. J., Bootman, M. D., & Roderick, H. L. (2003). Calcium signalling: Dynamics, homeostasis and remodelling. *Nature Reviews Molecular Cell Biology*, *4*(7), 517–529.
- Berridge, M. J., & Dupont, G. (1994). Spatial and temporal signalling by calcium. *Current opinion in cell biology*, *6*(2), 267–274.
- Berridge, M. J., & Galione, A. (1988). Cytosolic calcium oscillators. *The FASEB Journal*, *2*(15), 3074–3082.
- Berridge, M. J., Lipp, P., & Bootman, M. D. (2000). The versatility and universality of calcium signalling. *Nature Reviews*, *1*(1), 11–21.
- Bezprozvanny, I., & Ehrlich, B. E. (1995). The inositol 1,4,5-trisphosphate (insp3) receptor. *The Journal of Membrane Biology*, *145*(3), 205–216.

- Bezprozvanny, I., Watras, J., & Ehrlich, B. E. (1991). Bell-shaped calcium-response curves of Ins(1,4,5)P₃- and calcium-gated channels from endoplasmic reticulum of cerebellum. *Nature*, *351*(June 1991), 751–754.
- Busa, W. B., & Nuccitelli, R. (1985). An elevated free cytosolic Ca²⁺ wave follows fertilization in eggs of the frog, *Xenopus laevis*. *The Journal of cell biology*, *100*(4), 1325–1329.
- Callamaras, N., & Parker, I. (2000). Phasic characteristic of elementary Ca²⁺ release sites underlies quantal responses to IP₃. *The EMBO Journal*, *19*(14), 3608–3617.
- Camello, P., Gardner, J., Petersen, O. H., & Tepikin, A. V. (1996). Calcium dependence of calcium extrusion and calcium uptake in mouse pancreatic acinar cells. *The Journal of Physiology*, *490*(3), 585–593.
- Carreras-Sureda, A., Pihán, P., & Hetz, C. (2018). Calcium signaling at the endoplasmic reticulum: fine-tuning stress responses. *Cell Calcium*, *70*, 24–31.
- Carroll, J., Swann, K., Whittingham, D., & Whitaker, M. (1994). Spatiotemporal dynamics of intracellular [Ca²⁺] oscillations during the growth and meiotic maturation of mouse oocytes. *Development*, *120*(12), 3507–3517.
- Carter, T. D., & Ogden, D. (1997). Kinetics of Ca²⁺ release by insp₃, in pig single aortic endothelial cells: Evidence for an inhibitory role of cytosolic Ca²⁺ in regulating hormonally evoked Ca²⁺ spikes. *Journal of Physiology*, *504*(1), 17–33.
- Combettes, L., Champeil, P., Finch, E. A., & Goldin, S. M. (1994). Calcium and inositol 1, 4, 5-trisphosphate-induced Ca²⁺ release. *Science*, *265*(5173), 813–815.
- De Young, G. W., & Keizer, J. (1992). A single-pool inositol 1, 4, 5-trisphosphate-receptor based model for agonist-stimulated oscillations in Ca²⁺ concentration. *Proceedings of the National Academy of Sciences*, *89*(20), 9895–9899.
- Dufour, J.-F., Arias, I. M., & Turner, T. J. (1997). Inositol 1,4,5-trisphosphate and calcium regulate the calcium channel function of the hepatic inositol 1,4,5-trisphosphate receptor. *Journal of Biological Chemistry*, *272*(5), 2675–2681.
- Dupont, G. (1998). Theoretical insights into the mechanism of spiral Ca²⁺ wave initiation in *Xenopus* oocytes. *American Journal of Physiology-Cell Physiology*, *275*(1), C317–C322.
- Dupont, G., Berridge, M. J., & Goldbeter, A. (1991). Signal-induced Ca²⁺ oscillations: properties of a model based on Ca²⁺-induced Ca²⁺ release. *Cell calcium*, *12*(2-3), 73–85.
- Dupont, G., Falcke, M., Kirk, V., & Sneyd, J. (2016). *Models of calcium signalling* (Vol. 43).
- Dupont, G., & Goldbeter, A. (1993). One-pool model for Ca²⁺ oscillations involving Ca²⁺ and inositol 1,4,5-trisphosphate as co-agonists for Ca²⁺ release. *Cell Calcium*, *14*(4),

311–322.

- Ermentrout, B. (2002). *Simulating, analyzing and animating dynamical systems: a guide to xppaut for researchers and students* (Vol. 14). Philadelphia: SIAM.
- Falcke, M. (2003). On the role of stochastic channel behavior in intracellular Ca^{2+} dynamics. *Biophysical journal*, *84*(1), 42–56.
- Fill, M., & Copello, J. A. (2002). Ryanodine receptor calcium release channels. *Physiological Reviews*, *82*, 893–922.
- Finch, E. A., Turner, T. J., & Goldin, S. M. (1991). Calcium as a coagonist of inositol 1,4,5-trisphosphate-induced calcium release. *Science*, *252*(5004), 443–446.
- Fink, C. C., Slepchenko, B., Moraru, I. I., Schaff, J., Watras, J., & Loew, L. M. (1999). Morphological control of inositol-1, 4, 5-trisphosphate-dependent signals. *The Journal of cell biology*, *147*(5), 929–936.
- Fontanilla, R. A., & Nuccitelli, R. (1998). Characterization of the sperm-induced calcium wave in *Xenopus* eggs using confocal microscopy. *Biophysical journal*, *75*(4), 2079–2087.
- Foskett, J. K., White, C., Cheung, K. h., & Mak, D.-O. D. (2007). Inositol trisphosphate receptor Ca^{2+} release channels. *Physiological Reviews*, *87*(2), 593–658.
- Hagar, R. E., Burgstahler, A. D., Nathanson, M. H., & Ehrlich, B. E. (1998). Type iii InsP3 receptor channel stays open in the presence of increased calcium. *Nature*, *396*, 81–84.
- Hodgkin, A. L., & Huxley, A. F. (1952). A quantitative description of membrane current and its application to conduction and excitation in nerve. *The Journal of physiology*, *117*(4), 500–544.
- Höfer, T. (1999). Model of intercellular calcium oscillations in hepatocytes: synchronization of heterogeneous cells. *Biophysical journal*, *77*(3), 1244–1256.
- Joseph, S. K. (1996). The Inositol Triphosphate Receptor Family. *Cellular signalling*, *8*(1), 1–7.
- Jouaville, L. S., Ichas, F., Holmuhamedov, E. L., Camacho, P., & Lechleiter, J. D. (1995). Synchronization of calcium waves by mitochondrial substrates in *Xenopus* Laevis oocytes. *Nature*, *377*(6548), 438–441.
- Kaftan, E. J., Ehrlich, B. E., & Watras, J. (1997). Inositol 1, 4, 5-trisphosphate (InsP3) and calcium interact to increase the dynamic range of InsP3 receptor-dependent calcium signaling. *The Journal of general physiology*, *110*(5), 529–538.
- Kaouri, K., Maini, P. K., Skourides, P. A., Christodoulou, N., & Chapman, S. J. (2019). Mathematical biology a simple mechanochemical model for calcium signalling in embryonic epithelial cells. *Journal of Mathematical Biology*, *78*(7), 2059–2092.
- Katrik, V., Van Rossum, D. B., Patterson, R. L., Ma, H. T., & Gill, D. L. (2002). The

- cellular and molecular basis of store-operated calcium entry. *Nature Cell Biology*, 4(11), 36–38.
- Kline, D., & Kline, J. (1992). Thapsigargin activates a calcium influx pathway in the unfertilized mouse egg and suppresses repetitive calcium transients in the fertilized egg. *Journal of Biological Chemistry*, 267(25), 17624–17630.
- Kowalewski, J. M., Uhlén, P., Kitano, H., & Brismar, H. (2006). Modeling the impact of store-operated Ca^{2+} entry on intracellular Ca^{2+} oscillations. *Mathematical Biosciences*, 204(2), 232–249.
- Lechleiter, J., Girard, S., Peralta, E., & Clapham, D. (1991). Spiral calcium wave propagation and annihilation in *Xenopus Laevis* oocytes. *Science*, 252(5002), 123–126.
- Li, Y.-X., & Rinzel, J. (1994). Equations for InsP_3 receptor-mediated $[\text{Ca}^{2+}]_i$ oscillations derived from a detailed kinetic model: A Hodgkin-Huxley like formalism. *Journal of theoretical Biology*, 166(4), 461–473.
- Lytton, J., Westlin, M., Burk, S. E., Shull, G. E., & MacLennan, D. H. (1992). Functional comparisons between isoforms of the sarcoplasmic or endoplasmic reticulum family of calcium pumps. *Journal of Biological Chemistry*, 267(20), 14483–14489.
- Mak, D.-O. D., & Foskett, J. K. (2015). Inositol 1,4,5-trisphosphate receptors in the endoplasmic reticulum: A single-channel point of view. *Cell Calcium*, 58(1), 67–78.
- Mak, D.-O. D., McBride, S., & Foskett, J. K. (1998). Inositol 1,4,5-tris-phosphate activation of inositol tris-phosphate receptor Ca^{2+} channel by ligand tuning of Ca^{2+} inhibition. *Proceedings of the National Academy of Sciences*, 95(26), 15821–15825.
- Marchant, J. S., Callamaras, N., & Parker, I. (1999). Initiation of IP_3 -mediated Ca^{2+} waves in *Xenopus* oocytes. *The EMBO journal*, 18(19), 5285–5299.
- Marchant, J. S., & Taylor, C. W. (1998). Rapid activation and partial inactivation of inositol trisphosphate receptors by inositol trisphosphate. *Biochemistry*, 37(33), 11524–11533.
- Marks, A. R. (1997). Intracellular calcium-release channels: regulators of cell life and death. *American Journal of Physiology-Heart and Circulatory Physiology*, 272(2), H597–H605.
- Masamitsu, I. (1990). Biphasic Ca^{2+} dependence of inositol 1,4,5-trisphosphate-induced Ca^{2+} release in smooth muscle cells of the guinea pig taenia caeci. *Journal of general physiology*, 95(6), 1103–1122.
- MathWorks. (2020). *Matlab r2020a*. Natick, Massachusetts: The MathWorks Inc.
- Mauger, J.-P., Lièvremon, J.-P., Piétri-Rouxel, F., Hilly, M., & Coquil, J.-F. (1994). The inositol 1,4,5-triphosphate receptor: kinetic properties and regulation. *Molecular and cellular endocrinology*, 98(2), 133–139.
- Meyer, T., Holowka, D., & Stryer, L. (1988). Highly cooperative opening of calcium channels

- by inositol 1,4,5-trisphosphate. *Science*, *240*(4852), 653–656.
- Miyakawa-Naito, A., Uhlén, P., Lal, M., Aizman, O., Mikoshiba, K., Brismar, H., . . . Aperia, A. (2003). Cell signaling microdomain with Na,K-ATPase and inositol 1,4,5-trisphosphate receptor generates calcium oscillations. *Journal of Biological Chemistry*, *278*(50), 50355–50361.
- Mouillac, B., Balestre, M.-N., & Guillon, G. (1990). Positive feedback regulation of phospholipase c by vasopressin-induced calcium mobilization in wrk1 cells. *Cellular Signalling*, *2*(5), 497–507.
- Murray, J. D. (1989). *Mathematical biology, vol. 19 of biomathematics*. Springer, Berlin, Germany.
- Nuccitelli, R., Yim, D. L., & Smart, T. (1993). The sperm-induced Ca²⁺ wave following fertilization of the *Xenopus* egg requires the production of ins (1, 4, 5) p3. *Developmental biology*, *158*(1), 200–212.
- Parekh, A. B., & Penner, R. (1997). Store depletion and calcium influx. *Physiological reviews*, *77*(4), 901–930.
- Parekh, A. B., & Putney Jr, J. W. (2005). Store-operated calcium channels. *Physiological Reviews*, *85*(2), 757–810.
- Parys, J. B., & Bezprozvanny, I. (1995). The inositol trisphosphate receptor of *Xenopus* oocytes. *Cell calcium*, *18*(5), 353–363.
- Parys, J. B., Sernett, S. W., DeLisle, S., Snyder, P. M., Welsh, M. J., & Campbell, K. P. (1992). Isolation, characterization, and localization of the inositol 1, 4, 5-trisphosphate receptor protein in *Xenopus Laevis* oocytes. *Journal of Biological Chemistry*, *267*(26), 18776–18782.
- Patel, S., Joseph, S. K., & Thomas, A. P. (1999). Molecular properties of inositol 1,4,5-trisphosphate receptors. *Cell Calcium*, *25*(3), 247–264.
- Patterson, R. L., Boehning, D., & Snyder, S. H. (2004). Inositol 1,4,5-trisphosphate receptors as signal integrators. *Annual Review of Biochemistry*, *73*, 437–465.
- Politi, A., Gaspers, L. D., Thomas, A. P., & Höfer, T. (2006). Models of IP₃ and Ca²⁺ oscillations: Frequency encoding and identification of underlying feedbacks. *Biophysical Journal*, *90*(9), 3120–3133.
- Putney, J. W., Broad, L. M., Braun, F. J., Lievremont, J. P., & Bird, G. S. J. (2001). Mechanisms of capacitative calcium entry. *Journal of Cell Science*, *114*(12), 2223–2229.
- Sanders, J. R., Ashley, B., Moon, A., Woolley, T. E., & Swann, K. (2018). PLC ζ induced Ca²⁺ oscillations in mouse eggs involve a positive feedback cycle of Ca²⁺ induced InsP₃ formation from cytoplasmic PIP₂. *Frontiers in Cell and Developmental Biology*,

- 6(APR), 1–14.
- Shuai, J.-W., & Jung, P. (2002). Stochastic properties of Ca^{2+} release of inositol 1, 4, 5-trisphosphate receptor clusters. *Biophysical journal*, *83*(1), 87–97.
- Sims, C. E., & Allbritton, N. L. (1998). Metabolism of inositol 1, 4, 5-trisphosphate and inositol 1, 3, 4, 5-tetrakisphosphate by the oocytes of *Xenopus Laevis*. *Journal of Biological Chemistry*, *273*(7), 4052–4058.
- Smrcka, A. V., Hepler, J. R., Brown, K. O., & Sternweis, P. C. (1991). Regulation of polyphosphoinositide-specific phospholipase C activity by purified Gq. *Science*, *251*(4995), 804–807.
- Sneyd, J. (2007). Models of calcium dynamics. *Scholarpedia*, *2*(3), 1576.
- Sneyd, J., Tsaneva-Atanasova, K., Reznikov, V., Bai, Y., Sanderson, M., & Yule, D. (2006). A method for determining the dependence of calcium oscillations on inositol trisphosphate oscillations. *Proceedings of the National Academy of Sciences*, *103*(6), 1675–1680.
- Stehno-Bittel, L., Lückhoff, A., & Clapham, D. E. (1995). Calcium release from the nucleus by InsP3 receptor channels. *Neuron*, *14*(1), 163–167.
- Sun, X.-P., Callamaras, N., Marchant, J. S., & Parker, I. (1998). A continuum of InsP3-mediated elementary Ca^{2+} signalling events in *Xenopus* oocytes. *The Journal of Physiology*, *509*(1), 67–80.
- Swann, K. (2021). Personal Communication.
- Swann, K., & Lai, F. A. (2013). PLC ζ and the initiation of Ca^{2+} oscillations in fertilizing mammalian eggs. *Cell calcium*, *53*(1), 55–62.
- Swann, K., & Lai, F. A. (2016). Egg activation at fertilization by a soluble sperm protein. *Physiological reviews*, *96*(1), 127–149.
- Taylor, C. W., & Laude, A. J. (2002). IP3 receptors and their regulation by calmodulin and cytosolic Ca^{2+} . *Cell Calcium*, *32*(5-6), 321–334.
- Taylor, C. W., & Richardson, A. (1991). Structure and function of inositol triphosphate receptors. *Pharmacology & therapeutics*, *51*(1), 97–137.
- Taylor, C. W., & Traynor, D. (1995). Calcium and inositol trisphosphate receptors. *The Journal of Membrane Biology*, *145*(2), 109–118.
- Theodoridou, M., Nomikos, M., Parthimos, D., Gonzalez-Garcia, J. R., Elgmati, K., Calver, B. L., ... Lai, F. A. (2013). Chimeras of sperm PLC ζ reveal disparate protein domain functions in the generation of intracellular Ca^{2+} oscillations in mammalian eggs at fertilization. *Molecular Human Reproduction*, *19*(12), 852–864.
- Thomas, A. P., Bird, G. S. J., Hajnóczky, G., Robb-Gaspers, L. D., & Putney, J. W. (1996). Spatial and temporal aspects of cellular calcium signaling. *The FASEB Journal*,

- 10(13), 1505–1517.
- Uhlén, P., Laestadius, Å., Jahnukainen, T., Söderblom, T., Bäckhed, F., Celsi, G., ... Richter-Dahlfors, A. (2000). α -haemolysin of uropathogenic e. coli induces Ca²⁺ oscillations in renal epithelial cells. *Nature*, 405(6787), 694–697.
- Van Petegem, F. (2012). Ryanodine receptors: Structure and function. *Journal of Biological Chemistry*, 287(38), 31624–31632.
- Wakai, T., Zhang, N., Vangheluwe, P., & Fissore, R. A. (2013). Regulation of endoplasmic reticulum Ca²⁺ oscillations in mammalian eggs. *Journal of cell science*, 126(24), 5714–5724.
- Wallingford, J. B., Ewald, A. J., Harland, R. M., & Fraser, S. E. (2001). Calcium signaling during convergent extension in *Xenopus*. *Current Biology*, 11(9), 652–661.
- Watras, J., Bezprozvanny, I., & Ehrlich, B. E. (1991). Inositol 1, 4, 5-trisphosphate-gated channels in cerebellum: presence of multiple conductance states. *Journal of Neuroscience*, 11(10), 3239–3245.
- Yao, Y., & Parker, I. (1994). Ca²⁺ influx modulation of temporal and spatial patterns of inositol trisphosphate-mediated Ca²⁺ liberation in *Xenopus* oocytes. *The Journal of Physiology*, 476(1), 17–28.

Appendix A

A look into models with dynamic IP_3

An avenue for further work from this project is to derive a model with an ODE for dynamic IP_3 concentration, as suggested in Chapter 5. Sneyd et al. (2006) produced experimental data to prove that dynamic IP_3 is necessary in models for Ca^{2+} signalling in airway smooth muscle cells and pancreatic acinar cells. They also derived two models with IP_3 as a dynamic variable.

In Sneyd et al. (2006), an experiment was carried out where a artificial pulse of IP_3 is applied to two different types of cells. The results from the experiment on airway smooth muscle (ASM) showed that Ca^{2+} oscillations were present with constant IP_3 , and the extra pulse increased the frequency of oscillations. In pancreatic acinar cells (PAC), it was evident that the IP_3 concentration was oscillating. Once the pulse was added, IP_3 then lay outside the oscillatory range and there was a phase lag as the concentration of IP_3 decreased. Sneyd et al. (2006) studied a total of 13 different models and chose to illustrate their experimental results using the models of Atri et al. (1993) and Li and Rinzel (1994). Both the Atri model and Li-Rinzel model assume IP_3 concentration to be constant, and thus is a parameter in the system of equations. In both models, Ca^{2+} activates and inactivates the IP_3R , and the steady state of which follows the usual bell-shaped curve as a function of Ca^{2+} . A third equation for IP_3 is used to extend both the Atri and Li-Rinzel models.

An adapted Atri model with dynamic IP_3 :

Let us first look at how the paper by Sneyd et al. (2006) extends the Atri et al. (1993) model. The equations (2.1) and (2.2) are adjusted slightly to be as in equations (A.1) and (A.2) below. An equation for Ca^{2+} in the ER is incorporated (shown in equation (A.3)), as well as an equation for IP_3 (shown in equation (A.4)). We can see that the IP_3 concentration is

modulated by Ca^{2+} . The model is defined by

$$\frac{dc}{dt} = J_{channel} - J_{pump} + \delta(J_{in} - J_{pm}), \quad (\text{A.1})$$

$$\tau_n \frac{dn}{dt} = \frac{K_{inh}^2}{K_{inh}^2 + c^2} - n, \quad (\text{A.2})$$

$$\gamma \frac{dc_e}{dt} = - (J_{channel} - J_{pump}), \quad (\text{A.3})$$

$$\frac{dp}{dt} = v_4 \left(\frac{c + (1 - \alpha)k_4}{c + k_4} \right) - \beta_{osc}p + s(t). \quad (\text{A.4})$$

Fluxes are given by

$$J_{channel} = k_{flux} \left(\frac{p + \mu_0 K_{IP_3}}{K_{IP_3} + p} \right) n \left(\frac{K_{act}b + c}{K_{act} + c} \right) (c_e - c),$$

$$J_{pump} = \frac{V_e c}{K_e + c},$$

$$J_{in} = \alpha_1 + \alpha_2 v_4,$$

$$J_{pm} = \frac{V_p c^2}{K_p^2 + c^2}.$$

Parameter descriptions and values are given in Table B.6. Few parameter values have been adjusted from the Atri model. The leakage term, $J_{leakage}$, is now a more complex function dependent on cytosolic Ca^{2+} . The variable c_e , for Ca^{2+} in the ER, allows a coupling between equations (A.1) and (A.3). Equation (A.4) is an IP_3 production term (dependent on Ca^{2+}), a degradation term for IP_3 , and a source term, $s(t)$. The source term was present as a product of Heaviside step functions to model a pulse of IP_3 being added and causing a phase delay. The parameter γ is used to adjust the amplitude of the ER Ca^{2+} oscillations, as we know it is oscillating very slightly in comparison, and is passive.

Figure A.1 shows a plot of equations (A.1)-(A.4). We can see that Ca^{2+} in the ER has a very small amplitude in the oscillations. Therefore, for simplicity in the model one can eliminate equation (A.3) and consider Ca^{2+} in the ER to be constant. Once eliminated, ER Ca^{2+} can be taken as a value $14\mu M$. Now, since this is an order of magnitude greater than the range at which cytosolic Ca^{2+} oscillates, the term $(c_e - c)$ is actually doing very little in contribution to the system. It can just be taken as c_e on its own, which is a factor. When Ca^{2+} in the ER is taken as constant, we get a decoupling with the equation (A.1). The plot for this be seen in Figure A.1.

The model by Sneyd et al. (2006) is still based on the older data (Parys et al., 1992) that the Atri model was based on, and so it does not incorporate the more accurate data

on the IP_3R dynamics obtained by Mak et al. (1998). The Sneyd et al. (2006) model is one that should be taken into careful consideration for further work on the new model we have derived. It would be insightful to see how an IP_3 equation of this kind would work in a system with the IP_3R dynamics from Mak et al. (1998) incorporated.

A similar model was derived in the paper by adding the same ODE for IP_3 to the Li-Rinzel model. However, with this addition came the decision to consider n as a constant. This is not so relevant to our model as the fact our new model works on a gating system is crucial for the inclusion of the equation for P_O (3.2).

The third model we took a look at with dynamic IP_3 concentration was by Politi et al. (2006). The model presented was based around Li and Rinzel (1994), Lytton et al. (1992), and Camello et al. (1996). It is a system of four variables with cytosolic Ca^{2+} concentration, Ca^{2+} concentration in the ER, cytosolic IP_3 concentration, and the proportion of IP_3R that have not been inactivated by Ca^{2+} . The model assumes the IP_3 concentration to be highly dynamic, with oscillations in line with Ca^{2+} oscillations. They show that there is both positive and negative feedback of Ca^{2+} , and that IP_3 metabolism could mediate fluctuations in IP_3 .

The model presented accounts for the Ca^{2+} fluxes across the ER and plasma membrane, the IP_3R dynamics, and the formation and degradation of IP_3 . The model is as follows.

$$\frac{dc}{dt} = J_{channel} - J_{pump} + J_{leak}, \quad (A.5)$$

$$\frac{dc_e}{dt} = \frac{1}{\beta}(-J_{channel} + J_{pump}), \quad (A.6)$$

$$\tau_n \frac{dn}{dt} = 1 - n \frac{K_{inh} + c}{K_{inh}}, \quad (A.7)$$

$$\tau_p \frac{dp}{dt} = v_{PLC} - v_{deg}, \quad (A.8)$$

where

$$\begin{aligned}
J_{channel} &= \left(v_1 \left(n \frac{c}{K_{act} + c} \frac{p}{K_{IP_3} + p} \right)^3 + \epsilon \right) (c_e - c), \\
J_{pump} &= \frac{V_e c^2}{K_e^2 + c^2}, \\
J_{leak} &= v_{in} - v_{out} \\
&= \epsilon \left(v_0 + \Phi V_{PLC} - V_p \frac{c^2}{K_p^2 + c^2} \right), \\
v_{PLC} &= \frac{c^2}{K_{PLC}^2 + c^2}, \\
v_{deg} &= \left(k_{5P} + k_{3K} \frac{c^2}{K_{3K}^2 + c^2} \right).
\end{aligned}$$

Here we can see that Ca^{2+} flux through the IP_3R , $J_{channel}$, is modelled based on the Li and Rinzel (1994) model, that we have studied in Chapter 2. The SERCA pumps, J_{pump} , however, follows the model given in Lytton et al. (1992), and v_{out} follows that in Camello et al. (1996). The term J_{pump} is modelled with a Hill coefficient of 2, in contrast to 1 in both the Atri and Li-Rinzel models. It is important that future models respect the data and consider a Hill coefficient of 2. Ca^{2+} influx, v_{in} , represents a leak into the cell as well as a stimulation dependent influx. The parameter ϵ is a dimensionless constant that controls the relative strength of the cell plasma membrane's fluxes. This flux is cell type specific, or in an isolated egg, non-existent.

PLC produces IP_3 and depends on agonist dose and Ca^{2+} . PLC_β 's sensitivity towards Ca^{2+} is modelled by v_{PLC} . Within this, V_{PLC} depends on agonist concentration, and K_{PLC} characterizes the sensitivity of PLC to Ca^{2+} . IP_3 degradation happens through phosphorylation by IP_3P and phosphorylation by IP_3K , which is modelled by v_{deg} . Respectively, k_{5P} and k_{3K} are the IP_3 dephosphorylation and phosphorylation rate constants. The Ca^{2+} dependence of the IP_3K is described by a Hill function with half-saturation constant K_{3K} . Here, the model assumes that the two enzymes are not saturated with IP_3 , so a linear rate law in p is given. This assumption is based on the work of Fink et al. (1999) and Sims and Allbritton (1998).

The modelling of the IP_3 equation in this paper has been well thought out, and should be considered in any future models. The Hill equation in v_{deg} is a necessary component in any future model that assumes a dynamic IP_3 concentration. It is agreed that IP_3 production is catalyzed by phosphoinositide-specific phospholipase C isoforms (PLC), which are activated by Ca^{2+} . Furthermore, IP_3 levels fall by dephosphorylation through IP_3 5-phosphatase.

However, IP_3 degradation also happens by phosphorylation through IP_3 3-kinase (IP_3K). This is activated by Ca^{2+} , and hence in a mathematical model would need to show dependence on Ca^{2+} (Politi et al., 2006).

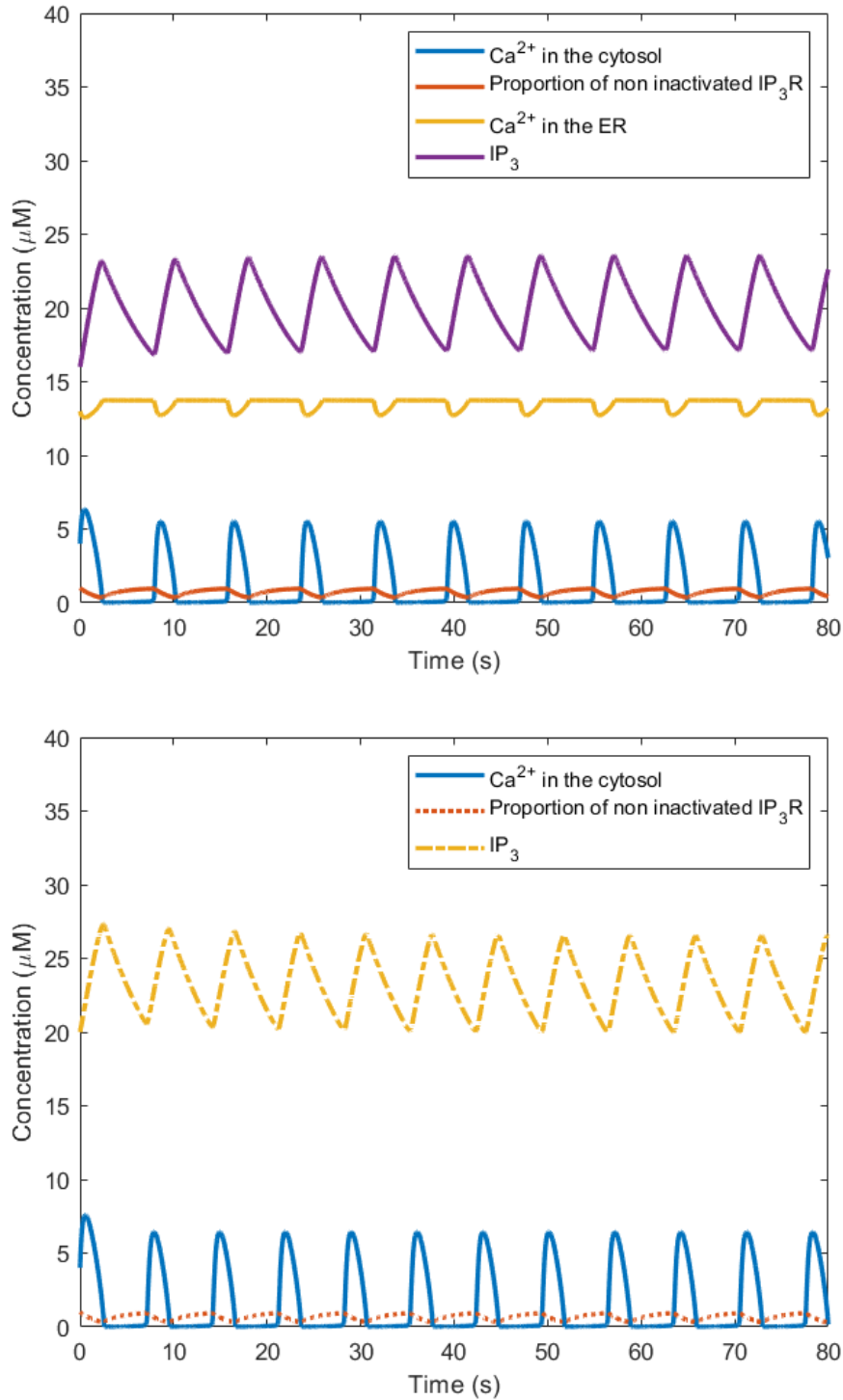


Figure A.1: The first graph shows Ca^{2+} and IP_3 oscillations arising as solutions of the equations (A.1)-(A.4). The second graph shows Ca^{2+} and IP_3 oscillations arising as solutions of the equations (A.1), (A.2) and (A.4) (Sneyd et al., 2006). Equation (A.3) for the Ca^{2+} concentration in the ER, c_e , has been omitted and c_e was set to $14\mu\text{M}$. Other parameters are taken as in Table B.6. *Software*: MATLAB.

Appendix B

Parameter Tables

Parameter	Biological representation	Value in Atri et al.
k_{flux}	Maximum total Ca^{2+} flux through all IP_3R	$8.1 \mu Ms^{-1}$
μ_0	Proportion of IP_3R that are activated at $IP_3 = 0 \mu M$ (site 1 activated in the absence of bound IP_3)	0.567
k_{IP_3}	Half-activation term for binding of IP_3 to site 1	$4.0 \mu M$
K_{act}	Half-activation term for binding of Ca^{2+} to site 2	$0.7 \mu M$
b	Proportion of IP_3R that have site 2	0.111
V_e	Maximal SERCA pump rate	$2 \mu Ms^{-1}$
K_e	Half-activation constant for SERCA term	$0.1 \mu M$
δ	Constant rate of Ca^{2+} influx into cytosol	$0.01 \mu Ms^{-1}$
τ_n	Time constant for dynamics of n (for activation of site 3)	2.0s
K_{inh}	Half-deactivation constant for Ca^{2+} binding to site 3	$0.7 \mu M$

Table B.1: Parameters used in the Atri et al. (1993) model, shown in equations (2.1), (2.2) in Chapter 2. A typical value of p used is $0.8 \mu M$.

Parameter	Biological representation	Value in Li-Rinzel
v_1	Maximal rate of Ca^{2+} release	$40s^{-1}$
k_μ	Half-activation constant for IP_3 binding	$0.2\mu M$
k_1	Half-activation constant for Ca^{2+} binding to activation site	$0.4\mu M$
ϵ	Ca^{2+} leak out of ER	$0.02s^{-1}$
c_1	Parameter used to adjust amplitude of ER Ca^{2+} oscillations	0.185
V_e	Maximal SERCA pump rate	$0.6\mu Ms^{-1}$
K_e	Half-activation constant for SERCA pumps	$0.18\mu M$
A	A parameter to characterize the slow time scale of Ca^{2+} inactivation	$1s^{-1}$
k_2	Half-activation constant for Ca^{2+} binding to inhibitory site	$0.4\mu M$

Table B.2: Parameters used the Li and Rinzel (1994) model, shown in equations (2.7), (2.8) in Chapter 2.

Parameter	Value in Li-Rinzel
δ	0.01
J_{in}	$0.8\mu Ms^{-1}$
V_p	$1.8\mu Ms^{-1}$
K_p	$0.1\mu M$

Table B.3: Parameters used in the Li and Rinzel (1994) Three-Variable model, (??)-(??) in Chapter 2.

Parameter	Biological representation	Value in Mak et al.
P_{max}	Maximal open probability of IP_3R	0.81
K_{act}	Half-activation constant for Ca^{2+} binding to activation site	$0.21 \pm 0.02 \mu M$
H_{act}	Hill coefficient for Ca^{2+} binding to activation site	1.9 ± 0.3
K_{inh}	Half-activation constant for Ca^{2+} binding to inhibitory site	
H_{inh}	Hill coefficient for Ca^{2+} binding to inhibitory site	3.9 ± 0.7
K_{∞}	Maximal inhibitory Ca^{2+} concentration	$52 \pm 4 \mu M$
K_{IP_3}	Half-activation constant for IP_3 binding to activation site	$50 \pm 4 \mu M$
H_{IP_3}	Hill coefficient for IP_3 binding to activation site	4 ± 0.5

Table B.4: Parameters used in the equation for open probability of the IP_3R by Mak et al. (1998), (3.2), in Chapter 3.

Parameter	Biological representation	Value in Kowalewski et al.
S_{ER}/V_{ER}	Surface-to-volume ratio of the ER	$1\mu M$
S_{ER}/V_{cyt}	Surface-to-volume ratio of the cytoplasm	$1\mu M$
$r_{ER} = V_{ER}/V_{cyt}$	Volume ratio of ER	0.185
β	Buffering factor	1
X	Relative amount of Ca^{2+} binding to SERCA	0.4
Y	Relative amount of Ca^{2+} binding to PMCA	0.6
I_{deg}	IP_3 degradation constant	$0.01s^{-1}$
t_0	G signalling start time	500s
k_G	G production rate	$0.2s^{-1}$
I_G	G degradation rate	$0.5s^{-1}$
$K_{1/2,G}$	G signalling inactivation constant	$0.5\mu M$
v_{IP_3R}	Maximum permeability across the IP_3R	$70nm/s$
d_1	IP_3 dissociation	$0.13\mu M$
d_2	Ca^{2+} inhibition dissociation	$0.5\mu M$
d_3	IP_3 dissociation	$9.4nM$
d_5	Ca^{2+} activation dissociation	$82.34nM$
v_1	Maximum Ca^{2+} channel permeability	$10\mu M/s$
V_{leakER}	Ca^{2+} leak permeability across the ER membrane	$2nm/s$
v_{SOC}	SOC permeability, per μM	$0.12nm/(s\mu M)$
$[Ca^{2+}]_{ER,min}$	Threshold concentration of ER Ca^{2+}	
V_{leakPM}	Ca^{2+} leak permeability across the cell plasma membrane	$0.012nm/s$
k_{SOC}	SOC production constant	$1.7\mu M/s$
I_{SOC}	SOC degradation constant	$0.002s^{-1}$
v_{CIF}	CIF permeability across the ER membrane	$1\mu m/s$
k_{CIF}	CIF production rate	$2 \times 10^{-4} s^{-1}$
$[CIF]_{max}$	Maximum CIF concentration	$0.1\mu M$
V_p	Maximum flux across PMCA	$0.147\mu m\mu M/s$
V_e	Maximum flux across SERCA	$1.9\mu m\mu M/s$
K_p	PMCA activation constant	$0.2\mu M$
K_e	Half-activation for SERCA pump	$0.5\mu M$

Table B.5: Parameters used in the model by Kowalewski et al. (2006), (4.1)-(4.8), in Chapter 4.

Parameter	Biological representation	Value in Sneyd et al.
k_{flux}	Maximum total Ca^{2+} flux through all IP_3R	4.8
μ_0	Proportion of IP_3R that are activated at $IP_3 = 0\mu M$ (domain 1 activated in the absence of bound IP3)	0.567
k_μ	Half-activation term for binding of IP_3 for domain 1	$4.0\mu M$
k_1	Half-activation term for binding of Ca^{2+}	$0.7\mu M$
b	Proportion of IP_3R that have domain 2	0.111
V_e	Maximal serca pump rate	$20\mu Ms^{-1}$
K_e	Half-activation constant for serca term	$0.06\mu M$
δ	Constant rate of Ca^{2+} influx into cytosol	$0.01\mu Ms^{-1}$
α_1	Constant influx	$1\mu Ms^{-1}$
α_2	Stimulation dependent influx	$0.2s^{-1}$
V_p	Maximal rate of leak out of cytosol over plasma membrane	$24\mu Ms^{-1}$
τ_n	Time constant for dynamics of n (for activation of domain 3)	2.0s
k_2	Half-deactivation constant for n	$0.7\mu M$
γ	Parameter used to adjust amplitude of ER Ca^{2+} oscillations	
v_4	Maximum rate of IP_3 production	6
k_4	Ca^{2+} sensitivity of PLC activity	1.1
α		0.97
β_{osc}	Linear rate of IP_3 breakdown/dephosphorylation rate	$0.08s^{-1}$

Table B.6: Parameters used in the model by Sneyd et al. (2006), (A.1)-(A.4) in Appendix A.

Appendix C

MATLAB Code

```
1 %Code used to simulate the Atri model
2
3 c0=0.1;
4 n0=0.5;
5
6 [t,y] = ode45(@ODE,[0,80],[c0,n0]);
7 plot(t,y(:,1),t,y(:,2),':', 'Linewidth', 2)
8
9 xlabel('Time (s)')
10 ylabel('Concentration (\muM)')
11 legend('Cytosolic Ca^2+', 'Proportion of non inactivated IP_3Rs')
12 ylim([0 5])
13 set(gca, 'fontsize', 15)
14 function dydt=ODE(t,yy)
15 c=yy(1);
16 n=yy(2);
17
18 Kflux=8.1;
19 p=1;
20 kip=4;
21 mu0=0.567;
22 mu1=0.433;
23 mup=(p+mu0*kip)/(kip+p);
24 %mup=1.5;
25 %mup=1;
26 %mup=0.5;
27 kact=0.7;
28 b=0.111;
```

```
29 V1=0.889;
30 Ve=2;
31 Ke=0.1;
32 B=0.01;
33 Jchannel=Kflux*n*((kact*b+(b+V1)*c)/(kact+c))*mup;
34 Jpump=Ve*c/(Ke+c);
35 Jleak=B;
36 kinh=0.7;
37 taun=2;
38
39 dydt= [Jchannel-Jpump+Jleak;
40 kinh^2/(2*(kinh^2+c^2))-n/taun];
41 end
```

Note that other MATLAB scripts written for this project using *ode45* are structured similarly.